ABSTRACT

Title of Thesis: ENABLING CO_2 ISOTHERMAL
                                             COMPRESSION USING LIQUID PISTON AND
                                             INTEGRATED GAS COOLER

                                             Timothy Kim, Master of Science, 2022

Thesis Directed By: Research Professor Yunho Hwang, Ph.D.
                                             Department of Mechanical Engineering

New avenues of decreasing environmental impacts and increasing the efficiency of

HVAC systems are constantly being explored in the race to reduce carbon emissions and global

warming. These new avenues have led to the exploration of the use of carbon dioxide as a

refrigerant in refrigeration applications. Many researchers have also investigated ways to reduce

the power consumption of compressors, which is typically the main source of power draw for

HVAC systems. One theoretical process to achieve this is through isothermal compression.

This thesis explores the idea of isothermally compressing CO_2 by using a liquid piston

and integrated gas cooler to achieve higher efficiencies with this transcritical cycle. A test

facility was designed, sized, constructed, and calibrated to emulate the suction and discharge

conditions of a typical CO_2 system for air conditioning applications. A prototype of the liquid

piston and integrated gas cooler chamber was designed and constructed as well. A simulation

model was built in Engineering Equation Solver in order to properly design the gas cooler

chamber. Other critical components have been carefully chosen to ensure smooth operation of

the system.

Results show isothermal efficiencies of up to 82.7% during steady-state operation and an isothermal efficiency of 91.2% during steady-state operation with the additional help of evaporative cooling. Comparing this to other conventional compressors give up to 34.2% absolute improvement in the isothermal compressor efficiency. These results show sufficient performance to warrant the design of a fully working prototype despite efficiency/capacity tradeoffs in the system. Challenges had been encountered such as the loss of refrigerant through the liquid piston, which will be accounted for in the next prototype. Discussion of the next prototype includes the use of a double-acting piston and a smaller tubed fractal heat exchanger design.

ENABLING CO$_2$ ISOTHERMAL COMPRESSION USING LIQUID PISTON AND
INTEGRATED GAS COOLER

By

Timothy Kim

Thesis submitted to the Faculty of the Graduate School of the

University of Maryland, College Park, in partial fulfillment

of the requirements for the degree of

Master of Science

2022

Advisory Committee:

Research Professor Yunho Hwang

Professor Bao Yang

Professor Jungho Kim

Dedication

To my family and God

Acknowledgments

I would like to thank Dr. Reinhard Radermacher for giving me the opportunity to learn, work and do research at CEEE. I would also like to give my biggest appreciation to Dr. Yunho Hwang for offering me a part-time job as a research assistant and recommending me to enroll in the graduate research program. Additionally, I would like to thank Jan Muehlbauer for his guidance and superb knowledge, and for pushing me to produce the best work possible. I would also like to thank Dr. Jiazhen Ling for his initial involvement in my project and support and hope the best in his next career. This project is also sponsored by the Department of Energy under award number DE-EE0009685. Many thanks for their support.

I am thankful to all other faculty, staff, and lab mates at CEEE. Special thanks to Ellery Klein, Jangho Yang, and Cheng-Yi Lee for their hospitality, aid in my research, and kindness as well as others in the lab.

Finally, I would like to thank my parents, my sister, and my extended family for their support in this endeavor.

Table of Contents

List of Tables

List of Figures

Nomenclature

A	Heat Transfer Surface Area	[m^2]
AHRI	Air-Conditioning, Heating and Refrigeration Institute	[-]
CAD	Computer Automated Design	[-]
CAES	Compressed Air Energy Storage	[-]
cc	Cubic Centimeters	[cm^3]
CEEE	Center for Environmental Energy Engineering	[-]
CFD	Computational Fluid Dynamics	[-]
COP	Coefficient of Performance	[-]
D	Compression Chamber Diameter	[mm]
DAS	Data Acquisition System	[-]
D_H	Hydraulic Diameter	[m]
DOE	Department of Energy	[-]
EC	Evaporative Cooling	[-]
EES	Engineering Equation Solver	[-]
E_{elec}	Electrical Energy	[kJ]
EIA	Energy Information Administration	[-]
E_{press}	Energy from Pressure	[kJ]
GPM	Gallons Per Minute	[Gal/min]
GWP	Global Warming Potential	[-]
HFC	Hydrofluorocarbons	[-]
HVAC	Heating, Ventilation and Air Conditioning	[-]
HXCC	Heat Exchanger Compression Chamber	[-]
h	Enthalpy	[kJ/kg]
Δh	Enthalpy Difference	[kJ/kg]
ISO	International Organization for Standardization	[-]
L	Compression Diameter Length	[m]
l	Tube Length	[m]

M	Molar Mass	[g/mol]
m	CO_2 Mass	[kg]
$\dot{m}$	Mass Flow Rate	[kg/s]
$\dot{m}_{inj}$	Injection Mass Flow Rate	[kg/s]
ORNL	Oak Ridge National Laboratory	[-]
P	Pressure	[kPa]
Δp	Pressure Drop	[Pa]
PAG	Polyalkylene Glycol	[-]
P_{elec}	Power Draw	[kW]
PET	Polyethylene Terephthalate	[-]
P_{final}	Final Gas Pressure	[kPa]
$P_{initial}$	Initial Gas Pressure	[kPa]
p_m	Intermediate Pressure	[MPa]
POE	Polyolester	[-]
$\dot{q}$	Heat Flux	[kW]
R	Ideal Gas Constant	[J mol^{-1} K^{-1}]
RTE	Energy Storage Roundtrip Efficiency	[%]
RPM	Rotations Per Minute	[1/min]
RTD	Resistance Temperature Detector	[-]
s	Entropy	[kJ kg^{-1} K^{-1}]
SS	Steady State	[-]
T	Isothermal Compression Temperature	[K]
ΔT	Temperature Difference	[K]
T_m	Intermediate Temperature	[°C]
U	Overall Heat Transfer Coefficient	[kW m^{-2} K-^{1}]
u_f	Overall Uncertainty	[-]
u_R	Random Uncertainty	[-]
u_S	Systematic Uncertainty	[-]
u_T	Total Uncertainty	[-]

u_{x_i}	Discrete Uncertainty	[-]
v	Piston Velocity	[m/s]
VCC	Vapor Compression Cycle	[-]
w_{actual}	Actual Specific Work	[kJ/kg]
w_{iso}	Isothermal Specific Work	[kJ/kg]
x_i	Nominal Variable Values	[-]
Z	Compressibility Factor	[-]

Greek

α	Injection Angle	[°]
f_D	Friction Factor	[-]
ρ	Density	[kg/m^3]
η_{pump}	Pump Efficiency	[%]
η_{motor}	Motor Efficiency	[%]
η_{iso}	Isothermal Efficiency	[%]
η_{iso_Comp}	Isothermal Compressor Efficiency	[%]
ν	Fluid Velocity	[m/s]

1 Introduction

The reversed Carnot cycle is an idealized refrigeration cycle, which consists of two isothermal processes and two isentropic processes as seen in Figure 1. From the cycle, the theoretical efficiency limit is reached, which is dictated by the temperature of the hot and cold reservoirs. Unfortunately, real-world systems do not resemble these processes due to irreversible friction, pressure drops, superheated vapor compression, and isenthalpic expansion, making the reversed Carnot cycle an unrealistic ideal cycle. However, isothermal compression processes can be realized, which is a more efficient process than isentropic compression, leading a system one step closer to Carnot cycle efficiency. This is especially true because the compressor is responsible for a considerable amount of the system's power input. Typical compressor isentropic efficiencies range from 65% to 90% [15], while reciprocating compressors particularly lean toward the lower efficiencies, giving more room for improvement.
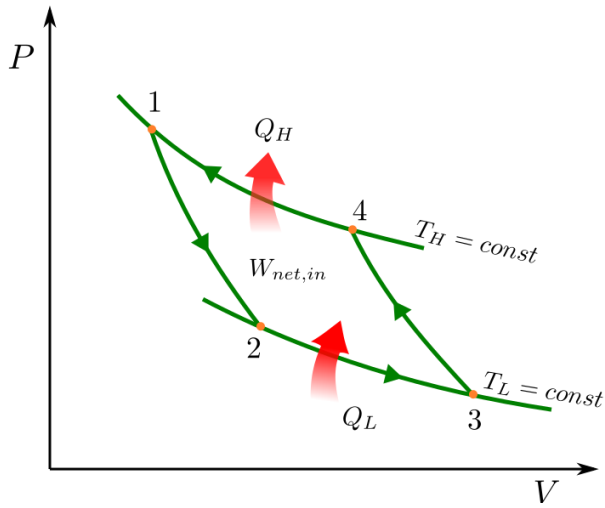
Figure 1: Ideal Reversed Carnot Cycle [10]

Looking at a simple vapor compression cycle (VCC) system, the basic components to drive the system are the condenser, expansion valve, evaporator and the compressor as seen in

Figure 2. The condenser is a heat exchanger that rejects heat, the evaporator is a heat exchanger that absorbs heat and the expansion valve is a device that allows the refrigerant inside to expand to a lower pressure. The compressor's function is to compress the working fluid, which results in an increase in pressure. This increase in pressure causes a pressure difference in the system, which is what drives the refrigerant inside to circulate, enabling constant mass flow.
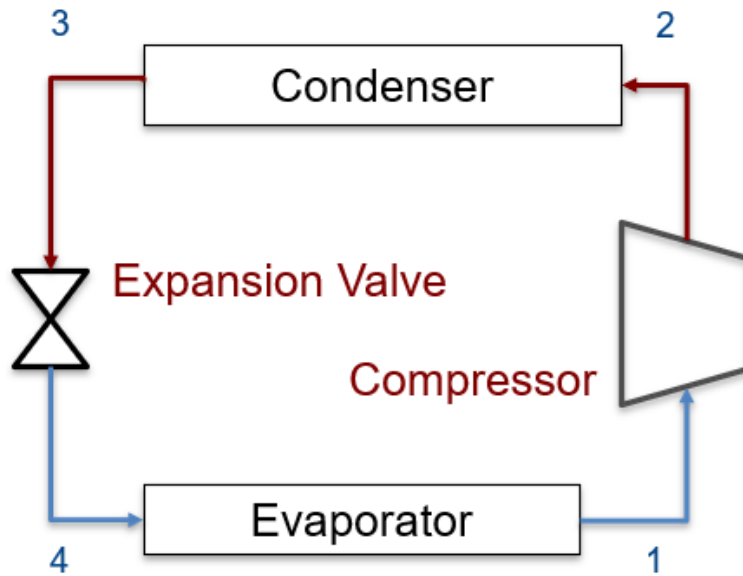
Figure 2: Simple Vapor Compression System

Many methods have been made to compress the gas but the most common is the use of a positive-displacement piston, which is essentially when the gas is forced into a smaller and smaller volume to compress the gas. Doing so increases not only pressure but temperature as well. This is due to a phenomenon called "heat of compression", which makes it harder to compress gas. Heat of compression describes the inefficiencies of compressing a gas where a lot of the energy is converted to heat instead of compressing the gas itself. If enough heat is rejected from the chamber as the gas is being compressed, then the same temperature can remain, hence the term, isothermal compression, the underlying principle. It can also be thought of as combining the roles of the compressor and condenser, which are happening simultaneously.

Motivation for the pursuit of this technology stems from the increasing concern for climate change in the world. The amount of CO_2 emissions has spiked since the industrial revolution which have led to an increase in the global climate by approximately 1 °C from 2011 to 2020 [58]. While this has resulted in relatively mild changes in the weather, higher global warming temperatures will have catastrophic effects. Knowing this, the Paris Climate Accords and Kigali Amendment to the Montreal Protocol were brought to fruition in 2016 [16]. This has led to the international recognition of the effects of climate change and first steps toward its mitigation and adaptation. One such step would be the gradual reduction of consumption of hydrofluorocarbons (HFC) due to their global warming potential (GWP). This means that common refrigerants such as R-134A will be phased out, leaving other environmentally friendly refrigerants to fill the void.

CO_2 has been one such potential refrigerant to replace what were industry standard refrigerants for households such as R-22 and refrigerators such as R-12. It has considerably lower GWP, is an abundant resource and is non-toxic. Figure 3 shows the energy distribution generated by the U.S. and shows a major part of the electricity generated goes to residential and commercial. Heating, Ventilation and Air Conditioning (HVAC) systems are a major contributor in energy consumption in residential and commercial buildings. A consensus survey done by the Energy Information Administration (EIA) in 2015 showed 55% of energy consumption for residential and 54% for commercial buildings comes from heating, cooling, ventilation, and refrigeration [53][54]. The Department of Energy (DOE) as well as many other organizations have set goals for themselves to combat climate change. If these conventional systems were to be replaced with CO_2 based systems with isothermal compression, then it is estimated that 1 quad of energy could be saved annually. This energy is equivalent to $1.055*10^{18}$ Joules.
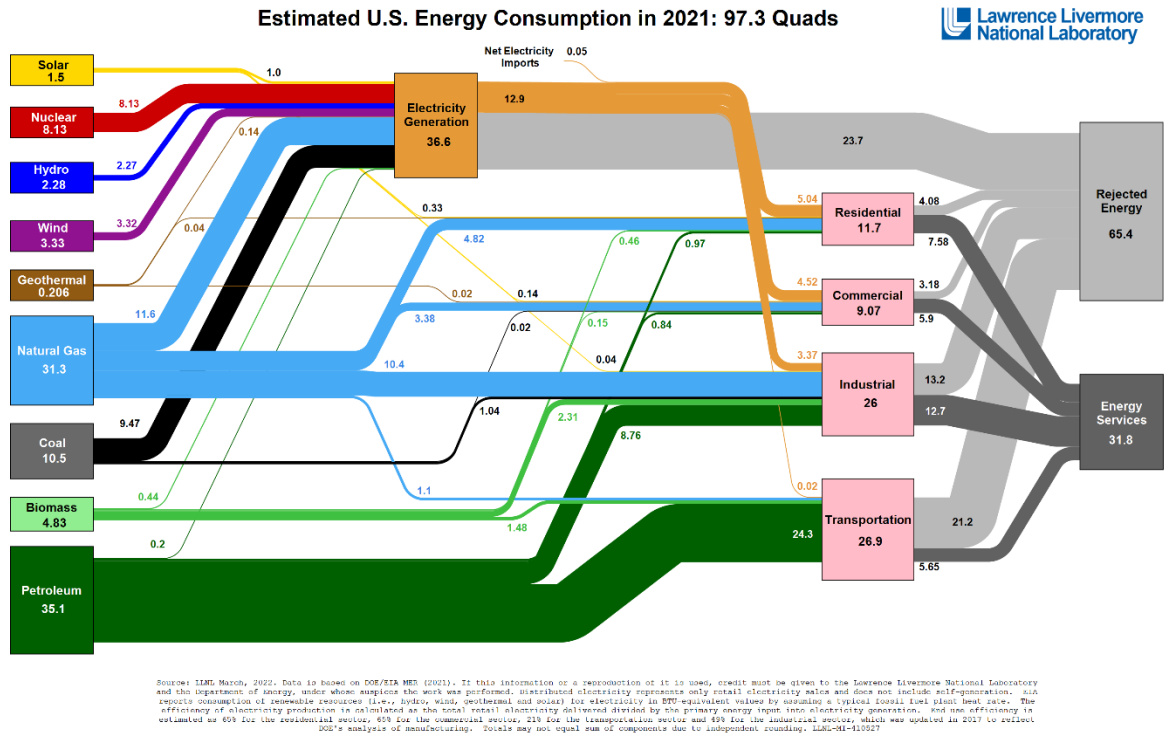
Figure 3: Estimated U.S. Energy Consumption in 2021 [28]

2 Literature Review

To effectively understand isothermal compression and come up with a design for a system, it is important to look at past work that has been done on isothermal compression. Work for two main applications have been explored: refrigeration and air compression applications. Research work for air compression applications have been on the rise in recent years with new, innovative approaches to isothermal compression while refrigeration applications have not seen much new development. The reason may be likely due to the global power generation rise in renewable energy, which has increased to 27% in 2019 [50]. As the world transitions into more renewables, storage becomes more and more of an urgent issue in which compressed air energy storage technologies have become a significant area of research. As the demand for wind and solar increases, more capacity is required, mainly because the power generation of these

renewables is intermittent. Therefore, energy storage technologies are needed, such as hydro and air compression storage, which promises large-scale energy storage. In particular, compressed air energy storage (CAES) has become more and more of a viable option thanks to research on isothermal compression. The idea of more efficient compressed air energy storage technologies via isothermal compression has become more desirable. But isothermal compression would not only benefit compressed air applications but also in refrigeration applications as reducing the worlds overall energy consumption will help lead to a path of carbon neutrality. The hope will be to apply applications from air compression to refrigeration. A complete breakdown of categories can be seen in Figure 4 below.
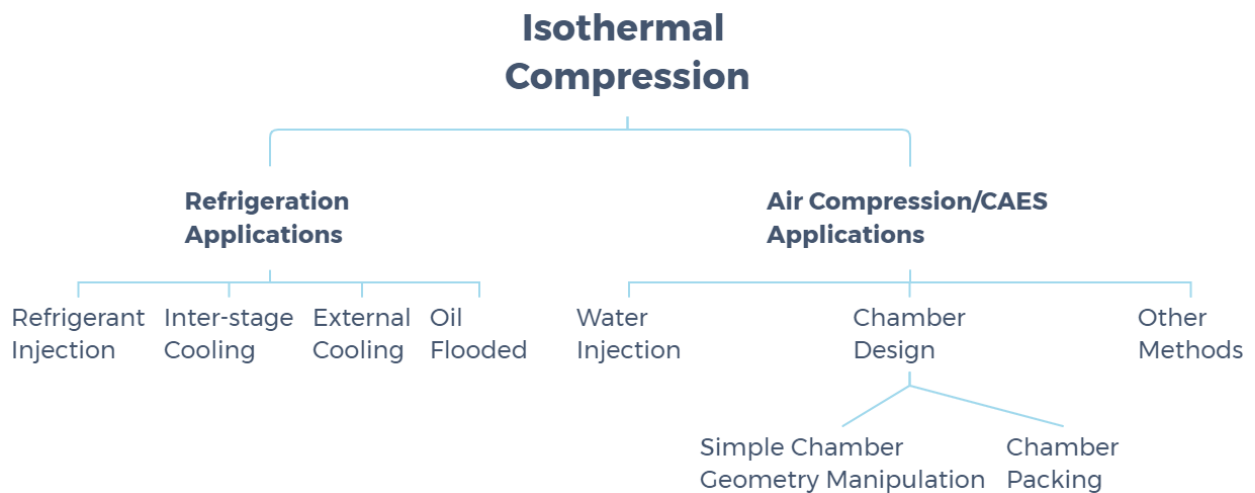
Figure 4: Breakdown of Isothermal Compression Technologies

2.1 Refrigeration Applications

The topics discussed in this section overview the methods explored to achieve isothermal compression in refrigeration applications, including refrigerant injection, inter-stage cooling, external cooling, and oil-flooded compression. Some of these methods have become mainstream applications to achieve this process, while others have remained a research topic. Most of these

methods can be an afterthought application to the already existing scroll compressors or other high-frequency counterparts.

2.1.1 Refrigerant Injection

Refrigerant injection has become a well-known research topic in the refrigeration community and is closely tied to inter-stage cooling. The liquid refrigerant injection is used to cool the compression gas, which can be used for isothermal compression. The benefits and limitations are similar for water injection in that surface area is greatly enhanced. Still, the equipment costs are also higher than some of the other techniques discussed in this review. Table 1 summarizes the findings in this section.

Cho et al. (2003) [13] tested the effectiveness of this strategy in a scroll compressor with the following parameters in mind: compressor motor drive frequency, injection pressure, injection ratio (ratio between injection and suction mass flow rate), and injection location. In short, high frequency leads to high performance, high injection pressure leads to a decrease in discharge temperature, and a rise in injection ratio leads to lower adiabatic efficiency. There are interesting corner cases where the normalized capacity is rapidly reduced at low injection ratios at the frequency test case for 45 hz.

Lee et al. (2015) [29] compared the effectiveness of liquid versus vapor injection on a scroll compressor. Performance metrics include the coefficient of performance (COP), subcooling, and discharge temperature. It should be noted that the authors goal was to decrease the discharge temperature by exploring the refrigerant injection to ensure a longer lifespan of the system while maintaining baseline performance. It should also be noted that the injections happen at the suction line of the compressor, making it a pre-mixed method. The discharge temperature decreases with increasing injection ratios, which increases compressor efficiencies

up to about 90%. However, at injection ratios greater than 10%, performance metrics such as the

cooling capacity and COP are negatively affected for liquid injection. In contrast, these

performance effects are seen linearly from the beginning for the vapor injection. Lee et al. (2015)

[29] recommended using liquid refrigerant injection at a 10% injection ratio in this case.

      Xu et al. (2011) [59] provided an excellent review of research in this field at the system

and the component level. The study described a paper that tested a two-stage CO_2 cycle with

vapor injection, which enhanced the COP by 16.5%. The refrigerant injection can be broken

down by cycle type (internal heat exchanger or flash tank), compressor type (screw, rotary,

scroll, and reciprocating), and performance parameters (injection port location, injection

pressure, and injection ratio), which are discussed in this paper.

Table 1: Refrigerant Injection Literature Summary

Author/year	Type	Details	Application	Findings
Lee et al. (2015) [29]	Experiment	• Compare the effectiveness of liquid and vapor injection at scroll compressor suction port • Working Fluid: R-22	Refrigeration	• Liquid injection recommended over vapor injection with an injection ratio of 10% • Liquid injection at suction port proves to be simple and effective means
Cho et al. (2003) [13]	Experiment	• Experimentally explore effects of refrigerant injection on scroll compressor • Vary the following parameters: Compressor frequency, injection pressure, injection ratio, and injection location • Working Fluid: R-22, Pressure Ratio: 0.63 – 2.15 MPa	Heat pumps	• 10% normalized increase in compressor efficiency • High frequency leads to high performance • High injection pressure leads to a decrease in discharge temp. as well as an increase in power input • A rise in injection ratio leads to lower adiabatic efficiency • Injection location at α=180° give slightly better performance

2.1.2 Inter-stage Cooling

      Inter-stage cooling has become commonplace as a tool to achieve higher efficiency

systems. The concept of inter-stage cooling proposes that if the working gas is compressed in

smaller discrete steps with cooling in between each compression, a more efficient compression

process can be attained. If you had an infinite amount of these discrete steps, theoretically, isothermal compression would be achieved. Dividing up the compression work among multiple compressors means that the gas's temperature is reduced, having the added benefit of using low-temperature material. Figure 5 shows a typical schematic of a two-stage compression system. The downside is the practical effects of pressure drop that will be more apparent with this cooling method. In addition, there will also be a steep increase in the number of equipment costs. To quote a paper, "The equipment is relatively expensive given the number of cylinders, valves, heat exchangers and pulsation dampers, which are required in a multistage unit" (Coney et al., 2002) [14]. Table 2 summarizes the findings in this section.
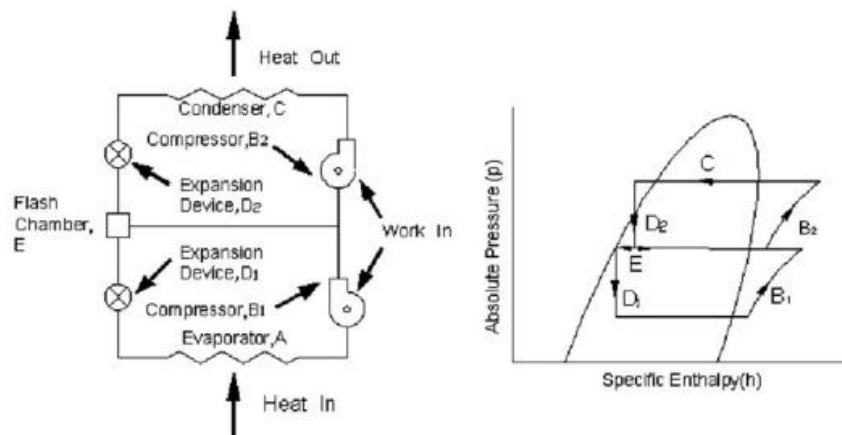
Figure 5: Schematic of Two-Stage Compression System with Associated P-h Diagram (Huang et al., 2007) [23]

Inter-stage cooling is also very niche in that a problem is being divided and conquered. Still, the cooling method in-between stages are mentioned in this review, such as refrigerant injection called pre-mixing, as aforementioned in Lee et al. (2015) [29]. The refrigerant injection is commonly used in these cases and is closely tied to inter-stage cooling. With inter-stage cooling, the refrigerant vapor is recirculated downstream after the expansion valve is back to the

line after each stage. The method for introducing it back into the stage is through refrigerant injection in Huang et al. (2007) [23]. More specifically, it is a borrowed technique used for impeller blades to provide a thin gas film to provide cooling called film cooling. Huang et al. (2007) [23] analyzed this for hole-injection type (3D flow field) and slot-injection type (2D flow field). The geometries of the two can be seen in Figure 6. In summary, there is pressure loss at larger injection angles but is less pronounced in hole injection. Also, better mixing results from this, which leads to lower temperatures. Higher injection velocities have a negligible influence on temperature or velocity uniformities.
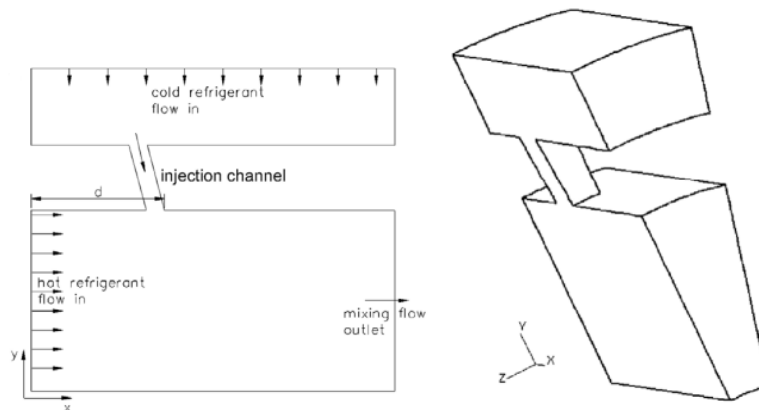
Figure 6: The Geometry of Slot Injection (left) and Geometry of Hole Injection (right)

(Huang et al., 2007) [23]

Röyttä et al. (2009) [44] explores using a flash intercooler in a two-stage compressor system. Flash intercoolers extract a portion of the flow from the condenser, expanding and evaporating in a heat exchanger that cools the main flow to the compressors. The goal was to simulate the system and obtain an optimal point based on calculated COP values tweaked by changing the compressor speed for two refrigerants. Higher COPs were seen at higher compression ratios and rotational speeds that were slightly lower than the optimal rotational speed for the compressor for R-245FA. The opposite happened in the case of R-134A.

Liu et al. (2019) [31] provided an interesting perspective on inter-stage cooling by exploring the antithesis of using inter-stage cooling, i.e., seeing the effects of not using inter-stage cooling on a multistage system. Liu shows performance hits for insufficient cooling and sees a primary trend in that for every 10 K increase in temperature; the isentropic efficiencies are reduced by about 1% at each stage for a four-stage compressor. There is a linear decrease in efficiencies as suction temperature goes up.

Table 2: Inter-Stage Cooling Literature Summary

Author/year	Type	Details	Application	Findings
Liu et al. (2019) [31]	Simulation	• Simulate an increase in suction temperature in increments of 10 to see resulting efficiencies and properties for multistage compressor	Air compression	• for every 10 °C increase in suction temperature, the volumetric efficiency of first-stage, second-stage, third-stage, and fourth-stage reduced by an average of 1.43%, 1.86%, 2.32%, and 2.56%, showing an increasing trend
Jin et al. (2018) [25]	Experiment/ Simulation	• Establish a coupling relationship between injection parameters (mass flow rate and specific enthalpy), the formation process of inter-stage parameters, and the compression process	Refrigeration	• Deviations between the simulated and experimental values of inter-stage parameters- m_{inj}, p_m, and T_m are 10-5%, 5-4%, and 17-5%, respectively • Specific enthalpy changes the direction of change in the state point • Mass flowrate determines the degree of change in the state point
Röyttä et al. (2009) [44]	Simulation	• Optimization of two-stage centrifugal compressor and flash intercooler model with two refrigerants: R-134a and R-245fa	Refrigeration	• Optimum point no optimum for both compressors due to model has shared shaft for both compressors • Modest COP values
Huang et al. (2007) [23]	Simulation	• A numerical study examining flow characteristics on slot and hole injection in a two-stage compressor	Refrigeration	• The recommended configuration is to use the hole-injection with an injection angle of 60° • Large injection angles and higher injection velocities lead to more significant pressure loss but better temperature mixing
Guo et al. (2017) [19]	Experiment/ Simulation	• Explore effects of precooling screw compressor	Refrigeration	• Energy consumption decreases by 0.65% for every 1°C drop in suction temperature

2.1.3 External Cooling

This section contains papers related to achieving isothermal compression through external cooling of the compression chamber. As opposed to more conventional ways of external

cooling, i.e., through multistage cooling, other unorthodox methods such as dripping condensate water on the compression chamber and applying tube-in-tube heat exchangers into the design of a compression chamber are explored. While these methods increase energy savings/efficiency, they are not as promising as other methods mentioned in this section. Table 3 summarizes the findings in this section.

Taghavi et al. (2021) [51] explored a highly novel concept of using the suction line piping to cool down the compressor, resulting in a 4% increase in COP. This minor change to the system would cost virtually nothing, and a significant performance boost would be seen, which could be applied to all refrigeration systems.

Nethaji and Mohideen (2017) [35] wasted no resources and utilized frost drip accumulated at the evaporator to cool the compressor. This experiment's premise is that there will be a substantial condensate in high relative humidity countries. They test an off-the-shelf unit (Electrolux makes frost-free cool type) with 150 watts of cooling, which uses R-134A refrigerant. At an outside dry bulb temperature of 29 °C and relative humidity of 72%, the average shell temperature and current consumption decreased, increasing the COP. While the compressor's efficiency is not reported, a 10.3% increase in COP would increase efficiency. This method's advantage is that an enormous temperature difference is achieved, which will help facilitate heat transfer from existing resources, so not much modification is needed. As seen in Figure 7, there are more hurdles in getting from the outside of the compressor to the winding and mechanism. Yet, substantial heat transfer is achieved thanks to the water droplets below ambient temperature.
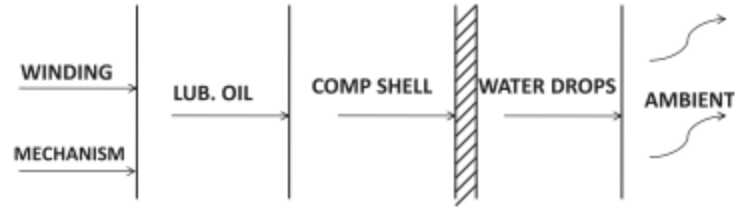
Figure 7: Heat Transfer Modes in Shell Cooling (Nethaji and Mohideen, 2017) [35]

Unlike Nethaji and Mohideen (2017) [35], Yusha et al. (2015) [61] require a considerable amount of more hardware and energy input, which is not desirable. These papers share the same concept: they are cooling the compressor chamber with a colder-than-ambient gas/liquid externally, which is not specified in this paper. Yusha essentially has a tube/in/tube heat exchanger. What is unique about this simulation is that they also take advantage of hydraulic diameter by presenting a slow-speed (0.5 – 2 s), long-stroke (0.2 -2 m) reciprocating compressor design. What is also interesting is that they also use ammonia/propane as their working fluid. Results show that this method is effective when the adiabatic coefficient is high (1.31) but does not influence temperature when it is relatively low (1.13).

Table 3: External Cooling Literature Summary

Author/year	Type	Details	Application	Findings
Nethaji and Mohideen (2017) [35]	Experiment	• Experimentally explore the effect of cooling market compressor (from Electrolux) by externally dripping defrost drip on compressor shell • Working Fluid: R-134a	Refrigeration Systems	• 8-10% energy savings from the method • 10.3% increase in COP • Use of already existing conditions
Yusha et al. (2015) [61]	Simulation	• Computationally assess the effect of externally cooling long-stroke reciprocating compressor while varying heat transfer coefficient and cycle time • Working Fluid: Ammonia/Propane	Natural Refrigerant	• Best effect when the adiabatic coefficient is 1.31 • When the coefficient is 1.13, external cooling does not influence temperature much
Wang et al. (2008) [56]	Simulation	• Reduce the power consumption of compressor two ways: cool motor by external means or make compression process isothermal • Simulate R-22, R-134a, R-410A, and R-744 cycle	Refrigeration Systems	• Cooling motor increases COP by 4% but does not reduce power consumption • Combined isothermal and isentropic compression can reduce power by 16% depending on operating conditions and fluid choice • More beneficial for refrigerants with a smaller molecular mass
Taghavi et al. (2021) [51]	Experiment	• Experimental study of the cooling compressor using suction line • Exergy analysis	Refrigeration Systems	• 12.6% reduction in total reversibility from baseline • 4% increase in COP • Virtually no cost to implement • Money saved from less charge required

2.1.4 Oil-Flooded Compression

Hugenroth et al. (2007) [23] proposed a liquid-flooded Ericsson cooler that uses liquid

flooding of the compressor and expander to approach isothermal compression and expansion. A

thermodynamic model was developed to analyze the idealized Ericsson system. Based on their

model, the input parameters, such as liquid specific heat, gas specific heat, pressure ratio, etc.,

could derive maximized cycle COP from the optimum amount of liquid flooding and pressure

ratio. The results show that the cycle has the highest second law efficiency when the evaporating

temperature is around -85 °C and condensing temperature at 32.2 °C. Such a high-temperature

difference indicates it may apply to the refrigeration industry. The study also mentions that the

practical approach for achieving liquid flooding would be to utilize oil in combination with a

scroll compressor, which could tolerate high oil volumes. Table 4 summarizes the findings in this section.

Bell et al. (2011, 2012a, 2012b, 2013) [4][5][6][7] continue the oil-flooded compression research. First, they analyzed the cycle performance adopting oil-flooding compression and suction line heat exchanger simultaneously by thermodynamic modeling (Bell et al., 2011) [4]. Comparing several working fluids in the parametric study, they found R-404A has the most impact using the technique, especially at a more significant temperature lift. Combining the oil-flooded compression and suction line heat exchanger, the isentropic efficiency could rise by 16.7% above the baseline cycle and further improve to 17.7% above the baseline cycle with a hydraulic expander. After that, they targeted the scroll compressor and scroll expander, developed a predicting model, and validated it through experiments (Bell et al., 2012a, 2012b) [5][6]. In their modeling, they break down the scroll machine model into the following sub-models: A volume calculation, which can calculate the scroll machine chamber as a function of the crank, a mass flow model, a heat transfer coefficient model for the gas-oil mixture, a temperature and pressure differential equation solver, and an overall solver for obtaining the lumped mass temperatures. The modeling prediction takes nitrogen as working gas and alkyl-benzene as refrigerant oil. If pure nitrogen were compressed from an inlet state of 400 kPa and 300 K to an outlet pressure of 1,200 kPa, the discharge temperature would be 480 K without flooding and 348.6 K with flooding. A test rig, following Figure 8 was built to validate and tune the modeling work. The mechanical simulation models show that for the scroll compressor and expander, the mixture mass flow rate and shaft power can be predicted to mean absolute error bands of 4.0% after tuning the model with experimental data. The validated models can also be

used to conduct parametric studies to evaluate the design parameters, such as the flank gap or ambient heat transfer coefficient.
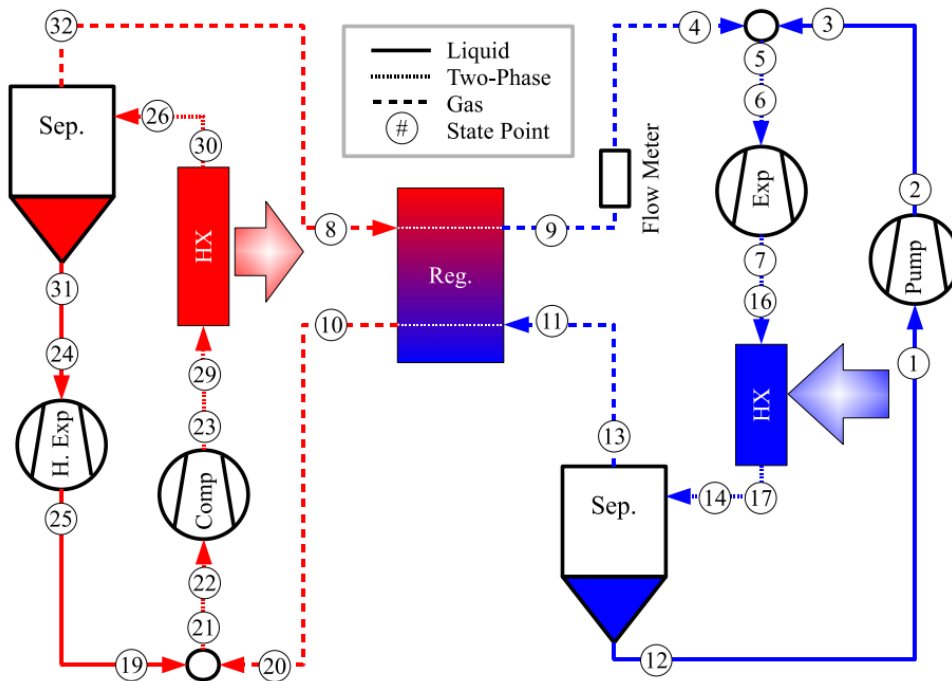
Figure 8: Schematic for Ericsson Cycle Test Rig (Bell et al., 2012b) [6]

Ramaraj et al. (2014, 2016) [45][46] tested an R-410A scroll compressor over a wide range of operating conditions while flooding POE oil into the compression chamber using a hot-gas bypass test stand. As shown in Figure 9, they customized a scroll compressor to inject oil into the chamber to avoid volumetric efficiency reduction and suction gas density increase. They found that oil-flooded compression increases refrigerant mass flow rate and decreases compressor discharge temperature.

Additionally, there is a tradeoff between reduced leakage and friction and increased pressure drops through the suction and discharge pathway. Ramaraj et al. (2016) [46] also evaluated the benefits of oil-flooded compression applied to heat pumps used in low-temperature climate regions. Given the hourly temperature distribution of Boston, Indianapolis, and

15

Minneapolis, the estimated COP could improve by approximately 9%, 10%, and 13% higher than the standard vapor compression cycle.
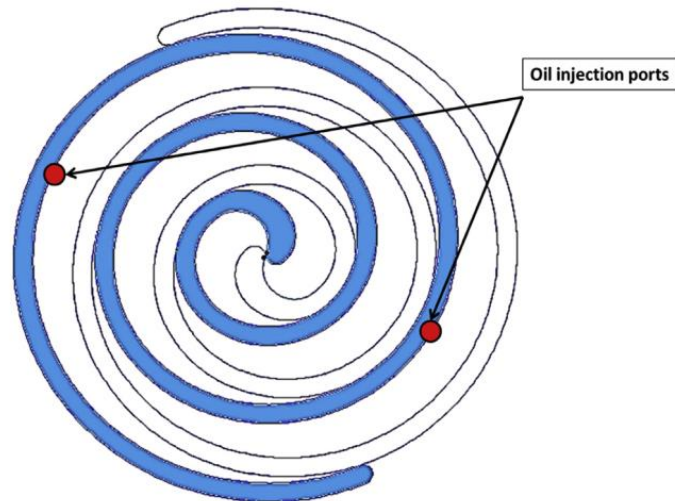
Figure 9: Location of Dual Oil Injection Port in the R-410A Scroll Compressor (Ramaraj et al., 2014) [45]

Luo (2016) [32] investigated the R-32 refrigerant performance and applied the oil-flooded technology theoretically. The isentropic efficiency improved by 3.6-7.3% because of less increased internal superheat from the compressor's suction port to the scroll chamber's actual suction port. The study shows that the heating and cooling capacity degraded, contradicting the previous R-410A experimental results.

Table 4: Oil-Flooded Compression Literature Summary

Author/year	Type	Details	Application	Findings
Hugenroth et al. (2007) [23]	Simulation	• Analytical models of liquid-flooded compression and expansion were developed using ideal gas, constant specific heat, and incompressible liquid assumption. • Parameters: Capacitance rate ratio, pressure ratio, a ratio of specific heat	Heat pump	• The concept uses the compressor and expander liquid flooding to approach the isothermal compression and expansion process. • For ideal components, the COP of the cooler approaches the Carnot COP as liquid flooding is increased. • The cycle has the highest second law efficiency at source temperatures in the range of -85°C and a sink at 32.2°C.
Bell et al. (2011) [4]	Simulation	• Evaluate oil-flooded compressor to achieve a quasi-isothermal compression process and use a regenerator to increase refrigerant subcooling. • Working Fluid: Ammonia, propane, R-134a, R-404A, R-410A, CO_2. Flooded Fluid: Polyalkyl glycol(PAG) oil, Pressure Ratio: 1.7-2.1	Refrigeration	• Efficiency improvement is increased by over 40% for supermarket refrigeration applications. For typical air-conditioning applications, 5% improvements are predicted. • The method has the most significant impact for R-404A and the most negligible impact for ammonia among the working fluid.
Bell et al. (2012a, 2012b) [5][6]	Experiment/ Simulation	• A detailed flooded scroll compressor and scroll expander models have been developed. • Then, the models have been validated and tuned using the experimental database. • Working Fluid: Dry nitrogen. Flooding Fluid: Alkyl-benzene refrigeration oil (Zerol 60)	Refrigeration	• The isentropic efficiency of the oil-flooded scroll compressor was up to 73%, and the volumetric efficiency was above 92%. • The mechanistic simulation models have been validated using experimental data, and the mass flow rate and shaft power can be predicted to be within 4.0%.
Bell et al. (2013) [7]	Experiment	• A residential air conditioning compressor has been modified to inject large quantities of oil into the working chamber. • The compressor was tested with oil injection mass flow fractions of up to 45%. • Working Fluid: R-410A Flooded oil: Polyol-ester (POE)	Refrigeration	• At an evaporating temperature of -10°C and condensing temperature of 30°C, the overall isentropic efficiency was up to 70% at the highest oil injection rate. • As the oil injection increased, the refrigerant mass flow rate and isentropic efficiency increased.
Ramaraj et al. (2014) [45]	Experiment	• An R-410A scroll compressor was tested over a wide range of operating conditions flooding POE oil into the compression chamber using a hot-gas test stand.	Refrigeration	• By fitting the experimental data, the semi-empirical compressor performance map is developed.
Luo (2016) [32]	Simulation	• An R-32 single-stage oil-flooded compressor model is developed to obtain a more accurate system-level improvement. • The heat transfer losses between shell and ambient, suction gas and motor, and high-pressure and low-pressure cylinders are considered.	Air conditioner	• The compressor's overall isentropic efficiency is improved by 3.6-7.3% at optimum oil mass fraction. • The COP in cooling improved 5.8-8.7%, and the COP in heating improved 8.6-16.4%.

2.2 Air Compression/CAES Applications

The topics discussed in this section overview the methods explored to achieve isothermal compression in air compression applications, including water injection, chamber design, which have subtopics in geometry manipulation and "chamber packing," and other miscellaneous methods. Most of these methods require using a liquid piston which has proven to pair well with the use case of applying these methods to air compression.

2.2.1 Water Injection

This section contains literature exploring water injection to achieve isothermal compression. This method encompasses the process by which you inject atomized water particles into the compression chamber to absorb the heat during compression, which can be visualized in Figure 10. There are quite a few papers on this idea. Hence, it is a highly explored topic of interest. Once again, these papers' focus lies in applications for air compression. This means that the piston fluid and working fluid are water and air for these papers. Most have achieved very high efficiencies, upwards of 98%. Water injection is the most promising since a high surface area is achievable, but it has shortcomings. Firstly, something must be done with the injected water after it has been injected, and it may mix with the working fluid, which requires separating the two afterward. This is extra work and equipment that must be accommodated with water injection. Table 5 summarizes the findings in this section.

Figure 10: Representative Model of Spray-Droplets in Liquid Piston (Patil et al., 2020b) [40]

Coney et al. (2002) [14] described a conventional reciprocating piston that uses water injection as the cooling mechanism. While cooling the working gas, water injection has the benefit of acting as its lubricant for the piston. In this case, the challenge is the water droplets' ability to disperse inside the compression chamber during compression uniformly. The process can be tricky because if it is injected too early, the droplets' velocity is slowed by the end of compression, where it would be most needed. Still, if injected too late, the working gas density may hinder the water droplets' ability to penetrate deep into the chamber. CFD simulations show this is the case as cooling is not seen at the chamber's core, so a combination of nozzles and different injection timings is adopted. This is interesting because better results are found in Patil et al. (2020b) [40], but a smaller chamber was used for this experiment. Uniform spray can be achieved with high injection pressure, but larger compressors with higher volume to surface area ratios will be more costly. This becomes even more costly with higher compression ratios because a higher injection pressure will be needed. Bigger water droplets are used, which is not a concern, unlike in Leibowitz and Karamchetty (1984) [30], and the water's atomization would

depend on the droplets colliding with each other. Problems with "hydro locking" are raised but report no issues in this area.

Patil et al. (2020b) [40] did the same experiment, except a liquid piston is used in this case, which opens the novel idea of recycling the water through the water piston. The parameters considered are nozzle angle, stroke time, and spray water injection pressure. Tests were performed with at least ten continuous compression cycles to ensure better reliability in the results. In summary, smaller nozzle angles and slower compression times, while small, better affected the efficiency. Spray pressure had the most significant influence on the isothermal efficiency, with the highest recorded efficiency of 95% at 70 psi spray pressure, which is relatively high. All parameters had diminishing returns on improving efficiency.

Qin and Loth (2014) [43] had a setup similar to Patil et al. (2020b) [40] using water injection and water pistons. The difference here is that this is a simulation and the fact that they explore the effect of pre-mixing the gas and water droplets upstream and direct injection, as seen in Figure 11. Pre-mixing would benefit from injecting the water at a lower pressure and prevents the likelihood of getting non-uniform dispersion. The disadvantage is that more water cannot be injected while the compression process is happening, which hurts the efficiency in this case. Two parameters were explored: droplet diameter and mass loading, virtually the total amount of mass of water used during the compression. Higher mass loadings and smaller droplet diameters lead to higher efficiencies, and overall, the direct injection method achieved higher efficiencies than the pre-mixed method. With this simulation, using direct injection with a mass loading ratio of 5 and a droplet diameter of 20 μm could lead to isentropic efficiencies up to 98% from a baseline of 71%.
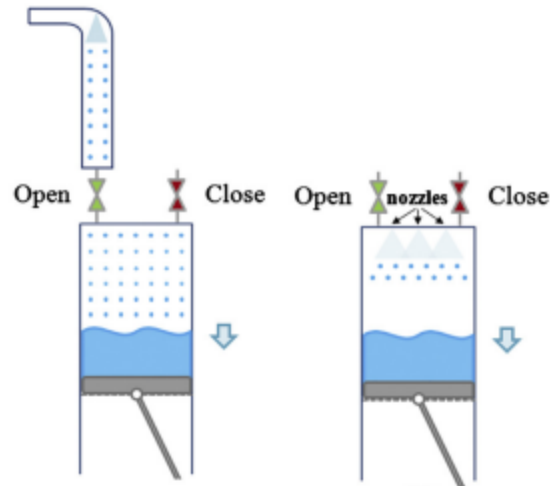
Figure 11: Premixing (left) versus Direct Injection (right) (Qin and Loth, 2014) [43]

Odukomaiya et al. (2016) [36] took the idea of recirculating water one step further by adding a heat exchanger component in line downstream with the spray nozzle. Three configurations were explored, where the base configuration is the adiabatic compression, configuration two is the compression with water injection, and configuration three is the water injection with the heat exchanger component, as seen in Figure 12. Configuration three would theoretically gain a better performance boost with the higher temperature difference, but this would need to be considered with the extra energy input required to do so.
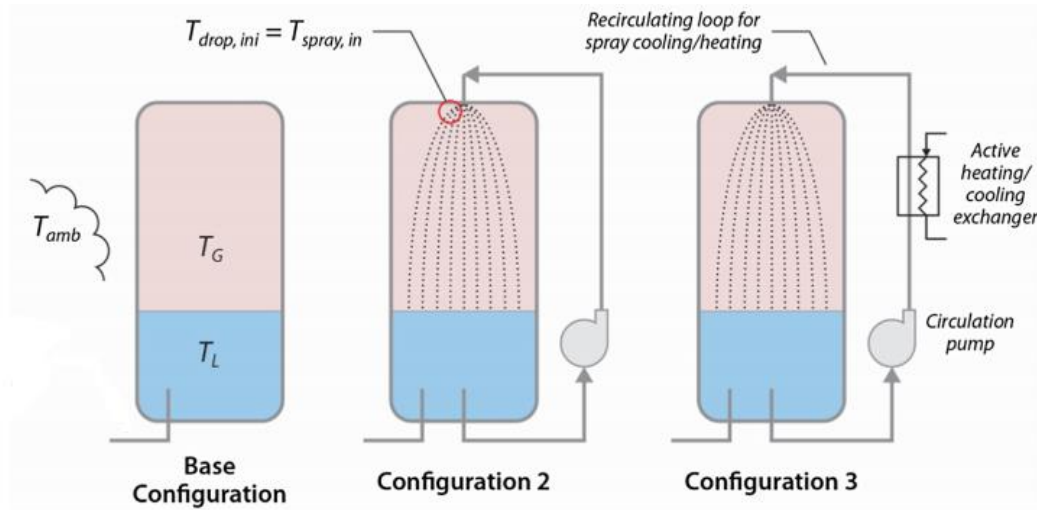
Figure 12: Investigated Configurations (Odukomaiya et al., 2016) [36]

The patent from Leibowitz et al. (1984) [30] used water injection by strategically placing holes in the centrifugal compressor's impeller. It would reduce the impact on the blades, but the droplets of water would still need to be small to minimize damage, especially at the frequencies that a centrifugal compressor would be going at. The water would also need to be extracted in some recovery system before being mixed with gas and ignited.

Table 5: Water Injection Literature Summary

Author/year	Type	Details	Application	Findings
Patil et al. (2020b) [40]	Experiment	• An Experimental study used water spray injection in a liquid piston air compressor. • Parameters: spray pressure 10-70 psi, 60 90 120-degree spray nozzles, different stroke times • Working Fluid: Air, Piston Fluid: Water, Pressure Ratio: 2.5	CAES	• The highest efficiency is seen with 70 psi spray at 95% but with a diminishing increase in spray pressure • The 60-degree nozzle makes the most difference • Spray angle makes a minimal improvement to efficiency (1-4%) • Baseline efficiency 75%
Odukomaiya et al. (2016) [36]	Simulation	• Evaluate transient, analytical, physics-based thermodynamic system model for three designs • Working Fluid: Air, Piston Fluid: Water, Pressure Ratio: 1.6	CAES	• Efficiency improvement is achieved via heat transfer enhancement and the use of waste heat. • Energy storage roundtrip efficiency (RTE) of 82% and an energy density of 3.59 MJ/m3 is shown.
Qin and Loth (2014) [43]	Simulation	• One-dimensional simulation of a sinusoidally driven piston in a 5 kW first-stage cylinder with various compression ratios and both pre-mixed and direct injection scenarios. • Working Fluid: Air, Piston Fluid: Water, Pressure Ratio: 10	CAES	• Compression efficiency 71% adiabatic process to as much as 98% with spray injection at a compression ratio of 10
Guanwei et al. (2018) [18]	Experiment	• Performance test of mechanical piston with water spray for different nozzle sizes • Volumetric compression ratio = 2, 0.1 – 1 mm diameter nozzles, 4 Hz frequency	CAES	• Compression efficiency improvement from 86.1% to 92.4% for 0.3 mm nozzle spray • Temperature reduction from 92.1 C to 32.4 C
Coney et al. (2002) [14]	Experiment/ Simulation	• Compared and benchmarked prototype compressor for CO_2 with an established predecessor compressor and other compressors • Experimental comparison of suction pressure, suction temperature, discharge pressure, discharge temperature, refrigerant mass flow rate, and compressor power consumption was measured • Working Fluid: CO2, Pressure Ratio: 1.6-3	Air compressor for power generation	• Lowered end cycle temperature from 120 °C to 80 °C • CFD analysis shows heat transfer limited by shallow water droplet penetration into the chamber • Volumetric efficiency 67-75%, isentropic efficiency 49-73%, overall isentropic efficiency 38-59% for prototype • Performance: Improved prototype > prototype > predecessor
Leibowitz et al. (1984) [30]	Patent	• Describes patent for isothermal compression of the rotary compressor using water injection • Patent used for Brayton cycle	Rotary compressor applications	• Nozzles strategically placed, so rotor blades are not impacted • 2-10 micron water droplets

2.2.2 Chamber Design

2.2.2.1 Simple Chamber Geometry Manipulation

This section contains literature dedicated to exploring the effects of using liquid pistons in air compressor applications instead of reciprocating pistons and using simple chamber geometry manipulations to enhance heat transfer. Liquid pistons are advantageous because there is no need for oil to use as a lubricant. They are inherently hermetically sealed and provide the flexibility needed to increase heat transfer by increasing the chamber's surface area by geometry manipulation. The tradeoff to this is its low power output, which is not a problem for air compression or CAES applications but will be for refrigeration applications if the user wants sufficient cooling. There may also be issues with working fluid dissolving in the piston with a liquid, further reducing power density and causing maintenance issues. In addition, there may be issues with cavitation as the piston's frequency increases, resulting in more splashing and, therefore, more low-pressure areas for the cavitation to occur (Van de Ven and Li, 2009) [55]. Table 6 summarizes the findings in this section.

Van de Ven and Li (2009) [55] showed improvement in switching from a reciprocating to a liquid piston. There is a design tradeoff between leakage and high sealing friction with reciprocating pistons, but as mentioned above, there are some issues with liquid pistons. Van de Ven and Li (2009) [55] addressed these problems by selecting low-soluble liquids or using a bladder to separate the two interfaces. This simulation shows a 13% uplift in efficiency against the reciprocating piston. The main parameter that was changed was the piston diameter, while the volume remained unchanged to increase the heat transfer area. After iteratively optimizing the diameter to be smaller and smaller, cylinder diameters reach below 0.001 m, which may seem unrealistic to manufacture, as seen in the left of Figure 13. Another result in such a small diameter is that while it improves heat transfer, it also negatively impacts the viscous pressure drop, and viscous forces decrease the Reynolds number, resulting in laminar flow. The graph on

the right of Figure 13 depicts the temperature versus % piston travel of the compressor. Most notably, the temperature begins to drop after a peak rise in temperature around 80% piston travel for the liquid piston. This suggests there is enough temperature difference and heat transfer area to decrease the temperature even at the final stages of the compression cycle.
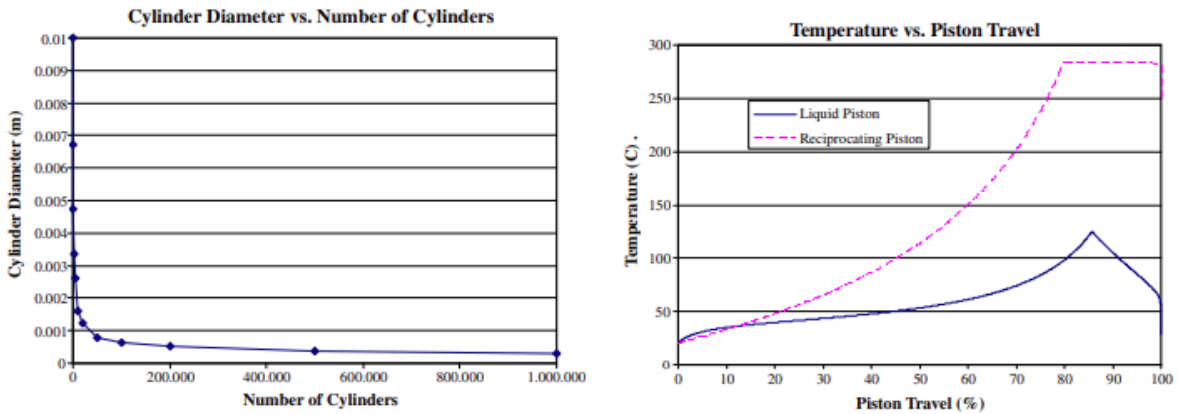
Figure 13: Cylinder Diameter versus Cylinder Iteration (left) Temperature versus Piston Travel (right) (Van de Ven and Li, 2009) [55]

On the other hand, Neu et al. (2020) [33] tested variations of multiple parameters such as chamber diameter, length, piston speed, and initial chamber pressures instead of vast iterations of one parameter. The results are predictable in that they do what they intuitively would do. The decrease in chamber diameter, increased length and decrease in piston speed all help to decrease the overall chamber temperature. Increasing the chamber's initial pressure offsets the temperature profile up while causing a more rapid intensification of convective heat exchanges (Neu et al. 2020) [33]. As seen on the left in Figure 14, all test variations would see a slight increase in temperature during compression, then dip at an inflection point where it would exponentially increase. Neu and Subrenat (2021) [34] also followed up with the study by analyzing the air velocity distribution within the chamber, and its transition to turbulent airflow as the piston compresses the air.
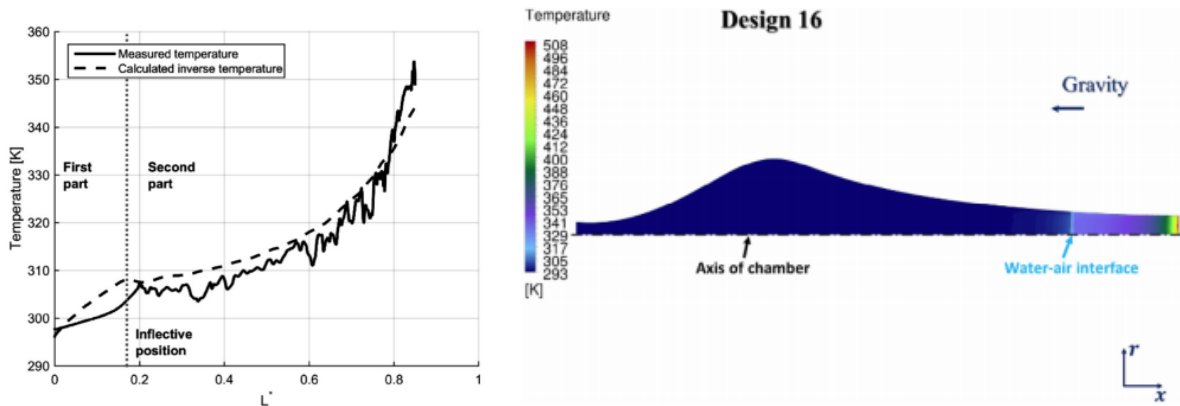
Figure 14: Temperature Function of Piston Length (left) (Neu et al., 2020) [33] Design 16 Temperature Distribution (right) (Zhang et al., 2016) [62]

Zhang et al. (2016) [62] interestingly approached geometric manipulation to take advantage of the liquid pistons' flexibility in that non-cylindrical gourd-like shapes are created to increase heat transfer by encouraging turbulent flow. After iterative design changes, the final design shape goes from an efficiency of 63% from design #6 to 69% for design #16, whose characteristics have a steeper slope and longer chamber length from the original design, as seen on the right of Figure 14. With this design, the flow is more agitated, creating better heat transfer conditions.

Finally, another interesting take on geometry manipulation is a patent from Gerstmann and Friedman (1979) [17]. This patent aims to take advantage of surface area by having multiple columns of chambers together in a manifold-like chamber geometry, which is a compromise between what was shown in Van de Ven and Neu's applications. The heat pump design operates in a thermally regenerated cycle without valves, closely approximating a Stirling cycle. Figure 15 shows the simplified liquid piston schematic.
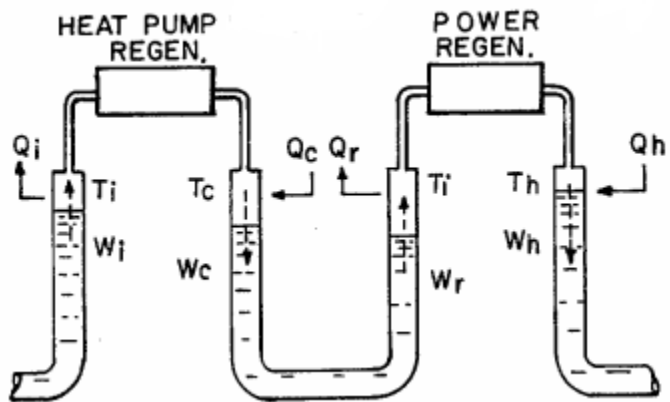
Figure 15: Simplified Liquid Piston Schematic (Gerstmann and Friedman, 1979) [17]

Table 6: Simple Chamber Geometry Manipulation Paper Summary

Author/year	Type	Details	Application	Findings
Neu et al. (2020) [33]	Experiment/ Simulation	• Experimental and numerical evaluation of liquid piston compression using an inverse method • Three chamber diameters, five-chamber lengths, different piston speeds, different initial pressures for a total of 73 test variants • Working Fluid: Air, Piston Fluid: Water, Pressure Ratio: 2.2	CAES	• For (D=100mm, v=0.12m/s, L = 6m) indicates transition into turbulent flow but inconclusive • Lowering hydraulic diameter, lowering piston speed, and increasing chamber length decrease final temp. • Did not consider air movement analysis • Satisfactory agreement from experimental and numerical data
Neu and Subrenat (2021) [34]	Experiment	• Measurement and analysis of flow distribution of air in the chamber with low stroke to bore ratio • Use of 2D particle image velocimetry	CAES	• Initial air velocity speeds are higher than piston speed • Displacement past 24% results in turbulent flow, causing Kelvin Helmlotz instabilities
Van de Ven and Li. (2009) [55]	Simulation	• Analyze liquid piston on efficiency • 1200 rpm cycle • Use a long, small-diameter piston with the same volume as reciprocating piston • Working Fluid: Air, Piston Fluid: Water, Pressure Ratio: 9.5	Air compression	• 19% reduction in energy consumption over the reciprocating piston • 83% efficiency versus 70% efficiency in liquid versus reciprocating, respectively • A slight increase in friction due to viscosity but the overall net gain in efficiency trumps this
Zhang et al. (2016) [62]	Simulation	• Design compression chamber as different gourd-shapes to encourage more agitation in gas, thus attaining better heat transfer • Water/air-liquid piston combination with "open-cell metal foam medium" (10 pores per inch, 93% porosity) • CFD simulation • Working Fluid: Air, Piston Fluid: Water	Air compression	• Best efficiency seen with designs with a high aspect ratio (long length, short diameter) and steep cross-sectional radius change • Design 16 achieves 69% efficiency • Enhanced mixing during compression
Gerstmann and Friedman(1979) [17]	Patent	• A patent describing heat-actuated heat pump with Stirling cycle using liquid pistons • Working Fluid: Air, Piston Fluid: Water	Heat pumps	• It has three liquid pistons with a heat pump regenerator and power regenerator • Liquid columns organized in a heat-exchanger-like fashion • Less moving parts

2.2.2.2 Chamber Packing

This section contains literature whose focus was to increase the compressor's efficiency

by increasing heat transfer through what this paper will call "chamber packing." Doing so is a

passive method of increasing heat transfer cost-effectively. It is concluded in many documents that a significant factor in making isothermal compression feasible is through an increase in heat transfer, which is highly correlated to the heat transfer surface area. In short, packing lots of material inside the compression chamber increases the efficiency of the compressor. Interestingly, the heat transfer medium's material provided little to no difference in the heat transfer rate, as referenced in (Patil et al., 2018; Xu et al., 2011) [37][59]. This means that even with the considerable increase in surface area, it is still a limiting factor in the transfer rate. While these references have applications for air compression, it is hoped that these techniques can be applied to refrigeration applications. Overall, there are significant efficiency improvements by increasing the surface area through wire mesh or other means. Table 7 summarizes the findings in this section.

In addition to the water injection paper mentioned previously, several papers were also written by Patil et al. (2018, 2019, 2020a) [37][39][38]. This is significant because direct comparisons between methods can be established to see which techniques worked the best under similar conditions. The test setup can be seen in Figure 16, where the chamber is submerged in a circulating water bath to eliminate a limiting factor in heat transfer. Their paper on using different chamber materials teaches that while it affects efficiency, there is slight variance. Efficiencies could be seen from 84-86%, where aluminum takes the lead. This surmises that thermal conductivities would not matter until the heat transfer area is significantly increased. It should also be noted that this was one of the few known papers to perform multiple continuous cycles (10 cycles). The water injection still holds the highest recorded efficiency among these experiments at 95%. Still, among the ones in chamber packing, the aqueous foam had the highest efficiency of a 4-8% improvement from the base efficiency of 86%, assuming that this base

efficiency is accurate. Patil's wire mesh experiment falls short but reports a 6-8% efficiency increase from 82-84% base efficiency. It could be argued that since these experiments are a year apart from each other, the base efficiencies could fall within error of each other. This means that regardless of the base efficiency, the percent increase in the wire mesh experiment has an overall higher growth than the aqueous foam experiment. Looking more into Patil's wire mesh experiment, the wire meshes are formed into a distinctive Archimedean spiral to help facilitate heat transfer in the axial and radial directions at a compression ratio of 2.8. Two types of materials are considered: Aluminum and copper. Two types of mesh densities; 8 and 16 wires/inch. Peak air temperature was reduced by 26-33 K, which translates to a 6-8% lift in compressor efficiency. The polycarbonate compression chamber dimensions are 88 mm diameter by 170 mm height. Similar temperature profiles in Aluminum and copper suggest thermal conductivity is not a limiting factor. Compression times vary from 3 to 6 seconds, concluding that longer compression times are favorable. The less-dense wire mesh also did better than the denser mesh, which suggests that there must also be a balance between surface area and thermal capacity. But this is not the case for porous inserts, as will be seen for Yan et al. (2015) [60].
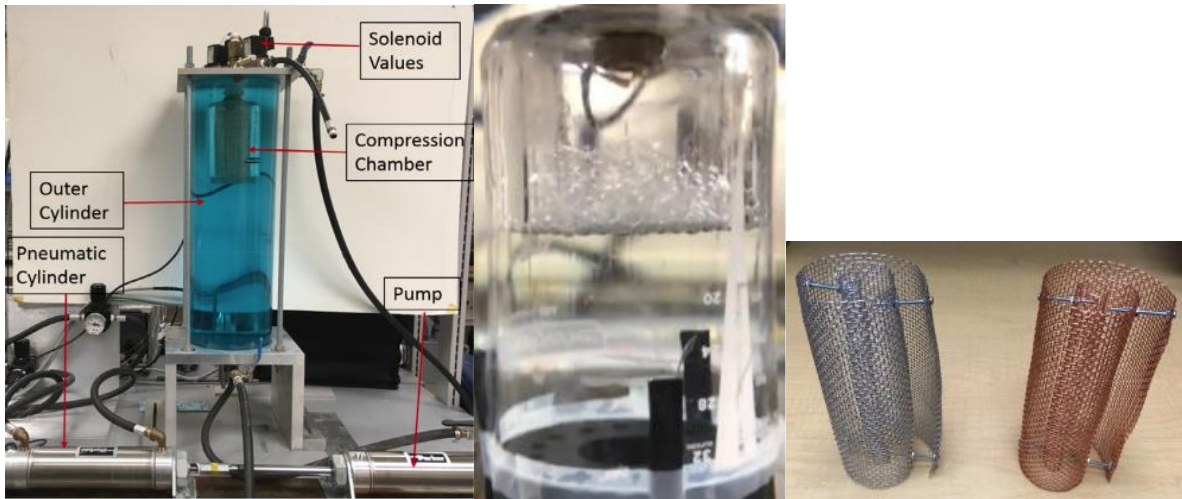
Figure 16: (left) Experimental Setup of Liquid Piston Compressor (Patil et al., 2020a) [38] (middle) Aqueous Foam Compression (Patil et al., 2018) [37] (right) Aluminum and Copper Metal Wire Mesh Spirals (Patil et al., 2020a) [38]

Yan et al. (2015) [60] performed an experimental study of chamber packing using what the author calls porous inserts, improving Patil's wire mesh idea. Several configurations are considered to vary in material and porosity. The polycarbonate compression chamber is 353 mm long and 50.8 mm in diameter. The plastics have interrupted plates (seen in Figure 17), which disrupt and restart the boundary layers, so heat transfer is enhanced and open structures to allow for low liquid drag. Essentially, they have vertical walls with spacing every discrete distance or so in a grid-like fashion. Yan plays with a range of compression times from 2 to 23 seconds and finds a better heat transfer seen at longer compression times. The author also concludes that interruption of the boundary layer also helps significantly in attaining better heat transfer. Another explanation is the small hydraulic diameters in porous media also induce higher local velocities. An optimized profile typically consists of segments of high flows at the beginning and end of the process and a slow (nearly isothermal) portion in the middle, which agrees with the Pareto optimization of Saadat et al. (2012) [48]. The thermal conductivity of the aluminum foam

(167 W/m K) is 1,000 times higher than that of the ABS plastic interrupted plates (0.19 W/m K). Results in this paper suggest that at the relatively low-pressure ratios of 6–10, these differences in conductivities and capacitances do not have significant effects. This analysis shows that because the thermal capacitance is sufficiently large compared to the thermal energy and the heat transfer coefficients in these low-pressure ratio experiments, the effect of thermal conductivities is, once again, insignificant.
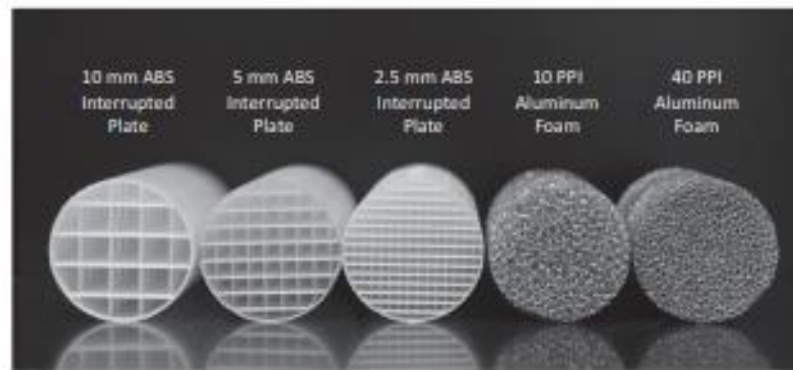
Figure 17: Types of Porous Inserts Used (Yan et al., 2015) [60]

Saadat et al. (2012) [48] expanded on the works of Van de Ven and Li (2009) [55] and put a little twist on it by taking all the tiny diameter tubes and putting them together in a bigger tube that encompasses them all. This would increase the heat transfer area inside the compression chamber but limit the heat transfer area on the outside. Simulations show a 10-40% increase in power density at 90% efficiency. Pareto optimizations also show that 91.45% can be achieved if the compression speed is varied for a cycle, i.e., having an initial fast compression followed by a long, relatively slow compression, then a final rapid compression to get to the final desired pressure.

Table 7: Chamber Packing Literature Summary

Author/year	Type	Details	Application	Findings
Patil et al. (2019) [39]	Experiment/ Simulation	• Experimental study of Liquid piston Air/water with different chamber materials and stroke times • Polycarbonate, PET, Aluminum, Copper • Working Fluid: Air, Piston Fluid: Water, Compression Ratio: 2.05-2.35	Air compression	• Compression efficiency of 84-86% • Overall, the heat transfer coefficient reaches a steady value towards the end of compression. • The convective thermal resistance of air contributes to the total resistance. • High thermal conductivity of chamber material helps with heat transfer at the initial phase of compression, but potential limit reach during the latter phase of compression
Patil et al. (2020a) [38]	Experiment	• Experimental study of Liquid piston Air/water with aluminum/copper wire mesh of varying diameters along with changing compression times • Working Fluid: Air, Piston Fluid: Water, Pressure Ratio: 101 – 280 kPa	Air compression	• Compression efficiency improved from 83-84% to 88-90% • Smaller wire diameter beneficial
Patil et al. (2018) [37]	Experiment	• Achieve isothermal compression of air using aqueous foam in compression chamber through experimentation • Tested for one stroke, which takes 4.2-4.4 sec • The aqueous foam generated by surfactant, i.e., DAWN ULTRA • Varied airflow speed for foam generation and % foam volume • Working Fluid: Air, Piston Fluid: Water, Compression Ratio: 2.5	Air compression	• 4-8% improvement in compressor efficiency • Provides higher heat transfer area as well as higher heat transfer coefficient
Yan et al. (2015) [60]	Experiment	• Experimentally determine the effects of different porous materials on heat transfer and efficiency • Use five unique inserts: three interrupted ABS inserts with plate spacing 2.5,5, and 10mm and two aluminum foam inserts sized 10 and 40 pores per inch • Working Fluid: Air, Piston Fluid: Water, Pressure Ratio: 10	CAES	• Increase in power density by 39 fold at 95% efficiency • The material type did not seem to matter when looking at heat transfer effectiveness • Provide better gas mixture during compression
Saadat et al. (2012) [48]	Simulation	• Pareto optimal compression profile for a liquid piston air compressor that maximizes given parameters • Working Fluid: Air, Piston Fluid: Water, Pressure Ratio: 10	CAES	• Optimized piston speed profile to compress faster in the beginning and ramp down toward the end • 10-40% increase in power density at 90% efficiency • The more general numerical approach

2.2.3 Other Methods

This section contains literature related to uncommon, unique methods of an isothermal

compression. While they can achieve very high efficiencies, they are grossly unexplored on

performance metrics due to patent protections or simply because of the niche applicability of the method. Table 8 summarizes the findings in this section.

Weiqing et al. (2020) [57] and Ren et al. (2020) [47] proposed similar ideas to use a mechanical piston in conjunction with a porous medium attached to the mechanical piston, which would be dipped into a circulating water reservoir as seen in Figure 18. This idea combines methods that have been discussed thus far, such as chamber packing, with the addition of other unique applications such as the mechanical piston and water reservoir. This specific design would have the advantage of achieving high compression speeds, increasing its capacity, and providing a more stable mass flow. Although, this will be limited by how well the heat transfer is between the air and the environment.
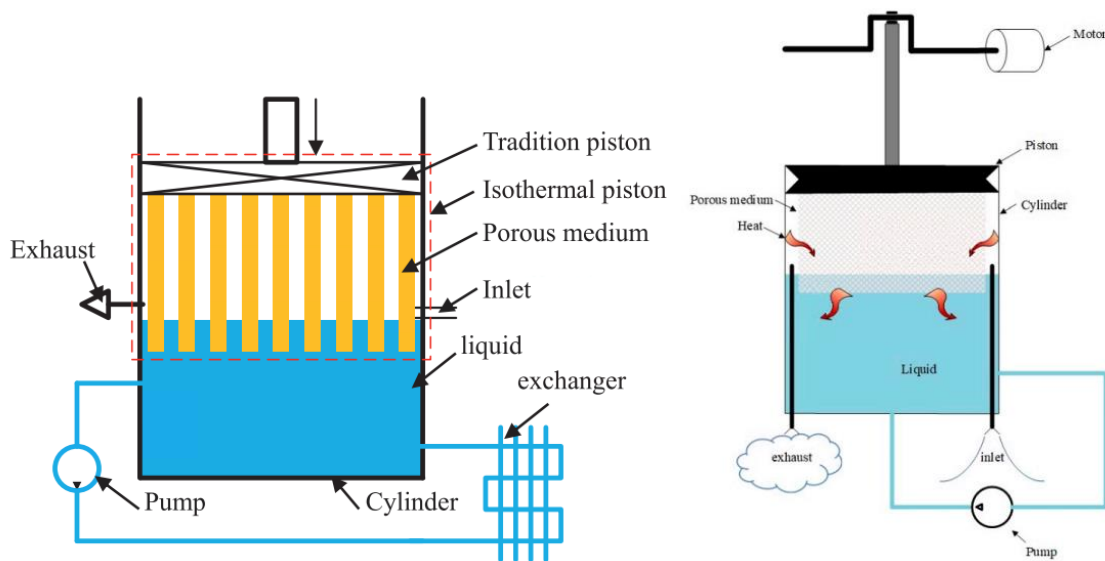
Figure 18: Weiqing Compressor Design (left, 2020) [57] Ren Compressor Design (right, 2020) [47]

Another unique method in enhancing heat transfer is called a "dry finned" piston, which is the opposite of a liquid piston in that it uses a solid physical piston, hence "dry." Heidari et al. (2014) [21] analyzed a patent submitted by Benson (1984) [3], as seen on the left of Figure 19.

Heidari et al. (2014) [21] showed analysis from the "pneumatic-electric" analogy perspective. What differentiates a dry finned piston and a dry piston is that the piston and the chamber have fins attached to them to increase the surface area. They are offset from each other, so they do not interfere when compressing the working gas. The main advantage of using such a piston is that its surface area remains constant while the compression process is happening, unlike liquid piston, whose heat transfer area is decreased as the piston compresses the working fluid more and more. This is especially advantageous since a large part of the gas's temperature increase happens towards the latter half of the compression cycle (Heidari et al., 2014) [21]. Of course, this opens it back to several of the disadvantages mentioned considering reciprocating pistons. Their analysis shows an improvement of 88% efficiency instead of a 78% efficiency for an adiabatic process.
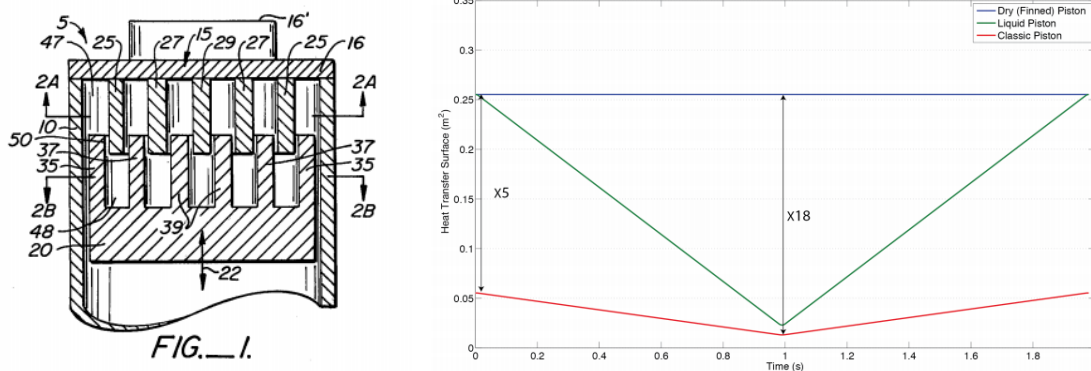
Figure 19: US patent by Benson (left, 1984) [3] and Heat Transfer Area for Liquid, Dry and Classic Piston (right, Heidari et al., 2014) [21]

Payne and Weinbrecht (2002) [41] described a compressor that compresses the working gas at a constant volume called the "reflux gas densifier" (Figure 20). Gas is taken in at the suction line, where the turning gears will create a pressure differential and pack more gas mass to the right, thus compressing the gas. The reflux conduits would recycle the compressed gas that

would be cooled at this point and mixed in with the fresh incoming gas in a closed-loop essentially. Though the current design does not have a means for heat removal during the process, one could be added right at the cavity after the turning gears. Calculations show a reduction in temperature from 300 to 22 °C at a pressure ratio of 10 on the theoretical curve compared to typical volumetric compression. Additionally, Langston and Faghri (1995) [26] described the use of heat pipes to extract the heat out of a turbine vane. Heat pipes are extremely good at moving heat because they take advantage of the heat of vaporization.
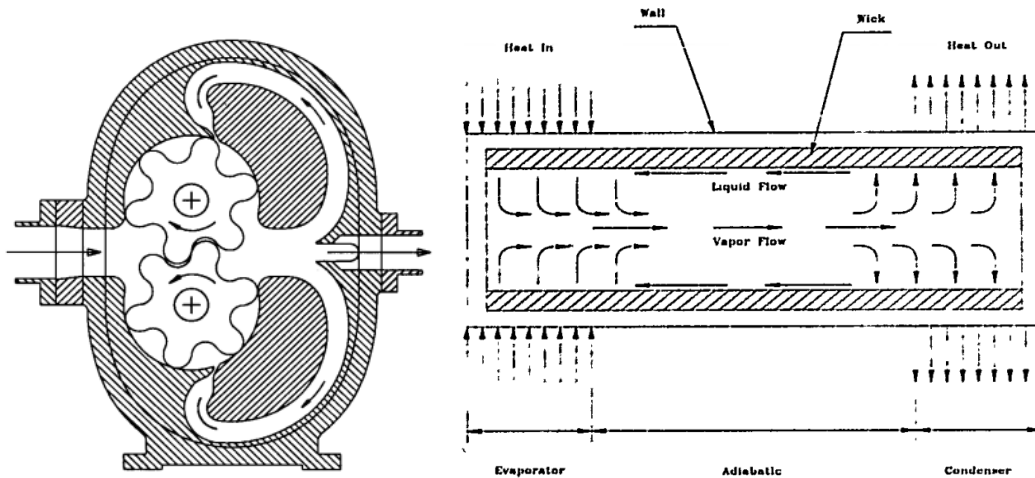
Figure 20: (left) Reflux Gas Densifier (Payne and Weinbrecht, 2002) [41] (right) Heat Pipe Flow Diagram (Langston and Faghri, 1995) [26]

Finally, an innovative method for isothermal compression, which was inspired by a trompe, was a patented device by a company called Carnot compression. They have two patents (Cherry et al., 2015, 2017) [11][12] concerning the device and from what can be gathered, the device, which is used for air compression, essentially is what can be described as the opposite of water injection. Air is extracted from the top, which creates an emulsion of air and water by bubbling air into the water with microchannel capillary tubes. A vortex is created from the water in the drum. As the bubbles are sent radially outward (the opposite from what is happening in the

left Figure 21), they get compressed from the centrifugal force, where it is somehow separated once it has reached the edge of the drum. Water is circulated to keep the process isothermal, which is advantageous because, in this design, there is essentially a large, constant-temperature reservoir. The company states that the only moving parts are the drum and radiator fan. This is a rough explanation of what is happening.
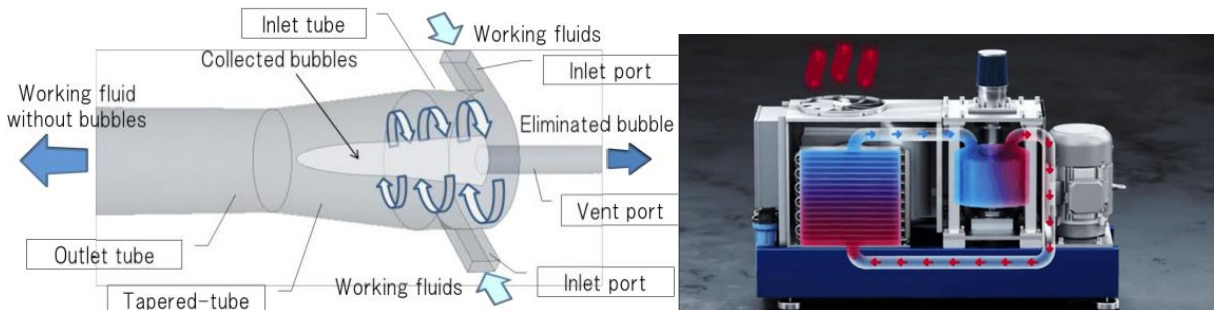
Figure 21: Hydraulic Bubbling (left, Sakama et al., 2012) [49] and Carnot Compression Concept (right, Carnot compression, 2021) [9]

Table 8: Other Methods Literature Summary

Author/year	Type	Details	Application	Findings
Heidari et al. (2014) [21]	Simulation	• Discuss and Analyze ways to achieve isothermal compression • Analyze dry "finned" piston design • Working Fluid: Air, Pressure Ratio: 100-580 kPa	CAES	• Identified heat transfer from gas to compressor chamber walls limiting factor • 88.4% efficiency compared to 78% for conventional piston • 0.25 m² surface area versus 0.05 m²
Heidari and Rufer (2014) [22]	Simulation	• Fluid flow analysis of finned piston using "pneumatic-Electric" analogy lumped method • Working Fluid: Air, Pressure Ratio: 100-580 kPa	CAES	• Concludes very effective in approaching isothermal compression thanks to the increase in heat transfer • The method proved to be an easier way of modeling • system of a complex finned piston
Benson (1984) [3]	Patent	• Patent explaining "dry finned" piston-type design and possible modifications to improve heat transfer • Used for heat engines	Solid piston reciprocating compressor applications	• Experimental performance of prototype shown in graph (non-flow thermizer performance) • Suggested modification to the heat sink by flow fluid through hollow fins • Limited against long-stroke or high-density applications
Payne and Weinbrecht (2002) [41]	Simulation	• Redesign of Gas Densifier • Shows iterative design process and some calculations on theoretical and actual performance • Working Fluid: Air, Pressure Ratio: 10	Natural gas vehicle fuel	• Calculation show a reduction in temperature from 300 to 22 °C at a pressure ratio of 10 on the theoretical curve compared to volumetric compression • Simple and rugged design • There are no valves and no contacting or rubbing parts. • High volumetric input
Langston and Faghri (1995) [26]	Experiment/ Simulation	• Present design ideas for implementing heat pipes to gas turbines • Discuss advantages and disadvantages of heat pipes versus conventional methods • Discuss testing methodology for experimental and simulated testing	Gas Turbine	• Heat pipe vane cooling offers isothermal cooling and prevents heat stress on the turbine • Increase in weight of the turbine • Extracted heat may take away from the cycle
Weiqing et al. (2020) [57]	Simulation	• Simulate the performance of compressor design: combines porous medium, mechanical piston, and liquid cooling	CAES	• Ka, the ratio of heat transferred from the air to heat generated from air, over 80 reduces the temperature of air by 80% • Compression efficiency diminishes with greater compression ratios • 28% increase in compressor efficiency at a compression ratio of 7
Ren et al. (2020) [47]	Experiment/ Simulation	• Simulate and experimentally validate isothermal compressor with mechanical piston and porous medium • Pressure Ratio: 4,100 rpm	CAES	• Reduced energy consumption by 45% • Air temperature lowered from 517 K to 342 K • Frictional forces negligible (0.21% of compression work)

2.3 Literature Review Summary

Isothermal compression is a very promising process that could drastically improve the efficiency of the compressor. Due to this, methods have been explored to apply this process to existing conventional compressors such as scroll compressors in refrigeration applications. At the same time, isothermal compression has been applied in more unconventional ways, such as with liquid pistons in air compression applications. To gather bearings on the progress of isothermal compression to discuss the benefits, limitations, and challenges of these methods, 47 papers/patents were reviewed and summarized.

These are the main takeaways from what could be extracted from the papers: A bulk of the ideas try to explore modifying the compression chamber in some fashion, particularly trying to increase the chamber's surface area. This suggests that surface area is an essential limiting factor in achieving isothermal compression.

This is mainly done by stuffing in material with a high surface area into the chamber to increase heat transfer inside the chamber uniformly. Other significant methods use water injection, which is analogous to refrigerant injection. Still, other niche methods include changing the chamber geometry to encourage mixing or even using programming to reach optimal compression speeds. More conventional ways have been to either do inter-stage cooling or refrigerant injection. Still, these methods take a more active part in cooling the working gas and usually have high initial and maintenance costs. Ideally, techniques such as stuffing material in the compression chamber with a more passive effect would be desirable, minimizing cost. Out of these methods, water injection seems to attain the highest efficiency in both simulation and experimentation.

In addition, chamber manipulation seems to do reasonably well. However, chamber manipulation may be more favorable as they still have high efficiencies while benefiting from being simple to apply. Other notable mentions are discussed in the following:

The dry "finned" piston is also a promising idea since its design can achieve a constant amount of high surface area throughout the compression process. Still, it presents issues with what typical reciprocating compressors will have. Tackling the challenge of isothermal compression can be looked at in four aspects: heat transfer coefficient, surface area, temperature difference, and time. Saadat et al. (2012) [48] discussed the idea of variable speed compression to achieve higher compression efficiencies discovered in their Pareto optimization. Having the concept of using programming to change the compressor's speed dynamically would be beneficial because temperature increase tends to spike at the latter half of the compression cycle. This would lower the compression time needed in one cycle and provide better overall heat transfer. There is also a need for long-term tests to ascertain each method's benefits fully. Many single-cycle tests are quick ways of getting data. Still, the reported efficiencies should be taken with a grain of salt as unforeseen long-term effects could impact the compressor's performance.

With all these aspects explored, it can be concluded that many studies that had applications for air compression can be applied to refrigeration. With all the possible methods explained to increase heat transfer, achieving near isothermal compression is feasible, while there may be challenges in achieving the desired power density. In addition, there seems to be a lack of experimental validation concerning isothermal compression. Many papers described ideas to increase heat transfer through simulations. It may be beneficial to explore experimental studies of isothermal compression, mainly applied to refrigeration applications.

3 Novel Approach

To take what has been learned in the literature review and apply it, the system that will be designed will take advantage of the CO_2 transcritical cycle and use a liquid piston. The transcritical cycle stands to benefit more from isothermal compression due to nature of transitioning to the supercritical state. Figure 22 compares conventional gas compression and desuperheating processes to achieve an isothermal compression in a transcritical cycle and a subcritical cycle. For the transcritical cycle, compressing from state A (1,000 kPa, 40 °C) to state B (10,000 kPa, 239 °C) and then removing the heat to get to state C (10,000 kPa, 40 °C) results in a huge amount of enthalpy that will need to be extracted to maintain isothermal conditions. This is due to not only the high compression ratios but also the fact that is enthalpy change is drastically changed past the critical point. Larger compressions will also result in larger temperature increase which, in turn, will make the heat transfer easier because of larger temperature differences. This will also result in larger improvement over the isentropic compression due to higher temperatures requiring more work to compress the gas. Compare this with a typical sub-critical cycle for R-410A and compressing from state A (1,000 kPa, 35 °C) to state B (2,138 kPa, 74.6 °C) and then removing the heat to get to state C (2,138 kPa, 35 °C) results in a more modest amount of required enthalpy to maintain isothermal compression. Cooling would have to stop at the edge of the vapor dome because wet compression is not ideal. Not much improvement can be gained from isothermally compressing the refrigerant. A liquid piston is used to compress the CO_2 which will be advantageous since it will be able to conform to almost any geometry in the designed chamber. This will be important since manipulating the geometry of the chamber will be needed to enhance the surface to facilitate heat transfer for isothermal compression.
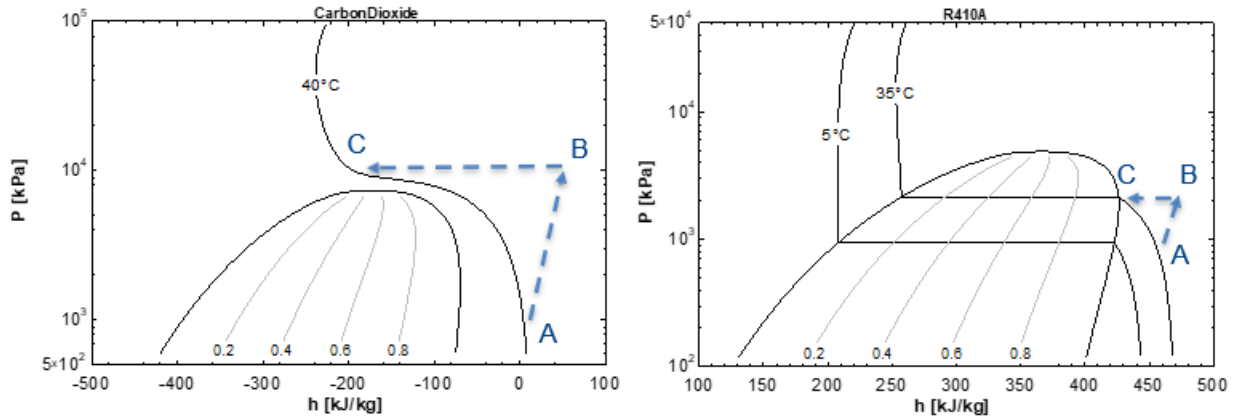
Figure 22: Enthalpy Difference Comparison Between CO$_2$ (left) and R-410A (right)

Shown in Figure 23, the chamber geometry will be designed as a one bank, single pass, bare tube heat exchanger which has been named the "compressor within heat exchanger" or "integrated gas cooler chamber" or heat exchanger compression chamber (HXCC). The compressor will work by driving the pump which will flow the liquid piston up through the bottom header, forcing the gas into a smaller and smaller space, effectively compressing it. As it is compressed and heats up due to the heat of compression, the chamber will act as a heat exchanger where a fan will blow air over the tubes to cool the gas. The geometry of the chamber should be designed so that the increase in surface area will allow sufficient heat transfer to keep the gas at isothermal conditions. Essentially, the job of the compressor and condenser are combined in one simultaneous process. This design is protected under the University of Maryland Invention Disclosure under PS-2018-077 [42].
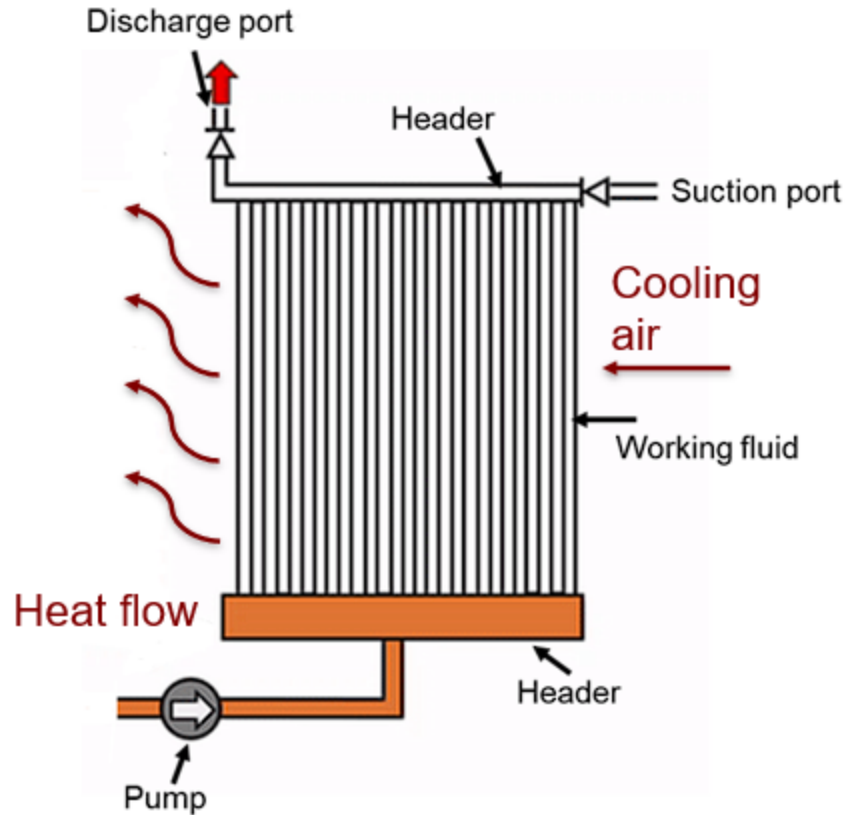
Figure 23: Integrated Gas Cooler Concept Design [42]

4 Objectives

The objectives of this research are focused on two major fronts: energy savings and isothermal capability. Objective goals include the following:

- Building fully working system
    - Design and build proof-of-concept test facility
    - Design and build prototype HXCC
    - Develop reliable level sensor for specific application
- Generate enough mass flow for 1.75 kW system
- Compress CO_2 above critical point up to 10 MPa
- Save up to 40% in energy savings compared to conventional compressors

- Compress as isothermally as possible

- Evaluate performance

    o Power draw

    o Mass flow

    o Compression temperature

    o Isothermal efficiency

- Develop improved prototype based on 1st prototype design

5 Cycle Modeling

A simple Engineering Equation Solver (EES) model was constructed to simulate the isothermal compression process of CO_2. The isothermal compression process was estimated as a quasi-equilibrium process with 100 discretized processes that is comprised of isentropic compression (process A-B) and isobaric cooling (process B-C). An exaggerated visualization of this process can be seen from Figure 24 below with the plotted P-h diagram. The red dots along the 40 °C isothermal line represent the 100 discretized processes. These discretized processes are done until state D is reached, at which point a condenser could be used to further cool down the working fluid and extract more cooling capacity of the system (process D-E). From process E-F, the working fluid would then expand down to the desired evaporating temperature and then heated up to state G where it will be superheated. Additional heating will be necessary to get back to state A which may be done with a suction line heat exchanger, exchanging heat between processes D-E and G-A.
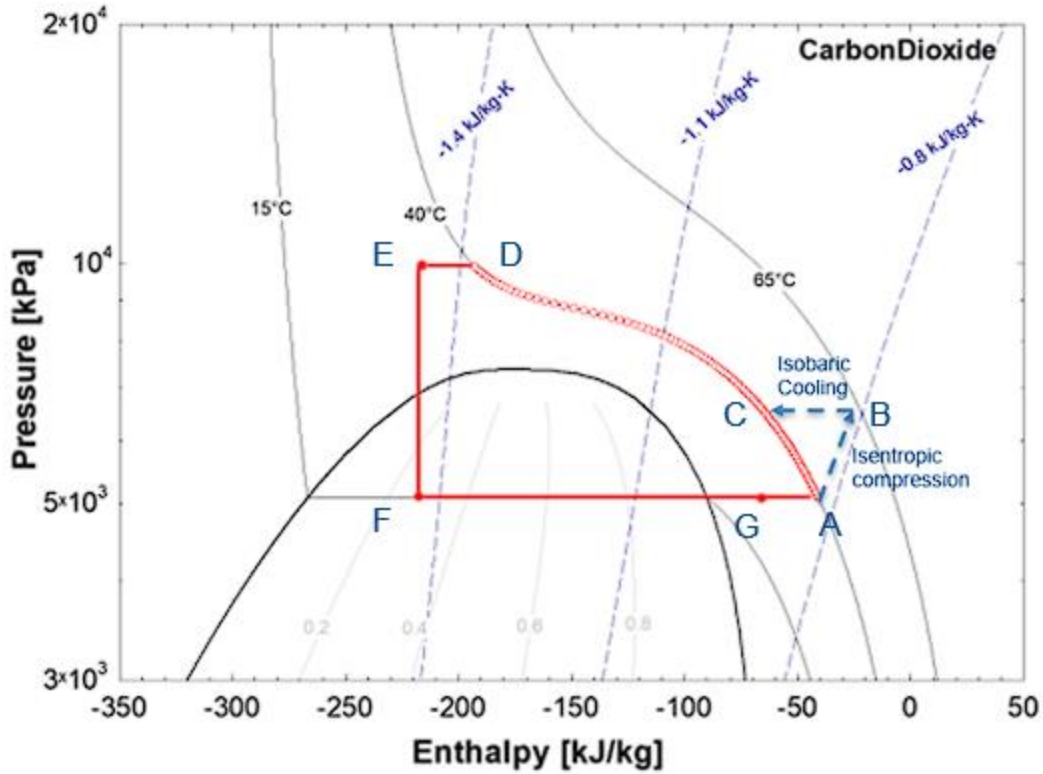
Figure 24: Transcritical CO₂ Cycle in EES Modeled

From each discretized process, all the isentropic compression work can be summed to obtain the total work for the isothermal compression process. Comparing this number with a conventional compressor with a typical isentropic compression efficiency, it is estimated that up to 40% in energy savings can be realized. This method of calculating the real isothermal work also matches with the method using the ideal gas law with the z compressibility factor, which would be done similarly by integrating the work using the real isothermal work equation for small pressure steps with changing z factors.

$$w_{iso} = Z \frac{RT}{M} ln \left(\frac{P_{final}}{P_{initial}} \right) \qquad (1)$$

Where Z is the compressibility factor, R is the ideal gas constant, T is the temperature at which the gas is being compressed at, M is the molar mass of the gas, $P_{initial}$ is the initial gas pressure and P_{final} is the final gas pressure. Calculating the isothermal work this way will be useful in future simulation prediction for near-isothermal compression experimental validations.

For the most accurate way to calculate the isothermal work, finding the difference of the enthalpy and entropy can also be used as shown in the equation below.

$$w_{iso} = \left[h\left(T, P_{final}\right) - h(T, P_{initial}) \right] - T\left[s\left(T, P_{final}\right) - s(T, P_{initial}) \right] \qquad (2)$$

Where h and s are the enthalpy and entropy and a function of the isothermal temperature T and pressure.

6 Experimental Setup

The following details the overview of the test facility, the major components of the test facility and prototype isothermal compressor, the types of sensors used which is accompanied by an uncertainty analysis and finally, the test conditions that were ran and how they were run.

6.1 Test Facility

A customized test facility was designed and built to test the isothermal compressor. Figure 25 details the layout of the test facility. The blue loop represents where the liquid piston exclusively resides and the red loop represents where the refrigerant resides, while the gray area represents the compression chamber and will have the liquid piston or the refrigerant at any given time. Additionally, the blue and gray areas are the isothermal compressor itself, while the red area is essentially the calorimeter.
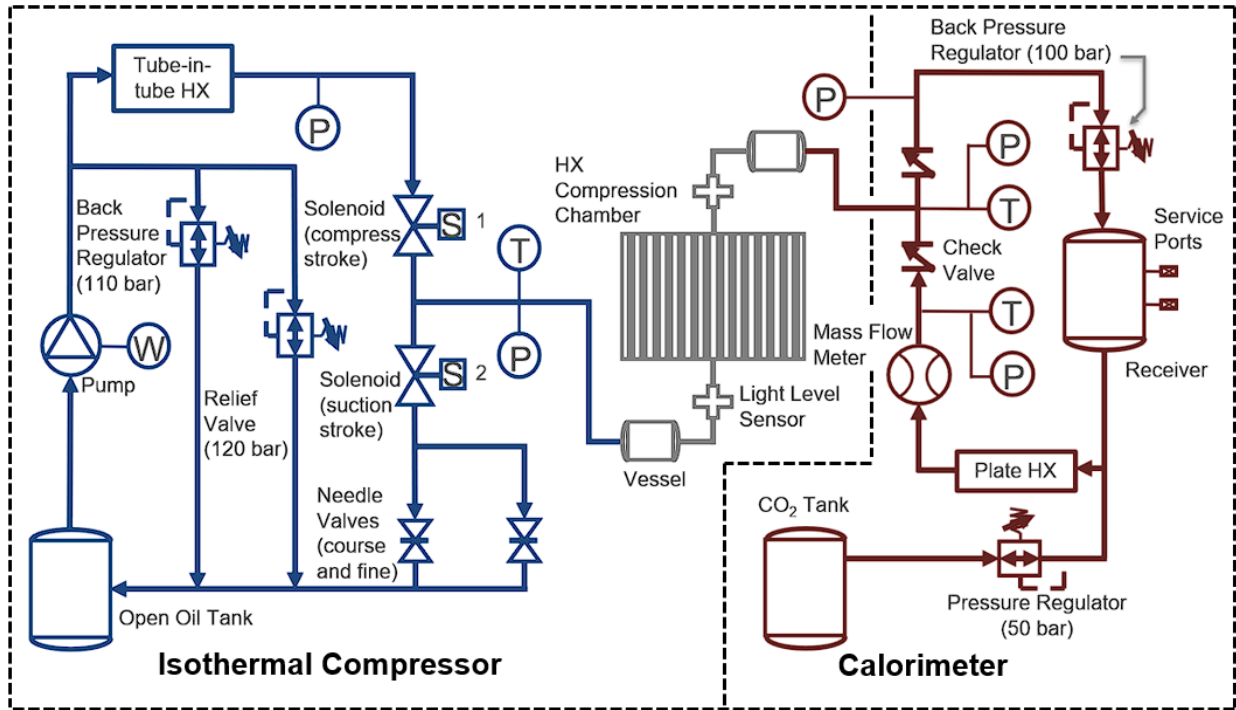
Figure 25: 1st Prototype Test Facility Diagram

An explanation of how the compressor works is detailed here. The compressor will have two phases: compression phase and decompression phase. During the compression phase, the pump pressurizes and brings the liquid up into the HXCC where it will compress the working fluid. At this point solenoid one is open, while solenoid two is closed. Once the working fluid has compressed and reached the desired pressure, the back pressure regulator will begin to allow the working fluid to flow through, passing through a check valve to ensure no backflow. The working fluid loops around to the inlet of the outlet pressure regulator as it expands and cools.

During the decompression phase, solenoid one closes, allowing for pressure to build up again from the pump for the next cycle as it will simply bypass through the back pressure regulator on the liquid piston side and recirculate. Solenoid two opens to allow the liquid piston to drain and decompress. A needle valve is put in place to control the speed of the decompression

and it is flowed back into the oil tank. The vacuum that is created will allow the working fluid to

flow back into the chamber from the suction side. This process is repeated to circulate the

refrigerant and create a cooling effect. Figure 26 below shows a front and back picture of the

built system.
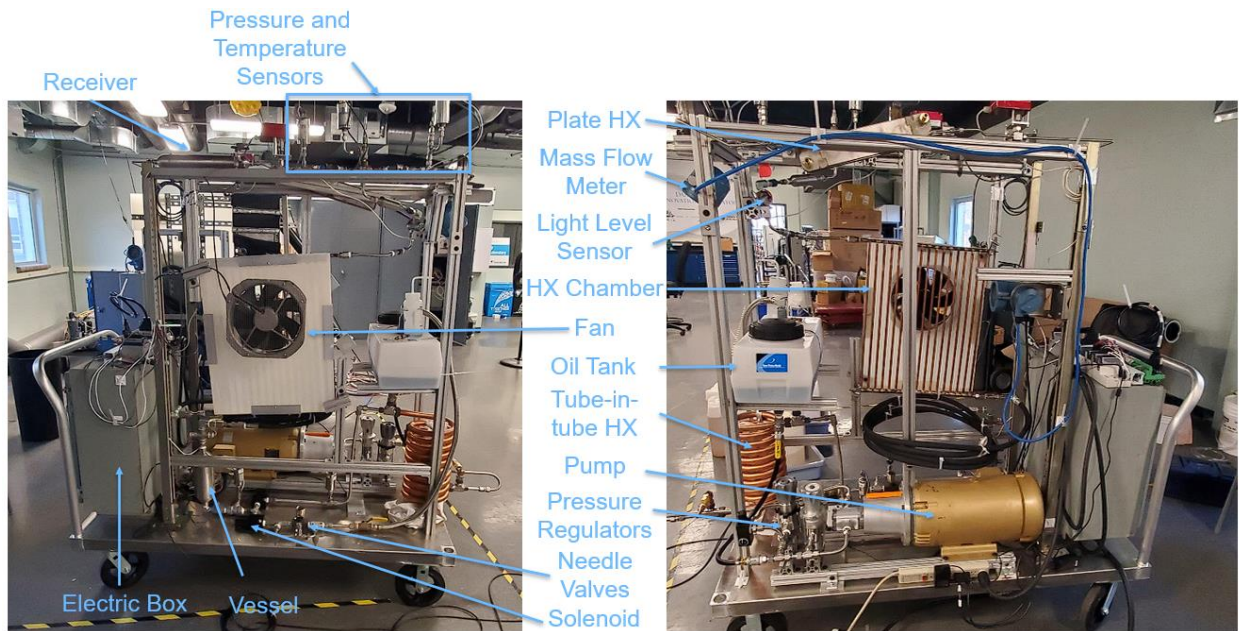
Figure 26: Picture of Front (left) and Back (right) of Built Test Facility

1.1.1 Pump

The pump that is used as a liquid piston in this prototype is an honor external gear pump

(manufacturer number 2GG1U09R) shown in Figure 27 with the following specifications:

Table 9: Gear Pump Specifications

In^3 per rev.	GPM @ 1750 RPM	Cont. PSI	Max PSI	RPM Range
0.58	4.39	3,500	4,200	600-4,000

Figure 27: Honor External Gear Pump

Gear pumps are beneficial in that they are cheap and can pump at consistent flow rates with high varying pressures. With these qualities, gear pumps become an excellent choice for liquid pistons. This pump is paired with a Baldor general-purpose, three-phase electric motor (part number EJMM3714T) which is rated at 10 hp and runs at 1,770 RPM maximum.

6.1.2 Liquid Piston

The liquid piston medium itself was chosen to be mineral oil. This conclusion was made from the following requirements:

- Viscosity: it is important to consider a liquid that has a medium viscosity. A low viscosity is beneficial since less power will be required to pump the liquid to compress the gas. Additionally, a low viscosity fluid will not stick to the sides of the integrated HXCC and impede heat transfer. It is also important when considering the integrated heat exchanger design and pressure drop as well. At the same time, a higher viscosity fluid will be

required to ensure the pump will be able to efficiently pump the liquid. Too low of a

viscosity will cause slippage.

- CO_2 solubility: a low solubility with CO_2 is the goal. Additional challenges comes with

  pumping a liquid with high solubility because of their potential to damage the pump.

  There are also possible challenges with bubbling occurring during the decompression

  process with its effect being worse with higher viscosity fluids.

- Non-toxic/non-corrosive: having a non-toxic and non-corrosive liquid will be beneficial

  for the environment and the systems longevity.

- Thermal conductivity: when using any type of oil, it is unavoidable that the oil will stick

  to the sides of the chamber while operating. Having an oil with a higher thermal

  conductivity will be beneficial in preventing thermal resistance from the refrigerant to the

  outside.

The mineral oil has the following physical properties:

Table 10: Mineral Oil Properties

Flash Point	Specific Gravity @ 25 °C	ISO Viscosity Grade
190 °C	0.818	10

A paper which had done investigation on the solubility of CO_2 with various oils is

referenced here [52] and it is seen that among the oils that were tested, mineral oil (listed as

paraffin oil here) had among them, the least solubility with CO_2 as seen in Figure 28.
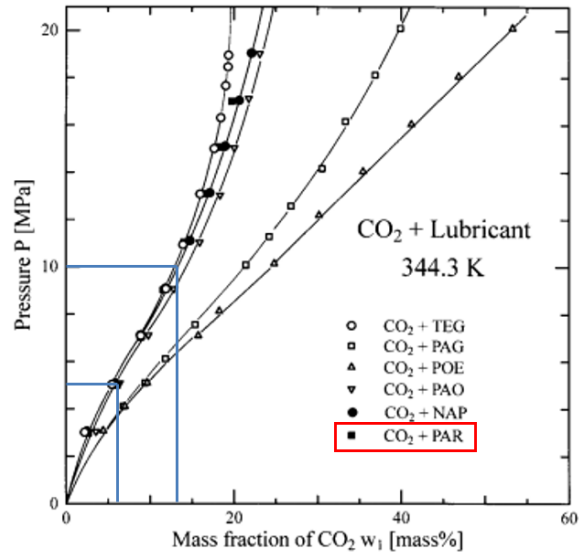
Figure 28: Solubility Graph Comparison of Various Oils [52]

Although mineral oil may be a potential candidate to be used as the liquid piston, testing is needed to compare the solubility effects of CO_2 in other liquids as well. The following two sections detail the crude testing that was performed to determine CO_2 solubility of various fluids to determine the best medium for the liquid piston.

6.1.2.1 Preliminary Test Setup

The following figures shows the test facility diagram as well as the actual facility for testing the solubility.
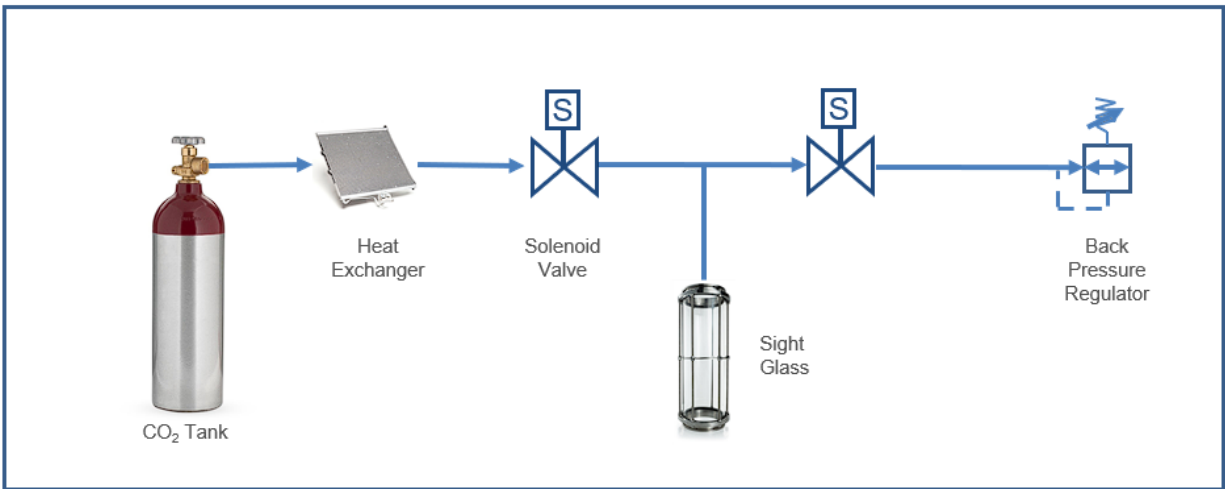
Figure 29: CO₂ Solubility Test Facility Diagram
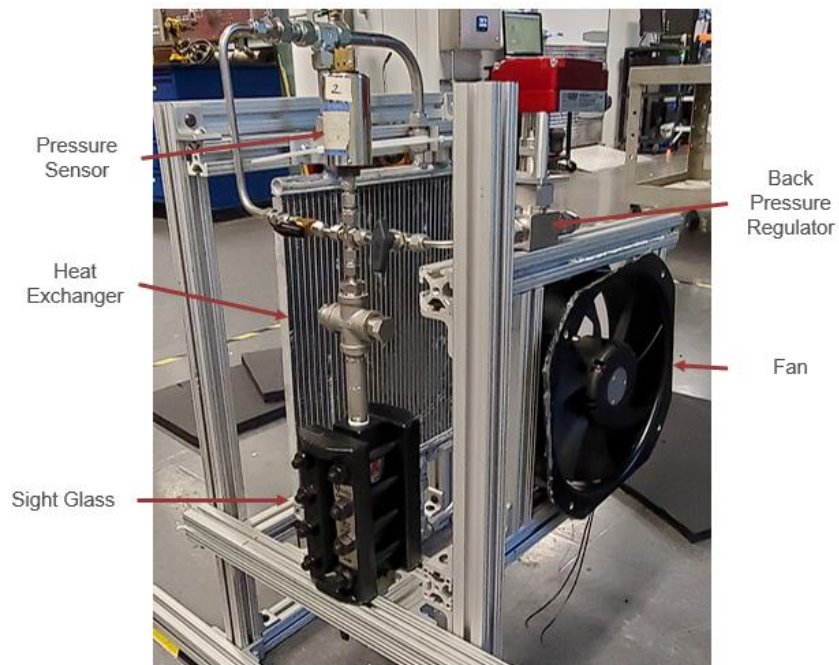
Figure 30: CO₂ Solubility Test Facility Picture

From Figure 29, because the CO_2 tanks can only be pressurized up to 5,750 kPa, the

facility needs to be put in a chamber at 40 °C to increase the pressure. A picture of the test

facility can be seen in Figure 30. A heat exchanger is added to the outlet of the tank to quickly

heat up the CO_2 up to the desired pressure. The first solenoid is opened while the second one is closed to allow the CO_2 to fill the sight glass where it is filled with the liquid that is being tested. Once time has allowed the CO_2 to saturate into the liquid, the first solenoid is closed while the second one is opened to allow the pressure to decrease. At this point, it can be visually confirmed if bubbling is occurring in the liquid. The test will be performed for five cycles, varying the pressure from 8,000 kPa to 3,000 kPa. According to Canales et al. (2015) [8], CO_2 is not a good solvent for liquids with high molecular weight, strong polarity or ionic compounds. With this knowledge, three liquids were tested due to their lack of solubility with CO_2: mineral oil, water and salt water. The reasoning behind salt water, in particular, is that literature also suggests that a salt solution in water also helps bring down solubility, which possibly fills up space in the water structure to prevent gases from dissolving and occupying those gaps in the structure (Hangx, 2005) [20]. The salt solution was 22% salt by mass.

6.1.2.2 Results and Discussion

To make a direct comparison between the liquids, the bubble height was measured. As can be seen from Table 11, water and mineral oil show no signs of bubbling at the tested pressure difference but salt water shows signs of bubbling. Since water and salt water have the ability to corrode the pipes within the liquid piston and react with CO_2 to make carbonic acid, mineral oil was chosen and further tested at larger pressure differences to see the extent of bubbling, which can be seen visually in Figure 31.

Table 11: CO₂ Solubility Results

Fluid	Bubbling Height (mm)
Water	0.0
Salt Water	2.1
Mineral Oil (5,000 kPa difference)	0.0
Mineral Oil (6,500 kPa difference)	6.1

Figure 31: Before (8 MPa left) and After (1.5 MPa right) Picture of Bubbling Occuring

6.1.3 Integrated Gas Cooler Chamber

This section details the process for designing the integrated gas cooler chamber. The table below summarizes the parameters used to help design the chamber.

Table 12: Key Chamber Design Parameters

Parameter	Unit	Value
Refrigerant	-	R-744
Compressing Temperature	°C	40
Evaporating Temperature	°C	15
Mass Flow Rate	g/s	13.3
Cooling Capacity	kW	1.75
Operating Pressure	kPa	5,000-10,000
Cycle Frequency	hz	0.1
Chamber Volume	cc	1,172

6.1.3.1 Prototype Design

As seen from Figure 24, the 40 °C isothermal line has an inflection point at around 9 MPa of pressure which is where the gas will experience the highest enthalpy difference due to its steep slope and therefore, will generate the most heat and have the highest temperature increase. For example, compressing the fluid from 5 MPa to 5.5 MPa will generate less heat than compressing the same amount of pressure at 9 MPa. This instantaneous point will be what the heat exchanger is designed for.

The design parameters will be to use carbon dioxide as the refrigerant and to get gas compression outlet and evaporating temperatures of 40 °C and 15 °C, respectively. Although the ultimate goal of the project is to use the system for commercial refrigeration applications, the aim for this first prototype will be to get an evaporating temperature of 15 °C, which is what would be needed for air conditioning. These temperatures will result in operating pressures between 5,000 to 10,000 kPa, which is a compression ratio of 2. The target cooling capacity is 3.5 kW of cooling, while the target capacity for the first prototype is 1.75 kW. Having the target capacity at hand and assuming an additional 5 °C of cooling is done on the refrigerant from the condenser side, the mass flow rate can be calculated which is estimated to be 13.3 g/s. This calculation was done in EES using a realistic non-isothermal CO_2 cycle. The required volume of the chamber can be calculated using the required mass flow rate and knowing the suction pressure and temperature to get the density of the refrigerant. For Figure 32, the following plot was created as a function of different compression frequencies.
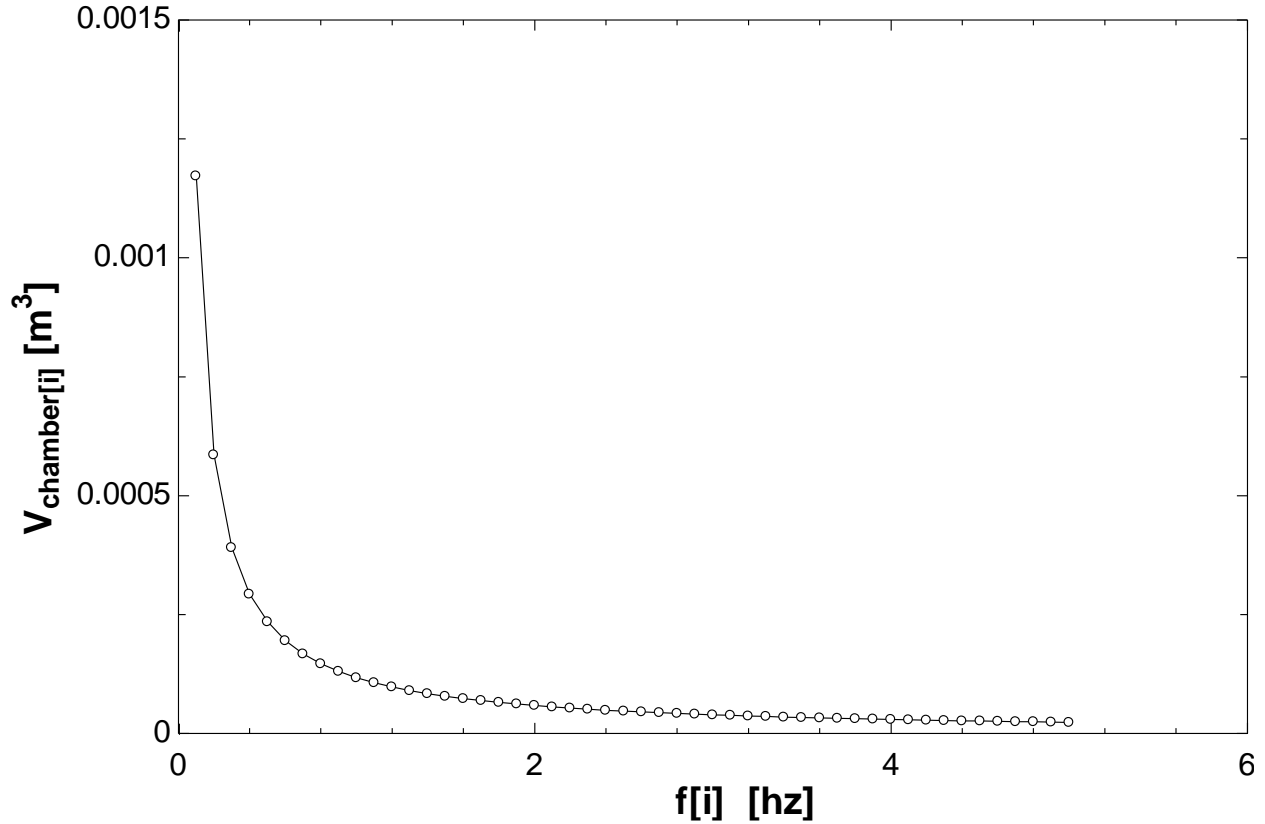
Figure 32: Chamber Volume Versus Frequency Plot

     The heat exchanger was built using k-type hard drawn copper tubes with stainless steel tubes used for the headers of the heat exchanger. The heat exchanger will be made as a single pass bare tube heat exchanger. Knowing the heat transfer area was composed of circular tubes, the surface area can be calculated based on the enthalpy difference and required mass flow rate as a function of the pressure. The following simple heat transfer equation was used to find the surface area. Effects from thermal conductivity of the tube are ignored.

$$\dot{q} = UA\Delta T \qquad (3)$$

The heat flux can be substituted by the enthalpy difference and mass flow rate. The convection coefficient can be given in per unit area. This can be rearranged to result in the following equation.

$$A = \frac{\dot{m}\Delta h}{U\Delta T} \qquad (4)$$

Where A is the heat transfer surface area, $\dot{m}$ is the mass flow rate, Δh is the enthalpy difference, ΔT is the temperature difference between the ambient air and the CO_2, and U is the overall heat transfer coefficient. CO_2 is assumed to be 40 °C. The heat transfer coefficient is assumed to be a constant 50 W/m²K while the ambient temperature was assumed to be 24 °C. Using this equation, the plot in Figure 33 is created.
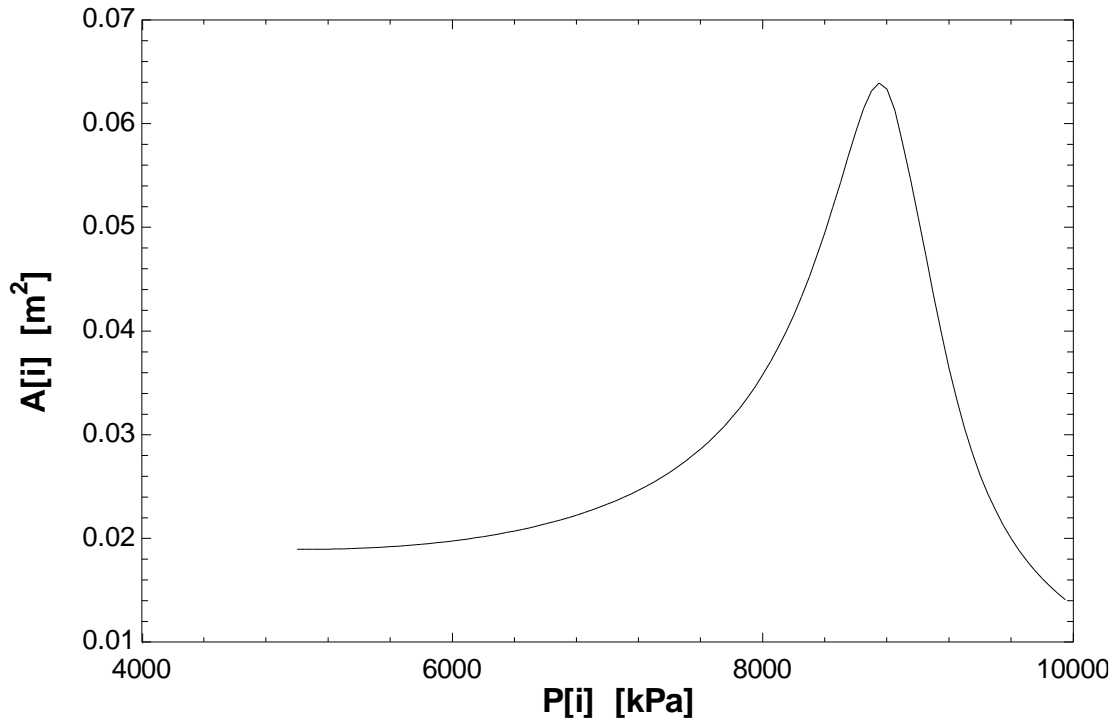
Figure 33: Required Heat Transfer Surface Area Versus Chamber Pressure

Looking at the plot, the maximum surface area that is needed is approximately 0.06 m^2 at its peak which is, once again, at the 9,000 kPa pressure point. This can be attributed to the isothermal curve and the increase in enthalpy difference to maintain the same temperature. Pressure drop is also considered inside the chamber for both CO_2 and the mineral oil. This is done using the Darcy-Weisbach equation as shown.

$$\frac{\Delta p}{l} = f_D \frac{\rho v^2}{2D_H} \qquad (5)$$

Where Δp is the pressure drop, l is the tube length, f_D is the friction factor, ρ is the fluid density, v is the fluid velocity, and D_H is the hydraulic diameter. Based on calculations, tube diameters around 5 mm show little to no pressure drop in the tubes. The final tube diameter that is commercially available are 6.2 mm inner diameter tubes with an outer diameter of 9.5 mm.

Based on the maximum required surface area, the chosen tube diameter, and the geometry, the resulting volume can be calculated. The required chamber volume can also be calculated based on the required mass flow rate and suction density of the CO_2. These two chamber volume values can be compared to ensure both heat transfer and mass flow requirements are being fulfilled and is sized accordingly. A cycle frequency of 0.1 hz was chosen to allow for more heat transfer time to achieve isothermal compression. This increases the chamber size but will also allow for more heat transfer surface area. Based on this comparison, the chamber volume is 1,172 cc with a copper surface area that is triple the necessary surface area. This is done to set a safety factor. This is depicted in Figure 34.

The HXCC was built in-house. Figure 34 shows a CAD model of the chamber with its plastic inserts between the copper tubes. These plastic inserts are installed to increase air flow velocity. Overall dimensions of the chamber are 0.61 m by 0.55 m.

Figure 34: Integrated HXCC CAD Model

Figure 35 shows the actual chamber as well as the side profile and tube pitch dimensions. It should be noted that the center-to-center tube pitch is 23.8 mm due to manufacturing. Brazing tubes very close to each other without melting the solder was thought to be difficult but with the use of a solder with a high silver content, it becomes hard to re-melt the solder without the aid of a solder flux. With the next prototype, a smaller tube pitch can be used.
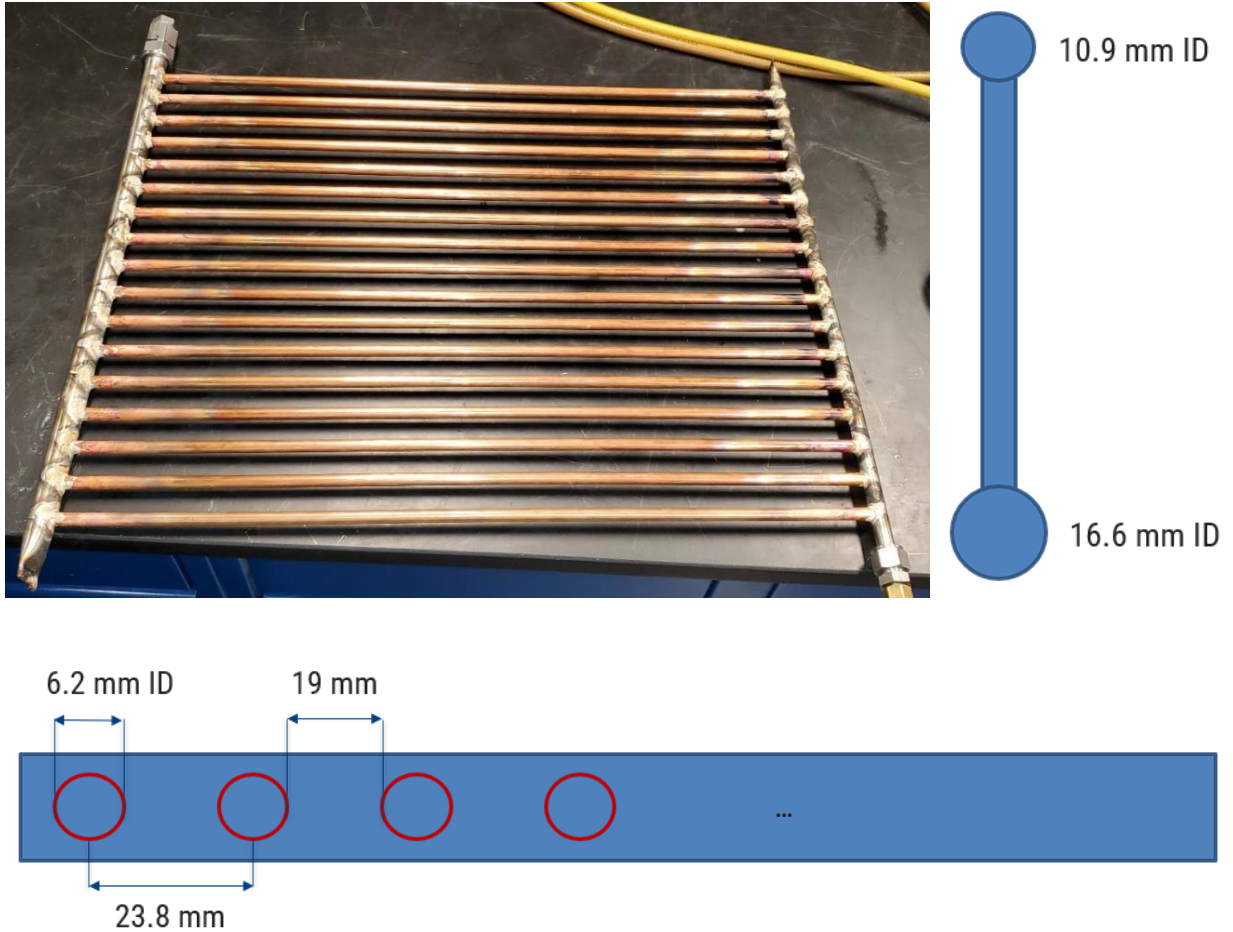
Figure 35: Picture of Integrated HXCC and Side Profile Dimensions (Top), Cross Section Tube Pitch Placement (Bottom)

A total of 17 copper tubes are used for the construction of the chamber. The tubes are k-type hard drawn copper tubes which have a higher yield strength than regular copper of 310 MPa. Tubes have a 6.2 mm inner diameter and a 1.65 mm tube thickness. This is a relatively thick tube thickness to account for the amount of pressure it needs to withstand. Installation of the chamber on the system is tilted on its side to ensure proper drainage of oil during decompression.

6.2 Instrumentation

This section specifies the type of instrumentation that was used as well as their specifications and installation locations.

6.2.1 Pressure Transducers

Figure 36: Picture of Setra Pressure Transducer

The pressure transducers that were used come from Setra Systems, Inc. (model 280E). Figure 36 shows a picture of the sensor. Five pressure transducers were installed at the following locations.

Table 13: Pressure Transducer Locations and Specifications

Location	Range	Full Scale Accuracy
Oil Side, Pump Outlet	0.1-20.7 MPa	0.11%
Oil side, HXCC Bottom	0.1-20.7 MPa	0.11%
Gas side, HXCC Top	0.1-20.7 MPa	0.11%
Gas side, Compressor Discharge	0.1-20.7 MPa	0.11%
Gas side, Compressor Suction	0.1-20.7 MPa	0.11%

Due to insufficient equipment, the pressure transducers could only be calibrated from a range of 0.1-3.4 MPa. Therefore, the pressures for the readings higher than 3.4 MPa would have to be extrapolated. Five equivalently spaced points were taken. Trend fitting for all pressure transducers showed at least a 99.99% fit.

6.2.2 Resistance Temperature Detector

The resistance temperature detectors (RTD) are 1/10DIN grade and were used for high accuracy temperature measurements at the following locations.

Table 14: RTD Locations of Specifications

Location	Probe Diameter	Accuracy from 0-100 °C
Oil side, HXCC Bottom	6.35 mm	0.03 – 0.08 °C
Gas side, HXCC Top	3.18 mm	0.03 – 0.08 °C
Gas side, Compressor Suction	6.35 mm	0.03 – 0.08 °C

6.2.3 Mass Flow Meter

Figure 37: Picture of Coriolis Mass Flow Meter

The mass flow rate of the CO_2 was measured using a Coriolis mass flow meter. Specifically, the mass flow meter is a Micromotion R-series flow meter with the model number R025P. It has an accuracy of ±0.75% of the mass flow for gases, zero stability at 0.165 kg/hr, maximum pressure of 10 MPa, maximum flow rate of 2,720 kg/hr and temperature range of -40°C to 60°C. The meter was installed at the suction side of the HXCC after the plate heat exchanger. The flow meter was calibrated in-house from a range of 0 to 65 g/s and had a trend fit of 99.99%. Figure 37 shows a picture of the sensor.

6.2.4 Watt Meter

Figure 38: Picture of AC Watt Transducer

A watt meter was installed on the system to measure the power consumption of the pump. This is important to calculate and compare the efficiencies of this compressor with industry-standard ones. The particular watt meter that was used was an AC Watt Transducer (model PC5-062D) from Ohio Semitronics, Inc. with an input of 0-300 VAC, 0-100 A and output of 0-10 VDC. It has an accuracy of ±0.5% full scale and an operating temperature range of -10°C to 60°C. This meter was factory calibrated at Ohio Semitronics. The watt meter was also set to

transform the power 4:1, setting the maximum power reading to 10 kW. Figure 38 shows a picture of the sensor.

6.2.5 Level Sensor

A level sensor was researched thoroughly to be used specifically for this unique application. The following sections outline the different types of sensors that were explored and an in-depth explanation of the chosen sensor.

6.2.5.1 Mind Map of Explored Sensors
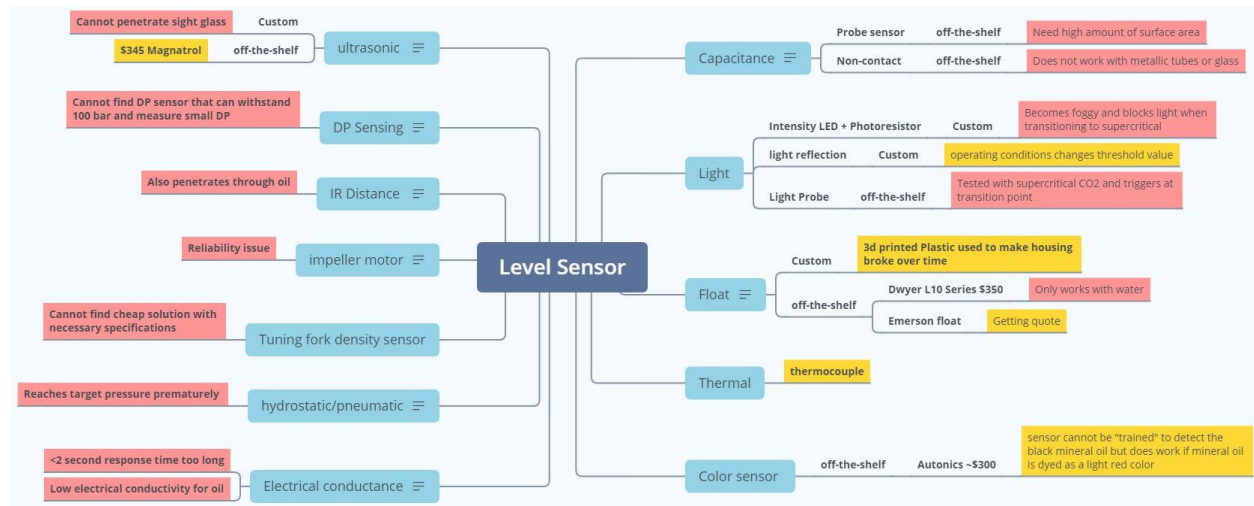
Figure 39: Mindmap of Explored Sensors

Figure 39 shows a map of the types of the sensors that were investigated as well as some of the limitations each one might have.

Among the sensing solutions listed, seven were determined to have the highest likelihood of working including the differential pressure sensor, float sensor, color sensor, light reflection sensor, thermal sensor, tuning fork density meter and ultrasonic sensor.

The differential pressure sensor is utilized by taking advantage of the dynamic and static pressure at two localized points to create a zone that will be able to detect the liquid piston since it will witness a spike in differential pressure. This was successfully tested with water in atmospheric conditions. The principle had worked but there were no commercially available sensors that could be found that could handle the extreme pressures of the system.

The float sensor is utilized by taking advantage of the buoyancy effects paired with a magnet to activate a reed switch to sense the liquid piston. Since conventional plastic floats are not sufficient to handle the pressures experienced in the chamber, cedar wood could be used because of its strong durability under pressure as well as its low density.

The color sensor sends white light which is reflected back into the receiver. Depending on the object in front of the sensor, it will absorb certain spectrums of the light, which will allow the sensor to create a profile for that object's color to sense its presence. Testing with an off-the-shelf sensor has shown that creating a profile for dark colored object (mineral oil dyed with dark dye) is unreliable but distinct colors (such as red) are reliably detected by the sensor.

The light reflection sensor utilizes a similar principle with the color sensor. There is a transmitter emitting a light (red light with the sensor that was bought) and a receiver. Depending on the intensity of the reflected light seen on the receiver, the sensor will trigger.

The thermal sensor utilizes a fast-acting thermocouple to sense the liquid. The liquid and the CO_2 can be set to different temperatures for the sensor to be able to tell the difference. The disadvantage of this sensor, however, is the need for cooling the liquid which may be costly due to high amounts of heat generation from the pump.

The tuning fork density meter is utilized by taking advantage of the difference in densities between the supercritical CO_2 and mineral oil (~200 kg/m^3 difference). A vibrating fork will oscillate at different frequencies depending on the density of the medium it is submerged in. Using this, one would be able to tell when the mineral oil has reached the sensor. However, an economically viable sensor is the limiting factor.

The ultrasonic sensor utilizes sound waves at ultrasonic frequencies to detect a liquid, similar to the tuning fork density meter. These waves propagate from the transmitter to the receiver with a gap in the middle. Depending on the liquid, the waves will travel through liquid at different speeds of sound.

6.2.5.2 LED and Photoresistor Sensor

Ultimately, a cheap, modified version of the light reflection sensor was chosen and made, which consists of an LED and photoresistor. A 3d printed housing was made to hold the LED and photoresistor as shown in Figure 40. A more in depth explanation of the principle are as follows: The light source will shine light into the sight glass where it will be reflected back to the receiver. Once the dyed mineral oil reaches the sensor, the amount of reflected light will be reduced. This is shown by the voltage reading of the photoresistor which can be used to determine when to stop the process.
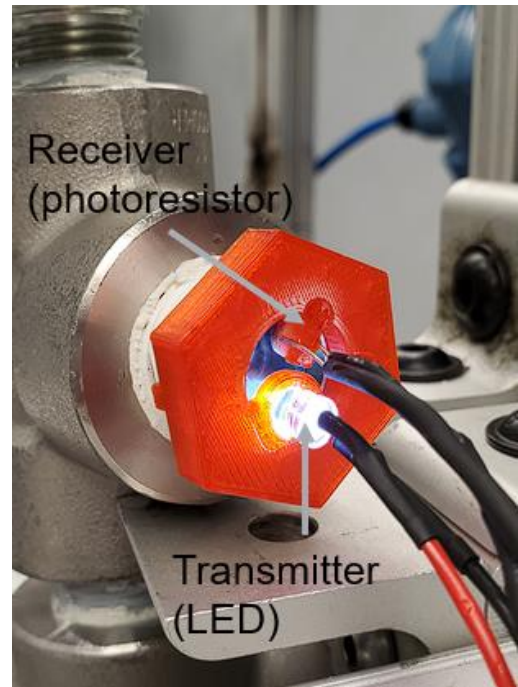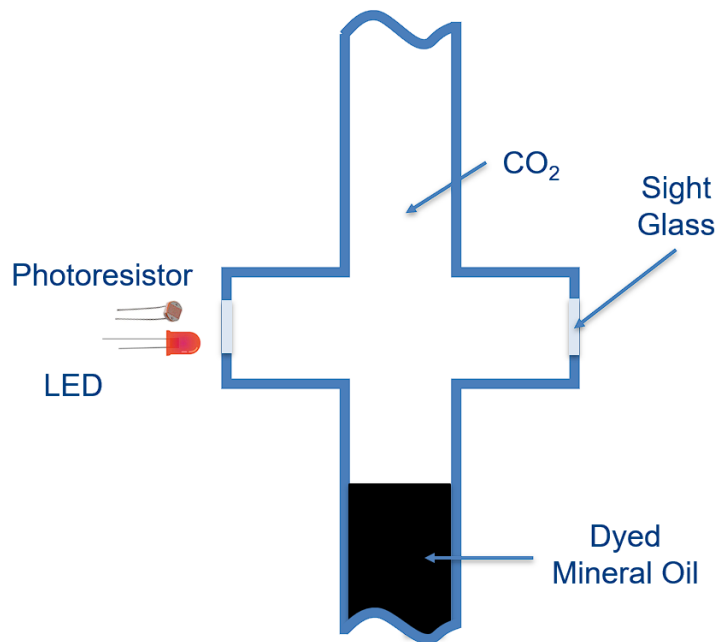
Figure 40: Reflect Sensor Diagram (left) Picture of Sensor Installed (right)

Testing of the sensor in Figure 41 shows a clear, significant drop in the voltage value from the photoresistor when the dyed oil reaches the cross connection. With this, a threshold value can be inputted and used to control the compression.
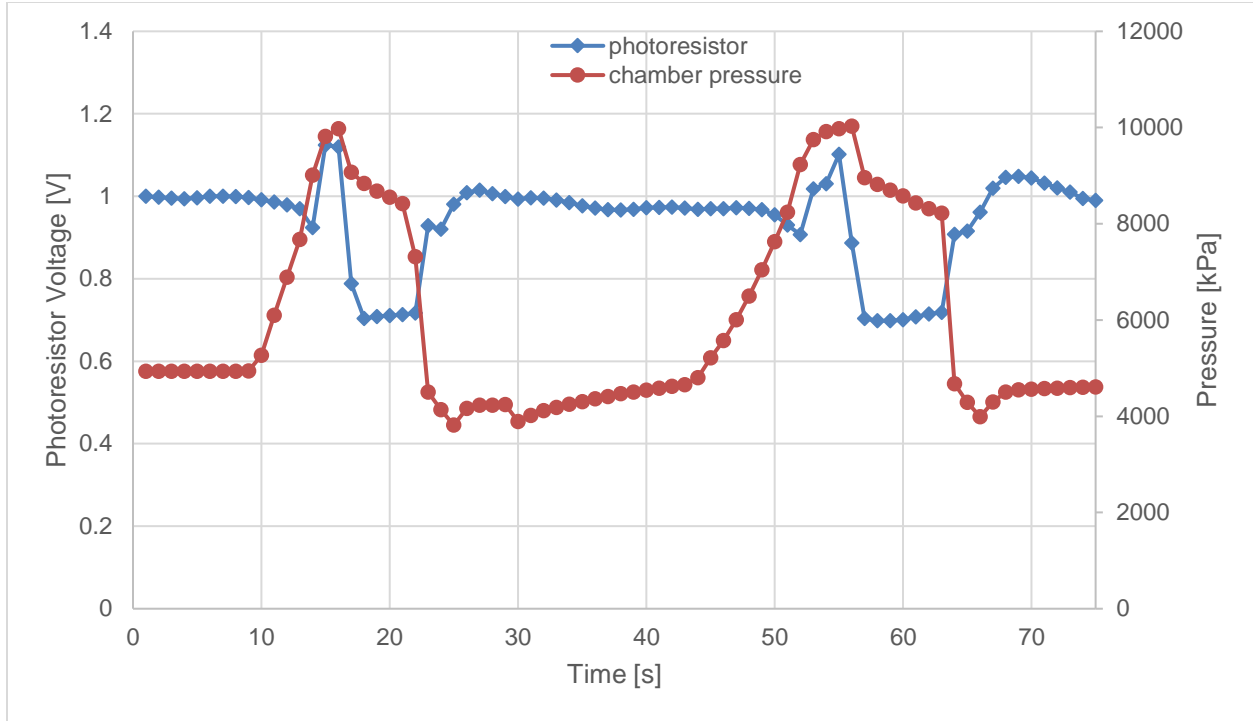
Figure 41: Testing of Reflect Sensor

6.3 Uncertainty Analysis

6.3.1 Systematic Error

Uncertainty of the experiment was determined using the Pythagorean summation of discrete uncertainties as shown in equation 6.

$$u_f = \sqrt{\left(u_{x_1}\frac{df}{dx_1}\right)^2 + \left(u_{x_2}\frac{df}{dx_2}\right)^2 + \cdots + \left(u_{x_n}\frac{df}{dx_n}\right)^2} \qquad (6)$$

Where u_f is the overall uncertainty of a function from individual uncertainties x_i, x_i are the nominal values of variables and u_{x_i} are the discrete uncertainties. Uncertainties are calculated based on the ASME PTC 19.1-2013 test uncertainty standards [1].

69

Table 15: Accuracy Tolerances of Different Measurement Parameters

Measurement	Accuracy
Temperature	±0.5°C
Pressure	±22.8 kPa
Mass Flow Rate	±0.038 g/s
Power	±0.05 kW
Isothermal Efficiency	±1.6 %

6.3.2 Random Error

The uncertainty for isothermal efficiency was determined using the uncertainty propagation in EES. The data used to calculate the random error comes from the shakedown test data for nitrogen at steady state. Average values and standard deviations were calculated using averages for a cycle for a period of five cycles with the exception of power and isothermal efficiency. It should be noted that for the calculation of the power and subsequently, isothermal efficiency, the power consumption was averaged over the compression process only. Therefore, the power input during decompression is ignored. Figures 42 and 43 show the pressure, power, temperature and mass flow versus time.
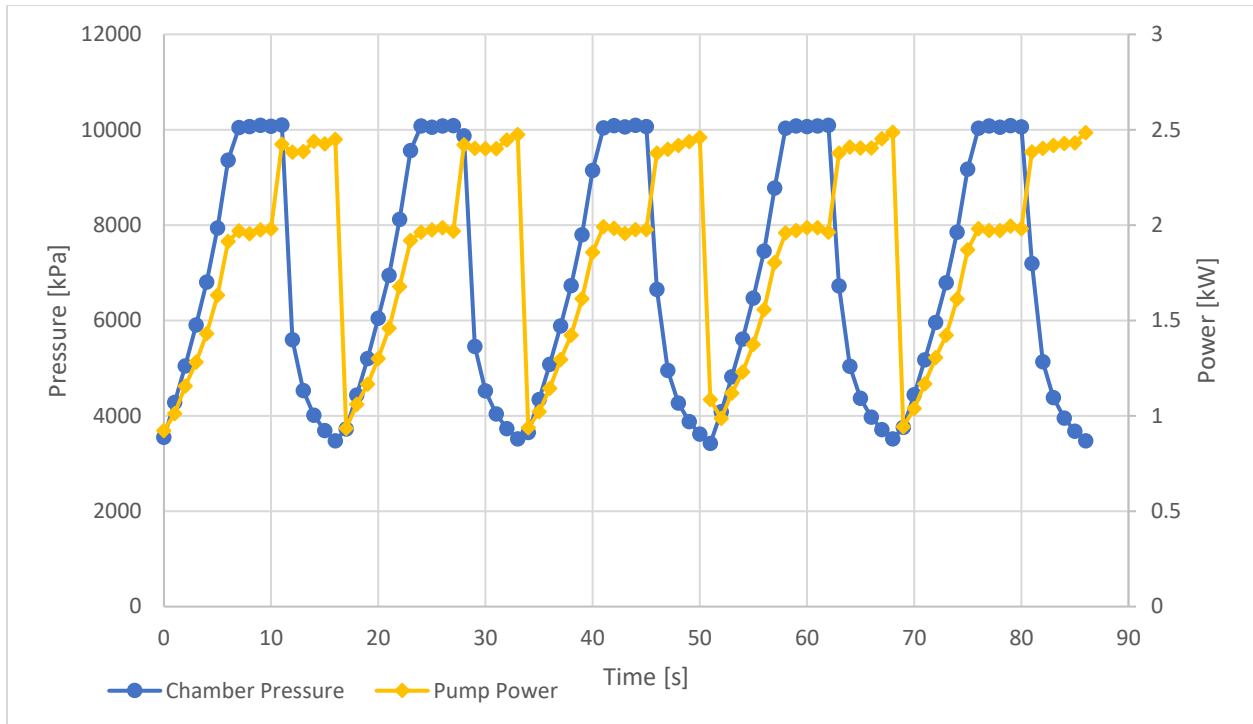
Figure 42: Pressure and Pump Power Versus Time Graph
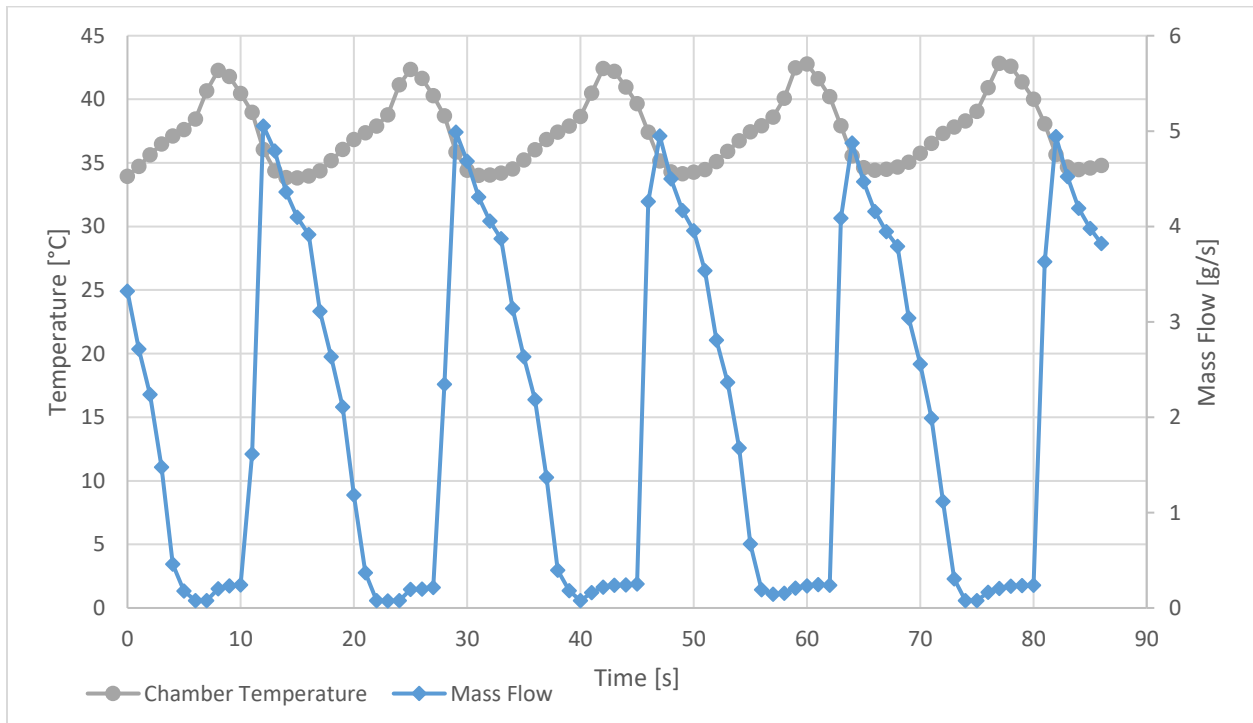
Figure 43: Temperature and Mass Flow Versus Time Graph

71

Table 16: Average Measurement Per Cycle

Cycle	Time [s]	Power [W]	P$_{chamber}$ [kPa]	T$_{chamber}$ [°C]	Mass Flow [g/s]	Isothermal Efficiency [%]
1	16.5	1378	6743	37.1	2.06	61.8
2	16.9	1400	6696	37.1	2.08	59.5
3	17.2	1371	6580	37.2	2.08	58.6
4	17.3	1351	6660	37.6	2.05	61.2
5	17.8	1380	6650	37.7	2.01	56.8

Table 17: Total Average Measurement and Standard Deviation

	Time [s]	Power [W]	P$_{chamber}$ [kPa]	T$_{chamber}$ [°C]	Mass Flow [g/s]	Isothermal Efficiency [%]
Cycle Averages	17.1	1376	6664	37.3	2.06	59.8
Random Error (Standard Deviation)	-	17.4	63.6	0.3	0.03	1.8

6.3.3 Total Error

The total error is calculated using the following equation according to ASME PTC 19.1-2013 standards [1]:

$$u_T = 2\sqrt{u_S{}^2 + u_R{}^2} \qquad (7)$$

Where u_T is the total uncertainty, u_S is the systematic uncertainty and u_R is the random uncertainty. The total error is therefore calculated within a 95% confidence interval.

Table 18: Measurement Error Calculation

	Time [s]	Power [W]	$P_{chamber}$ [kPa]	$T_{chamber}$ [°C]	Mass Flow [g/s]	Isothermal Efficiency [%]
% Random Error	-	1.3	1.0	0.8	1.5	3.0
% Systematic Error	-	3.6	0.3	1.3	1.8	3.8
% Total Error	-	7.7	2.1	3.1	4.7	9.7

As can be seen, the errors for the pressure and temperature are low, relative to the other errors. This is good, especially for the pressure since they could not be calibrated to the operating pressures that were tested here. All other errors are quite high (power, mass flow and isothermal efficiency), which is expected due to near minimal operation limit for the mass flow, the nature of having a prototype system and the slow transient cycle of values fluctuating, which contribute to random error.

6.4 Data Acquisition

All system measurements are taken using the National Instruments' Data Acquisition System (DAS) modules. These modules allow for streamlined data acquisition and communicate with Labview, a data acquisition software package.

A total of nine channels were used to collect data including pressure, temperature, mass flow rate, and power consumption. Additional internal sets of data were captured in the software including compression and decompression time as well as sensor voltages. Data is captured in one second intervals.
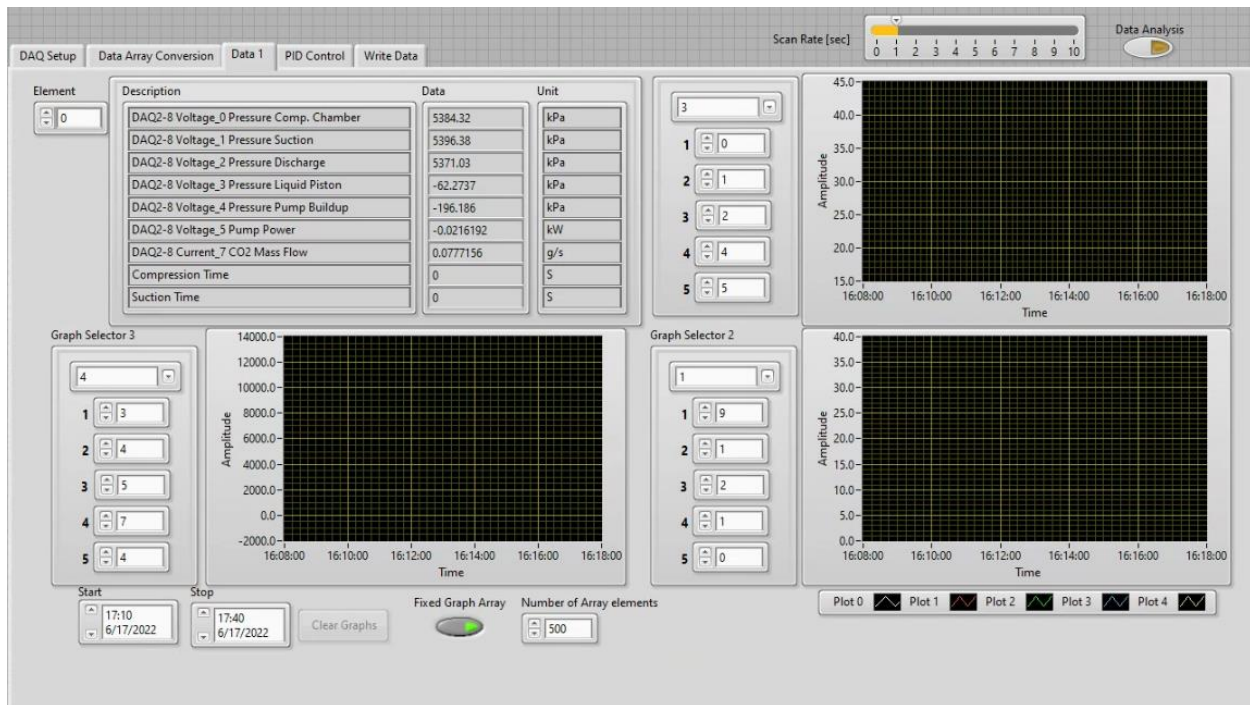
Figure 44: Screenshot of Labview Software User Interface

6.5 Shakedown Testing and Safety Implementation

Shakedown tests and safety implementations, both physical and virtual, were implemented to ensure safe use of the system. Several shakedown tests were performed to ensure proper use of the system:

- Pressure bypass test

- Liquid piston test

- Safety measure test with nitrogen

- Compression and decompression with nitrogen

- Run continuously with nitrogen

The pressure bypass test is performed to ensure that the back pressure regulator and relief valve on the pump is working properly and the desired pressure can be reached. The liquid piston

test is performed to ensure that the liquid level sensor also works properly without pressure before moving on to the compression and decompression with nitrogen test.

Safety measures in the Labview code are also implemented and tested to ensure proper function. First, there is a time factor which can be set for the compression and decompression which stops the current process it is in after the set time is exceeded. Second, there is a pressure factor for the compression process which will stop the compression and go into a routine of decompressing the chamber if a certain pressure is exceeded. Third, there is a temperature factor which monitors the temperature at the bottom of the chamber, in between the solenoid valves, which stops the decompression process if there is a significant change in temperature, meaning the oil has gone too far and the gas has entered that region. Error codes will flash if any of the three safety measures trigger as shown in Figure 45. Finally, there is a LED safety measure which monitors the connections of the LED light on the light level sensor to ensure that a process cannot be run if there is a disconnection.

The compression and decompression test with nitrogen was performed as a final test to ensure full functional operation for single cycle tests. Similarly, the run continuously with nitrogen test was performed to ensure functional operation when running the system continuously.

The figure below shows the control module for the DAS. Several modes can be chosen from the dropdown menu on the top left: manual, compression, suction, run compressor, emergency off and calibrate. Manual mode allows the user to control the 4 manual control buttons seen below the dropdown menu. Compression mode automatically runs the compressor to compress one time and then returns back to control mode. Suction mode automatically decompresses the liquid piston and allows the refrigerant to flow back in, one time. LED

indicators labeled "oil at top" and "oil at bot" are added to show the user where the liquid piston is at any time. This indicator is also used by the program to ensure compression or suction is not allowed twice in a row. Run compressor mode automatically cyclically runs the compression and suction continuously until stopped by the user. These processes can be stopped in the middle of their routine using the "stop process" button. The reset button is used to reset the error code LED indicators. Emergency off mode turns off all devices. Calibrate mode allows the user to get an average value for the level sensors to determine where the threshold values should be. These values can be inputted into the operating parameters. Time limits for the suction, suction wait, compression, and compression wait can also be inputted. The state tells the user what process the system is currently in. Below this, is the information that tells what the suction time, compression time and cycle frequency are. The program will also tell the user the estimate compression time for a give pump speed percentage. The DAQ Data will also tell the user the real time values for the sensors.
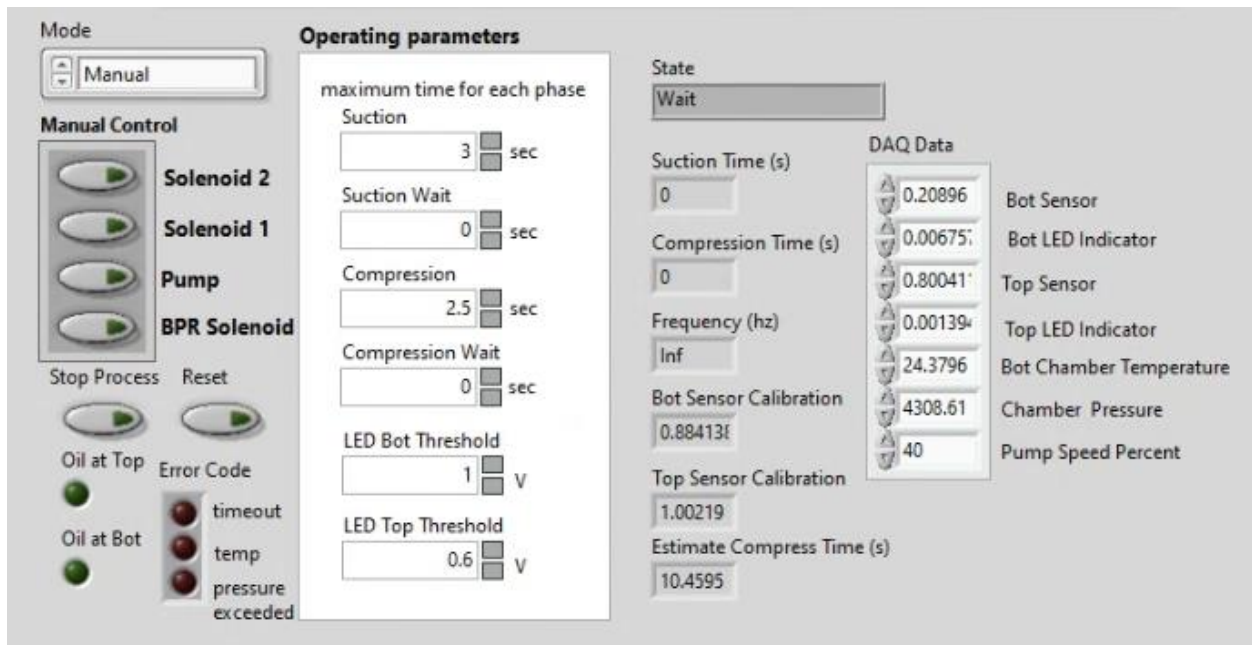
Figure 45: Screenshot of Labview Control Module

76

6.6 Test Procedure

A test procedure was developed to ensure the same conditions for all tests to be able to make fair comparisons. The goal is to obtain 10 to 20 minutes of steady state data. For single compression tests, only one cycle is performed. Before the actual test is run, the following checklist should be audited.

Preliminary Checklist

- Check that the back pressure regulator and pressure relief valve are properly set to the desired pressure (typically 11 MPa for the back pressure regulator and 12 MPa for the relief valve). This can be done by closing the compression solenoid, running the pump and reading the pressure sensor.

- Check that the two needle valves located after the second solenoid valve are properly adjusted. This may require a single compression and suction routine to determine the suction time.

- Ensure that the liquid level sensors are properly calibrated.

- Check that the back pressure regulator for the gas is properly set (typically 10 MPa).

- Check that the pressure regulator from the CO_2 tank is properly set (typically 4 MPa).

- Check that all the ball valves are open (three in total).

Running the Facility

1. Turn on the chamber to the desired temperature
2. Turn on the water baths and set the desired temperature
3. Turn on red button from the facility
4. Turn on the DAS and ensure that all values are measuring correctly

5. Wait for temperatures from the chamber and water baths to stabilize

6. Turn on the fan if needed

7. Select 'write data' from the write module

8. Select 'run continuously' from the control module ('single compression' if running single compression)

9. Let the system run until data has been collected

10. Stop the test by de-selecting the 'write data' button and selecting 'manual'

11. Turn off the fan and the water baths

12. If the test stopped during the compression phase, select 'suction' from the menu

13. Close the ball valve to the chamber

14. Turn off the chamber and the facility

6.7 Test Conditions

The following tables outline the test matrix for single compression tests as well as steady state (SS) tests. Tests ended up being tested at 4,000 kPa due to poor control of the suction pressure even though the HXCC was designed for 5,000 kPa. Test conditions are based on AHRI Standard 571 for CO_2 [1]. For single compression tests, a sensitivity analysis is done on the isothermal efficiency of the prototype design. Variables that are changed are the fan speed, oil temperature and pump speed. A repeat test of the baseline is done to determine the repeatability of the tests. A final test is done which employs a known combination of these three variables to get the best isothermal efficiency. For steady state, tests are run from 10 to 20 minutes where the last 5 cycles of the test are taken for analysis. The process is automated to ensure consistent cycles. SS-1 and SS-2 are run to see if the fan has more of an impact on efficiency than the single compression tests and to see the effect of having a lower suction temperature than the

ambient temperature. SS-3 and SS-4 are run to compare the effect of pump speed once again

with the baseline in a continuous operation. Interplay between combined effects were also

explored. SS-EC is the test that will utilize evaporative cooling to try to achieve higher

isothermal efficiencies and see its effect. Water spray on the chamber is done with water that is

at ambient air temperature.

Table 19: Single Compression Test Matrix

Test #	Chamber Volume (cc)	Compression Time (s/LPM/%)	Fan Speed (m^3hr^{-1} /%)	Air Temp. (°C)	Oil Temp. (°C)	CO_2 Suction Pressure (kPa)
Baseline	1,172	9/7.6/45	0/0	35	35	4,000
Repeat	1,172	9/7.6/45	0/0	35	35	4,000
1-1	1,172	9/7.6/45	481/25	35	35	4,000
1-2	1,172	9/7.6/45	960/50	35	35	4,000
1-3	1,172	9/7.6/45	1,141/75	35	35	4,000
1-4	1,172	9/7.6/45	1,920/100	35	35	4,000
2-1	1,172	9/7.6/45	0/0	35	25	4,000
2-2	1,172	9/7.6/45	0/0	35	30	4,000
2-3	1,172	9/7.6/45	0/0	35	40	4,000
2-4	1,172	9/7.6/45	0/0	35	45	4,000
3-1	1,172	6.4/11/65	0/0	35	35	4,000
3-2	1,172	7.5/9.1/55	0/0	35	35	4,000
3-3	1,172	12/6.1/35	0/0	35	35	4,000
3-4	1,172	21/3.8/20	0/0	35	35	4,000
3-5	1,172	42/1.9/10	0/0	35	35	4,000
Best	1,172	21/3.8/20	1,920/100	35	25	4,000

Table 20: Cycle Operation Test Matrix

Test #	Chamber Volume (cc)	Compression Time (s/LPM/%)	Fan Speed (m³hr⁻¹/%)	Air Temp. (°C)	Oil Temp. (°C)	CO₂ Suction Temp. (°C)	CO₂ Suction Pressure (kPa)
SS-B	1,172	12/6.1/35	0/0	35	45	~35	~4,000
SS-1	1,172	12/6.1/35	0/0	35	45	~27	~4,000
SS-2	1,172	12/6.1/35	1,920/100	35	45	~27	~4,000
SS-3	1,172	5/12.5/75	1,920/100	35	45	~35	~4,000
SS-4	1,172	24/3.0/15	1,920/100	35	45	~35	~4,000
SS-EC	1,172	10/7.2/40	1,920/100	35	31	~40	~4,000

7 Test Results and Analysis

This section discusses the results of the tests and compare between the single compression and steady state data as well as other compressors and research done on isothermal compression.

7.1 Single Compression

Results from the single compression tests are summarized in the table below. The temperature increase for all tests are seen to be almost the same except for test 3-5, which saw a significantly lower temperature lift. The error for most tests falls under 2% with the tests running for longer periods due to slower compression, seeing higher errors up to 4.5%. Isothermal compressor efficiency is also recorded which considers the pump and motor efficiencies.

Table 21: Single Compression Results

Test #	Temperature Increase [K]	Isothermal Efficiency [%]	Error [%]	Isothermal Compressor Efficiency [%]
Baseline	12.1	70.2	±1.90	50.7
Repeat	12.2	69.5	-	-
1-1	11.9	70.4	±1.85	50.8
1-2	12.0	69.0	±1.83	49.8
1-3	11.8	70.4	±1.94	50.9
1-4	11.7	71.4	±1.97	51.5
2-1	12.1	69.0	±1.80	49.8
2-2	11.8	70.0	±1.91	50.5
2-3	12.1	58.3	±1.39	42.1
2-4	11.9	59.5	±1.45	43.0
3-1	12.0	48.8	±0.85	35.2
3-2	12.3	67.2	±1.61	48.5
3-3	11.3	77.1	±2.68	55.6
3-4	10.4	84.4	±3.66	57.2
3-5	7.5	80.9	±4.53	46.3
Best	11.2	85.8	±3.89	58.1

7.1.1 Isothermal Efficiency Calculation

In order to compare efficiencies of these tests, isothermal efficiency must be defined. Other papers in the air compression research space have defined it as the capability of the compressor to maintain working fluids initial temperature during the compression process. Here, it is proposed that the classic thermodynamic definition is used as shown in equation 8.

$$\eta_{iso} = \frac{w_{iso}}{w_{actual}} = \frac{w_{iso}m}{(E_{elec} - E_{press})\eta_{pump}\eta_{motor}} \qquad (8)$$

Where E_{elec} is the measured electrical energy in kJ, m is the mass of CO_2 being compressed in kg, w_{iso} is the required isothermal specific work in kJ/kg, E_{press} is the necessary electrical energy to maintain the pump at a certain pressure in kJ, η_{pump} is the pump efficiency and η_{motor} is the motor efficiency. Normally isothermal work can be calculated with the ideal isothermal work equation, but it cannot be assumed that CO_2 is an ideal gas, so the work is calculated in EES using the model described in the cycle modeling section. Efficiency of the motor and pump is also accounted for in this case. The electrical energy to maintain the initial pressure is also subtracted as a specific offset to ensure isolation of only work done to compress the gas. Without this, work on compressing the liquid from atmospheric to the initial pressure would be included. Since this work recovery is not utilized in this design, as it would be with conventional compressors, it is not included as part of the actual energy. The liquid may also not be assumed to be incompressible, therefore energy would be wasted to compressing the liquid.

7.1.2 Repeatability

A repeat test of the baseline was performed to determine the repeatability of these tests. This is determined through standard deviation of the average temperature, isothermal efficiency and average power. From the results, it is seen that the average temperature deviates 0.2 °C from

each other. The isothermal efficiency deviates 1.0 % from each other and the average power

deviates 0.02 kW from each other. This would indicate that the test could be reproduced with a

fair amount of certainty. Results are summarized in Table 22.

Table 22: Repeatability of Baseline Test

Test	Average Temperature [°C]	Isothermal Efficiency [%]	Average Power [kW]
Baseline	39.6	70.9	1.59
Repeat	39.2	69.5	1.57
Standard Deviation	0.2	1.0	0.02

Figure 46 shown below plots the temperature versus pressure plot of the two tests which

show very close results through the compression process.
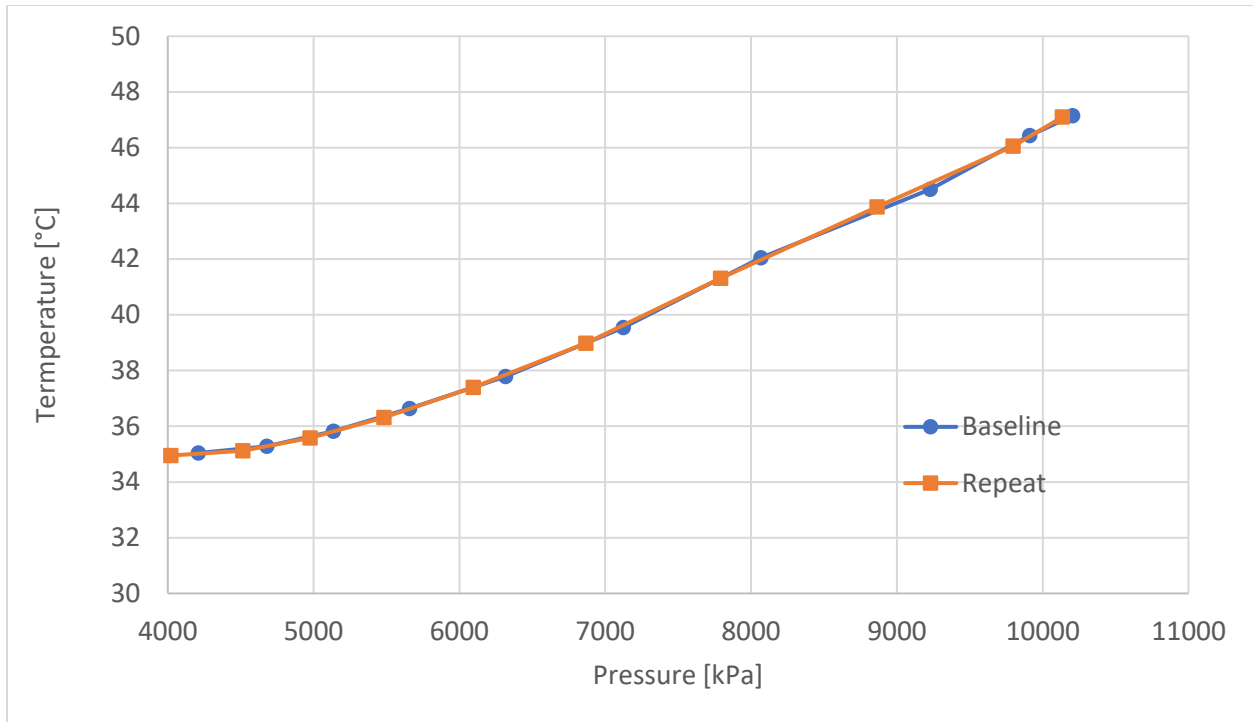
Figure 46: Temperature Versus Pressure of Baseline and Repeat

Figure 47 below shows the power draw through the compression process and shows a similar amount of power draw with slight deviation at the last part of compression.
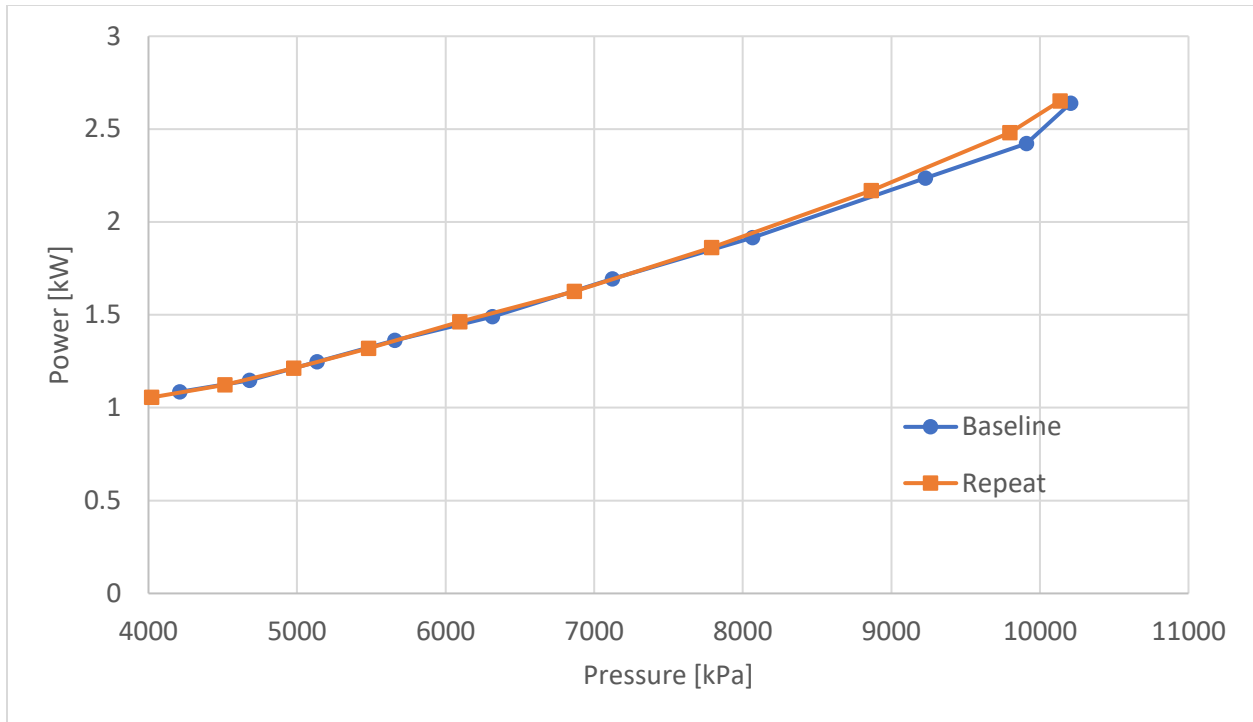
Figure 47: Power Versus Pressure of Baseline and Repeat

7.1.3 Data Analysis

Looking at the bar plot in Figure 48, the baseline gives an isothermal efficiency of 70.2%. This baseline uses 0% fan speed, 35 °C oil temperature and 45% pump speed. The bars in blue show isothermal efficiencies with varying fan speeds up to 100%. For these sets of tests, the effect of the fan speed seems to have little to no effect on the efficiency. This may be because the thermal mass of the HXCC may be enough to absorb all the heat during the single compression and therefore, the fan is not needed. So, during steady state operation the effect of the fan may be more significant. However, the fan still has influenced the temperature profile, as seen in Figure 50. Figure 55 shows the specific work where test 1-1 showed a major increase in power consumption on the latter half of the compression compared to the other tests, interestingly.

The gray bars show the effect of oil temperature on the efficiency. For the first tests, which are of lower oil temperature, it seems to have little to no effect on the efficiency while the other two tests (2-3, 2-4), which are of higher oil temperature significantly impact the efficiency. This may be due to natural convective heat transfer occurring during compression as the liquid piston flows into the HXCC, which heats up the working fluid, but it is not supported by the temperature profiles in Figure 51, which are very similar for those subset of tests. Tests 2-1 and 2-3 had the higher temperature profiles while tests 2-2 and 2-4 had the lower temperature profiles. Another possibility could be that the viscosity of the oil decreases with higher temperature which hurts the efficiency of the pump. This efficiency is assumed to be constant as consulted by the manufacturer. Interestingly, test 2-1 had the highest power consumption profile as shown in Figure 56. This may be due to the higher viscosity of the fluid at the lower temperature.

The yellow bars show the effect of pump speed. With higher pump speeds, the efficiency of the compressor suffers. Lower pump speeds resulted in higher efficiencies with diminishing returns where the benefits stop when the pump speed is lower than 20%. The motor efficiency also drops past this point, but it has been accounted for. The temperature and specific work profiles in Figures 52 and 57, show lower overall temperature and work, which would expect a higher efficiency. Figure 54 shows the effect of pump speed compared to all the other tests and Figure 57 shows the effect among the other tests in its category. An explanation for this drop in efficiency may lie in the pump efficiency but a full performance curve on the specific pump used is not available. One other noteworthy explanation may be due to the fact that although the power usage is lower, running the pump at 10% speed compared to 20% speed resulted in more

than twice as long compression times, which would lead to overall higher power consumption and, therefore, lower efficiency, a net loss.

The last test in green combined the knowledge of all three parameters and picked the best configuration. Overall, the best test beats the baseline efficiency by 15.6%, which is dominated by the effect of the pump speed. The addition of the fan and cooler oil temperature increases the efficiency over test 3-4 by 1.4% but is within the margin of error. As seen in Figure 53, the temperature profile is similar to the baseline in the first half of the compression but is considerably cooler in the latter half. Figure 58 shows lower power consumption compared to the baseline.
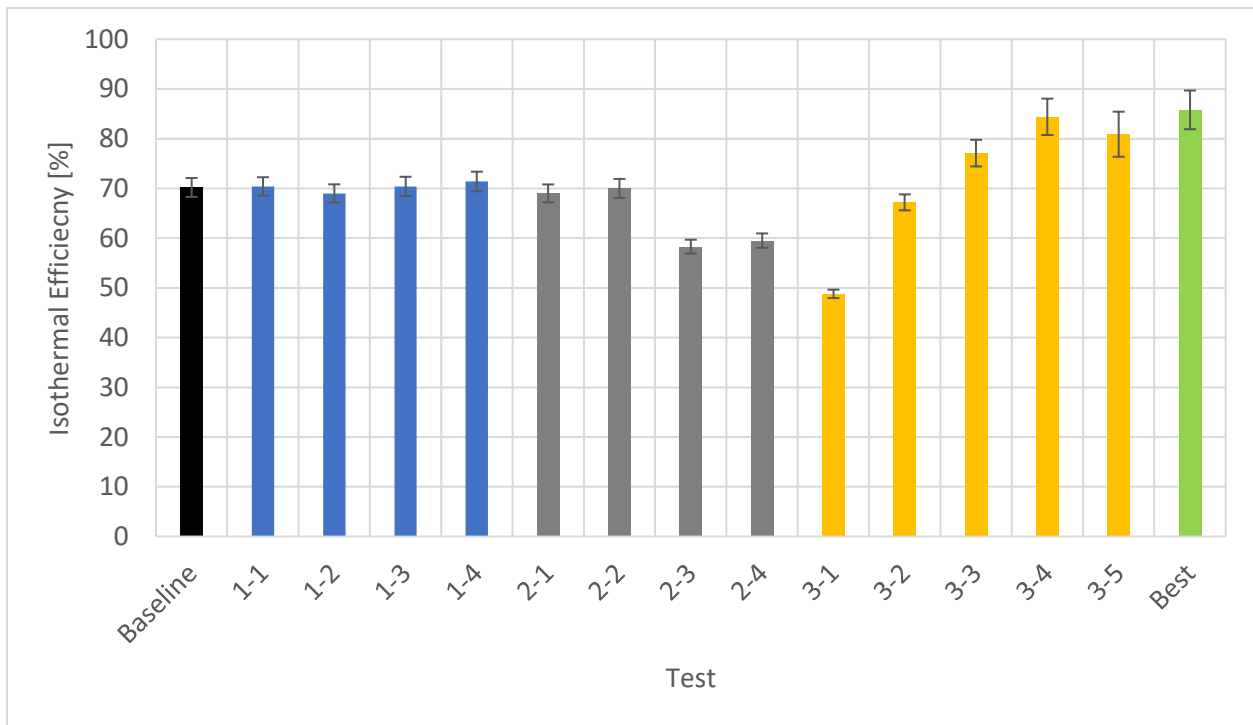
Figure 48: Isothermal Efficiency Bar Plot
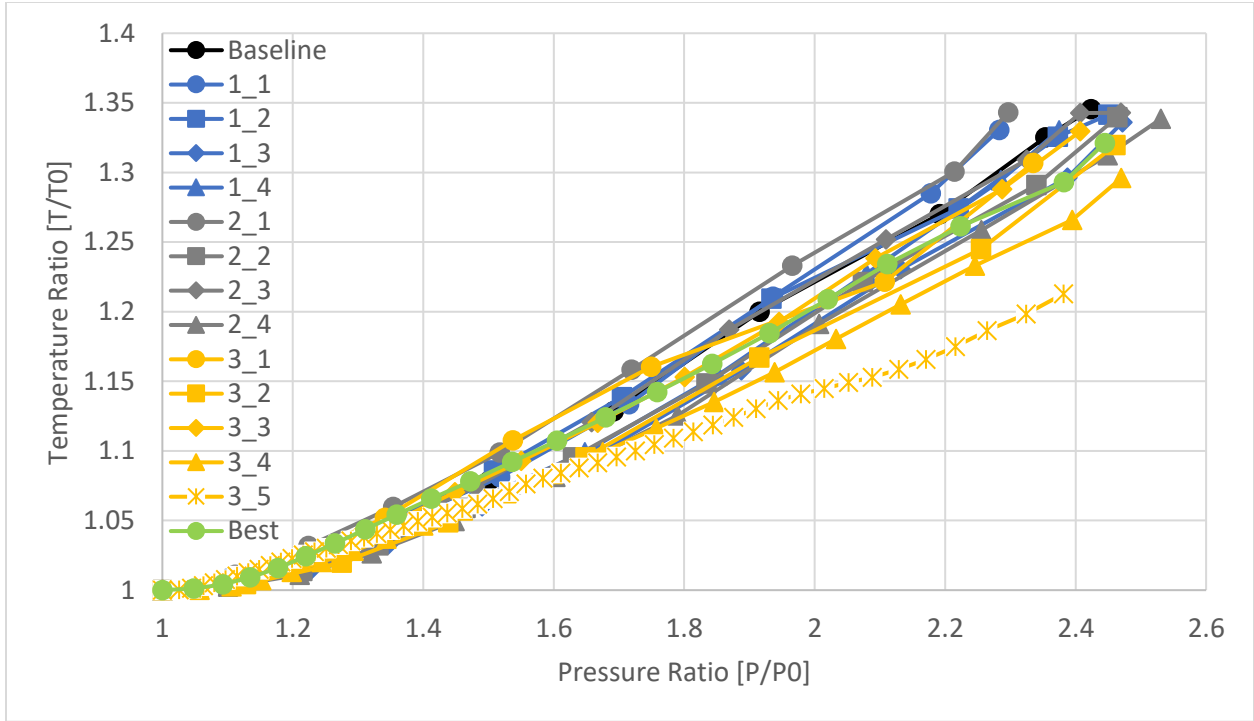
Figure 49: Temperature Ratio Versus Pressure Ratio For All Single Compression Tests
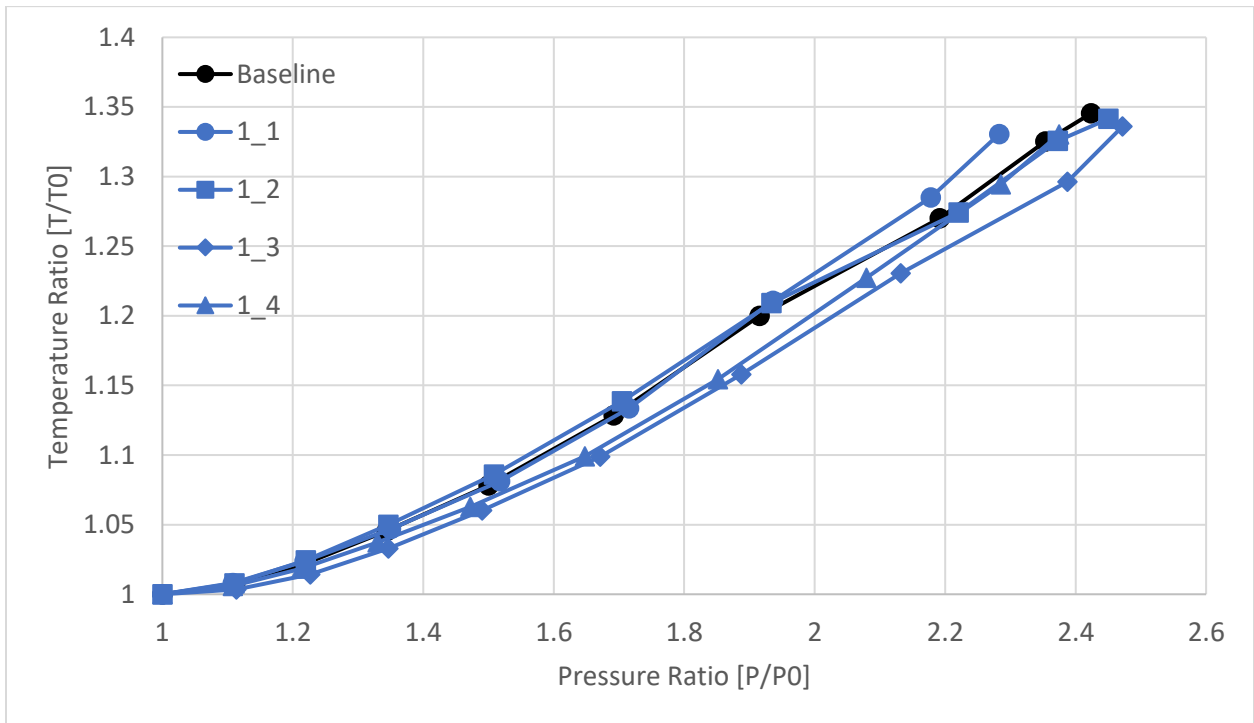
Figure 50: Temperature Ratio Versus Pressure Ratio For 1-X
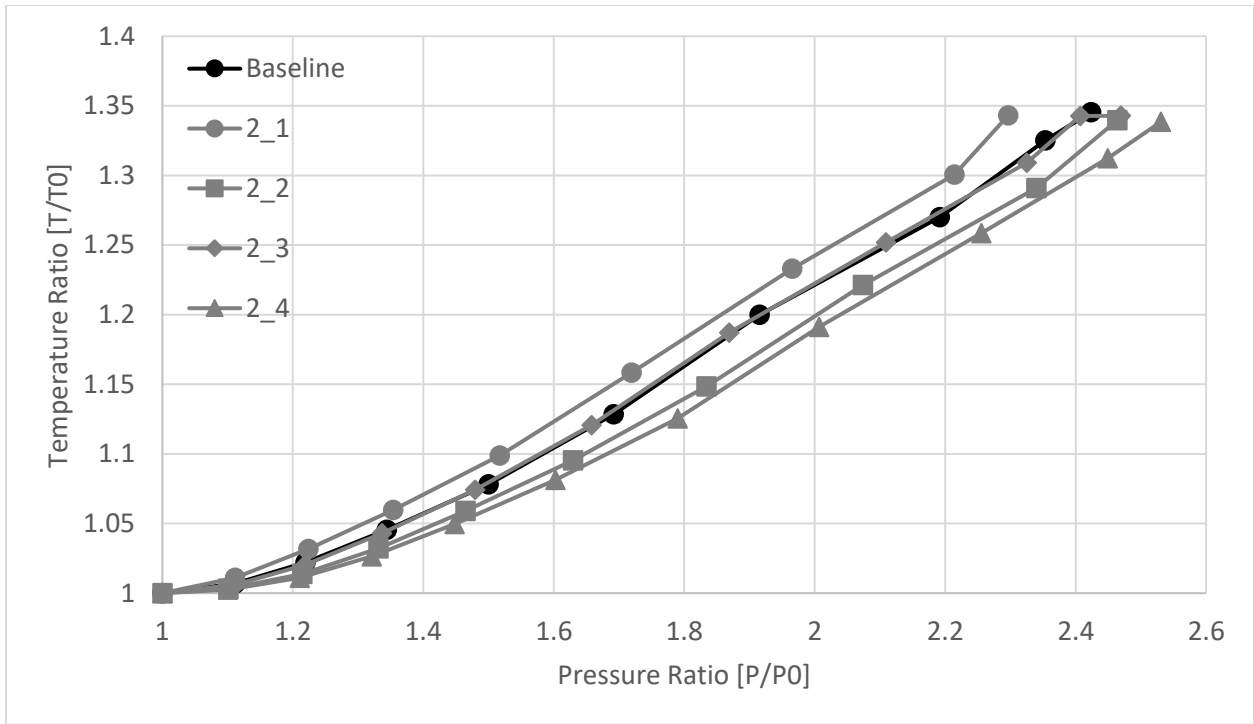
Figure 51: Temperature Ratio Versus Pressure Ratio For 2-X
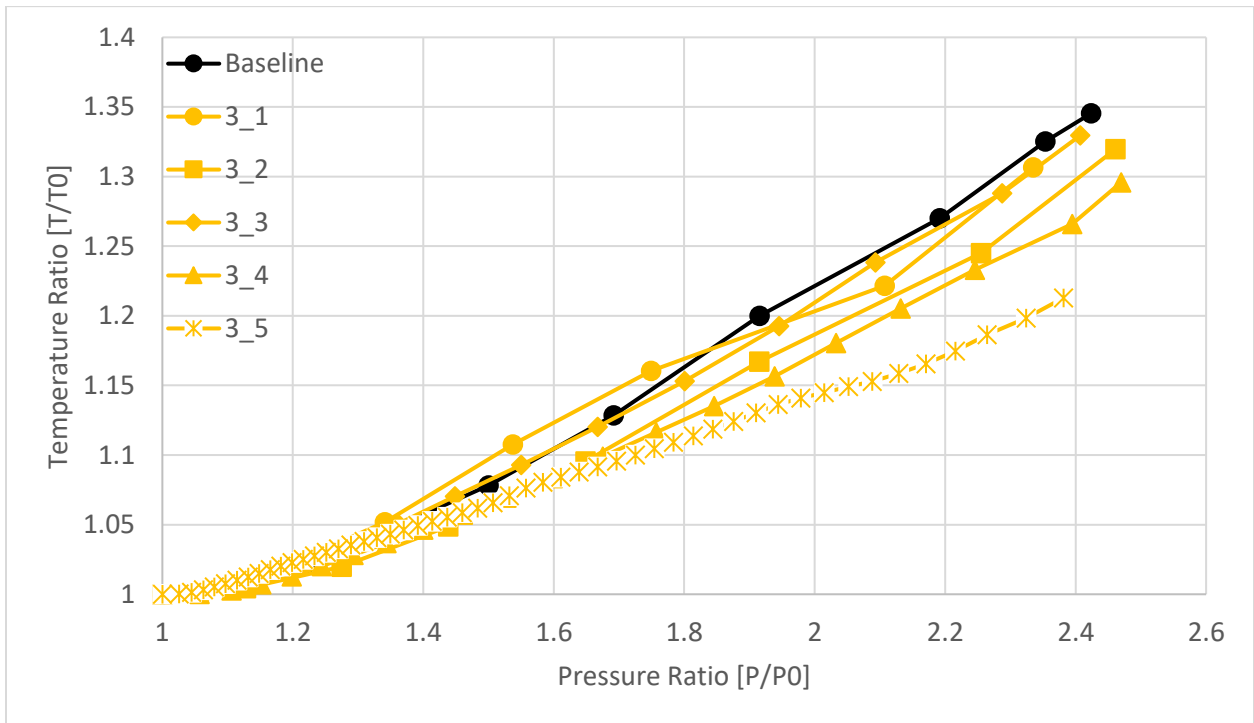
Figure 52: Temperature Ratio Versus Pressure Ratio For 3-X
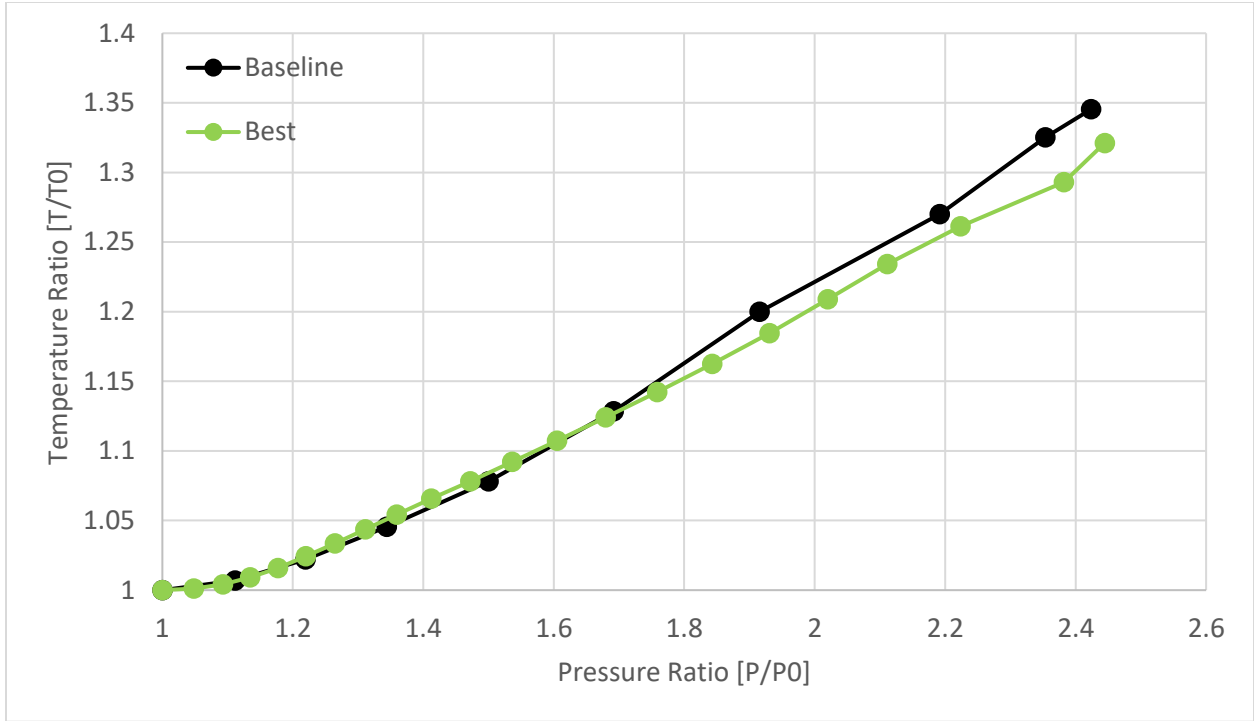
Figure 53: Temperature Ratio Versus Pressure Ratio Best Test
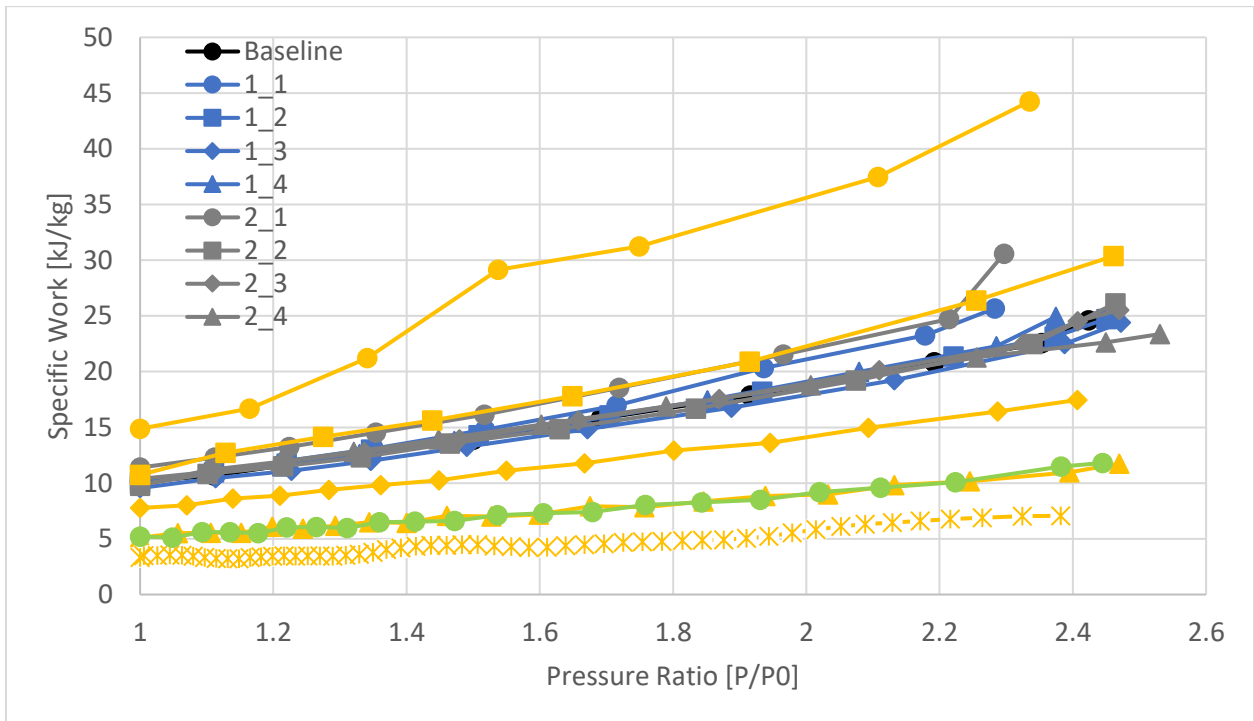
Figure 54: Specific Work Versus Pressure Ratio For All Single Compression Tests
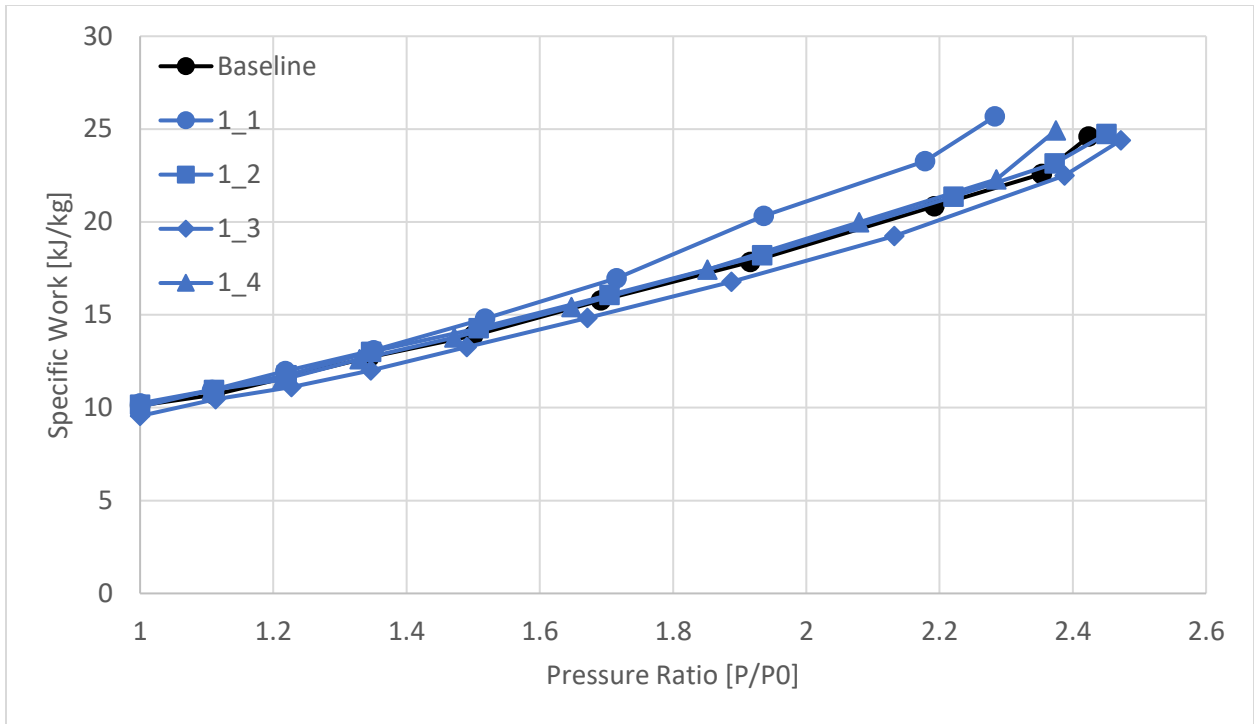
Figure 55: Specific Work Versus Pressure Ratio For 1-X
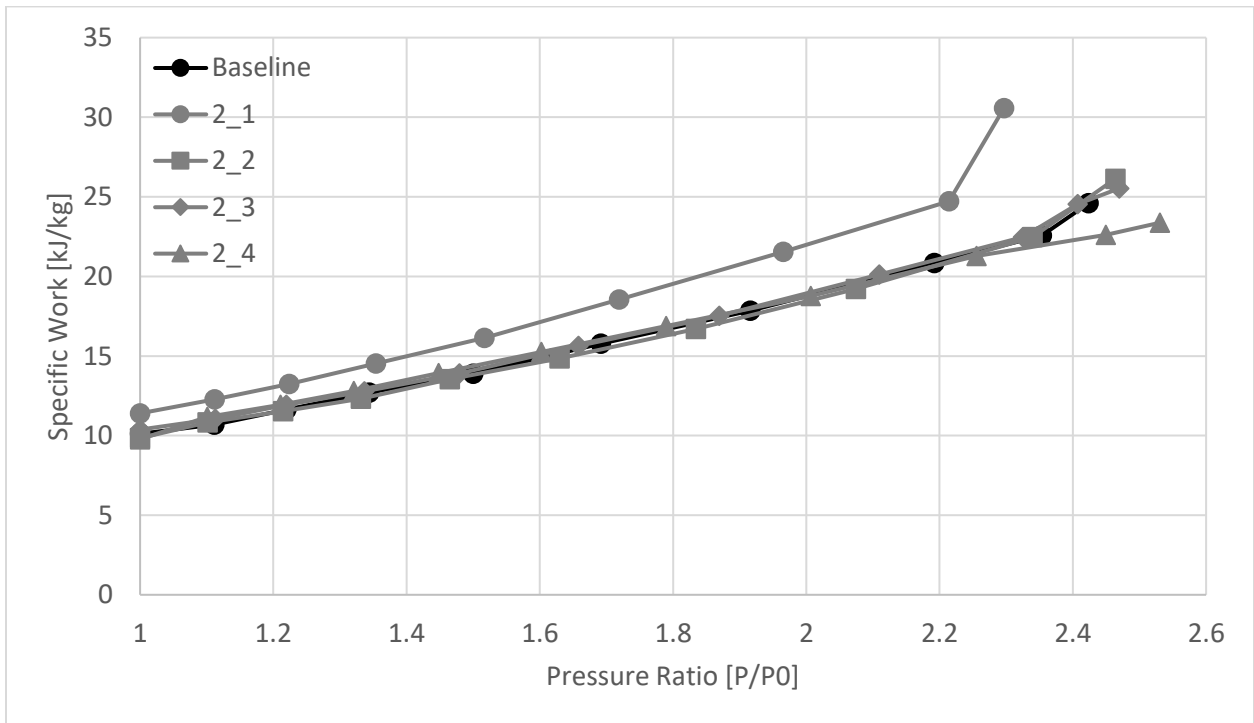
Figure 56: Specific Work Versus Pressure Ratio For 2-X
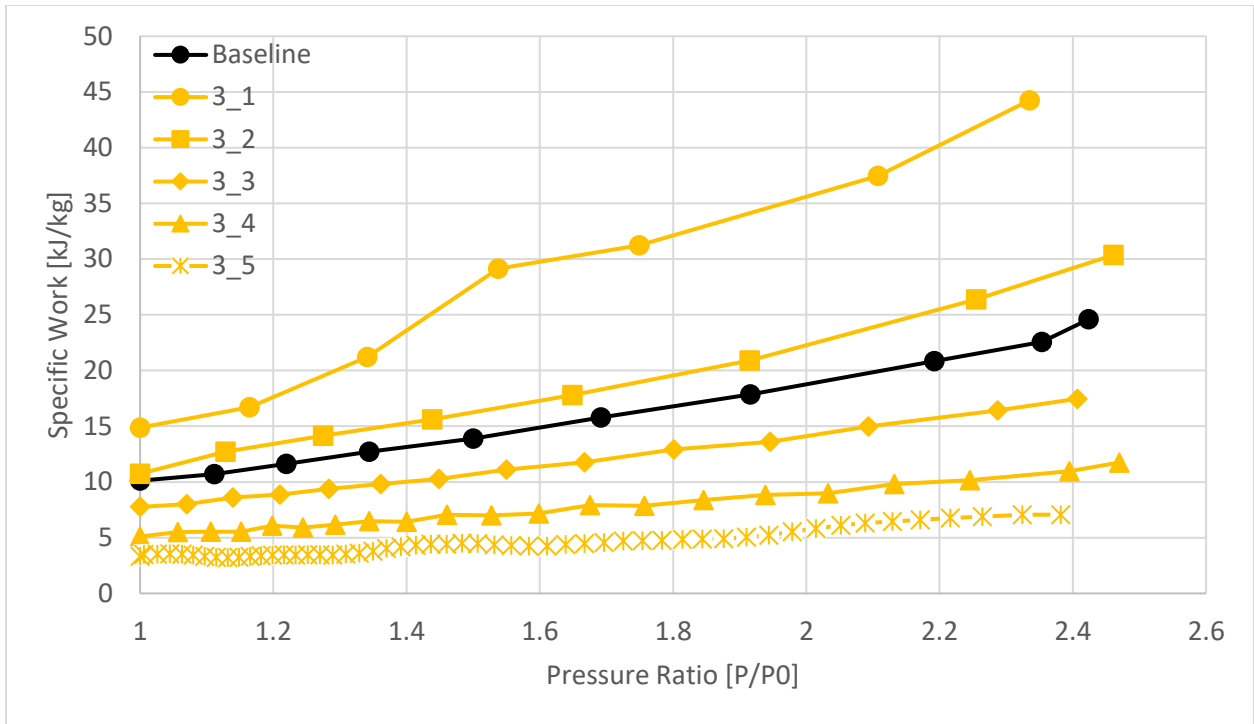
Figure 57: Specific Work Versus Pressure Ratio For 3-X
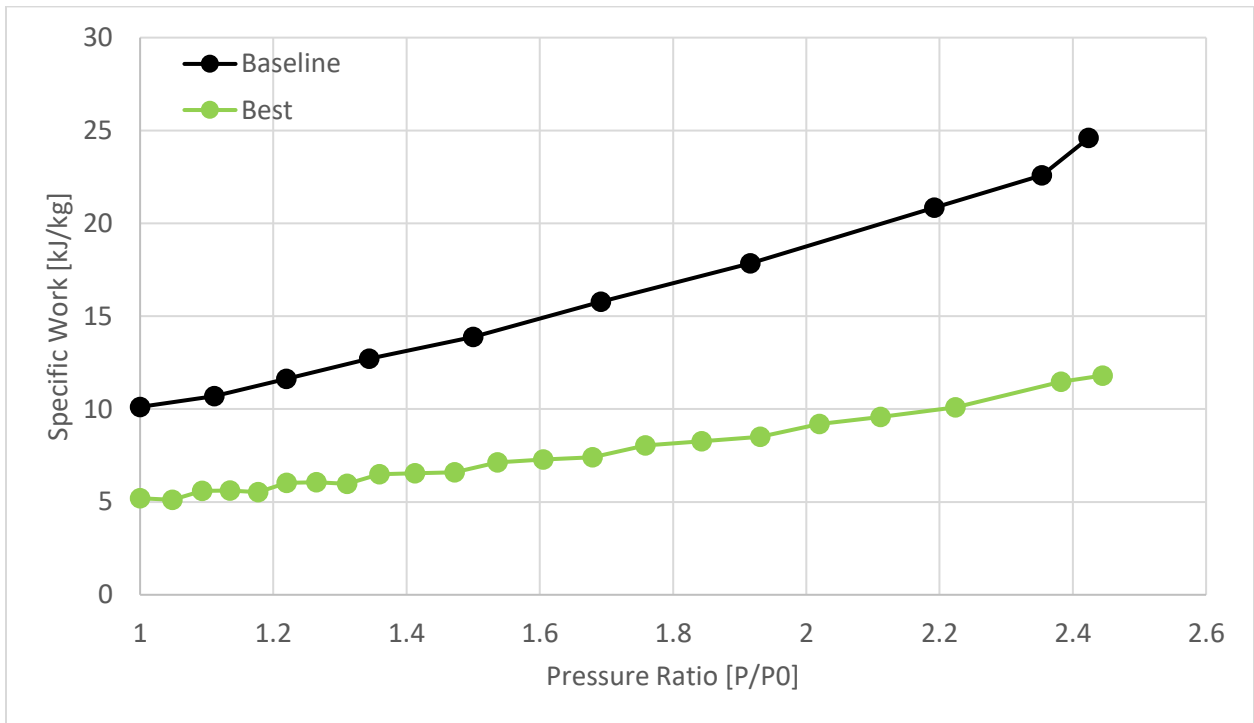
Figure 58: Specific Work Versus Pressure Ratio For Best Test

93

Two P-h diagrams are plotted. Figure 59 plots the best efficiencies from each case as well as the baseline and best-case tests which can be compared with the isentropic and isothermal case. Figure 60 plots the best temperature profiles from each case as well as the baseline and best-case tests. Comparison of all temperature profiles can be seen previously in Figure 49. The final temperature for the isentropic case would be 111.2 °C. Single compression tests show anywhere from 63.9 °C to 68.7 °C decrease from the isentropic case. Most notably, test 3-5 has the closest isothermal compression profile with only a 7.5 K temperature increase.
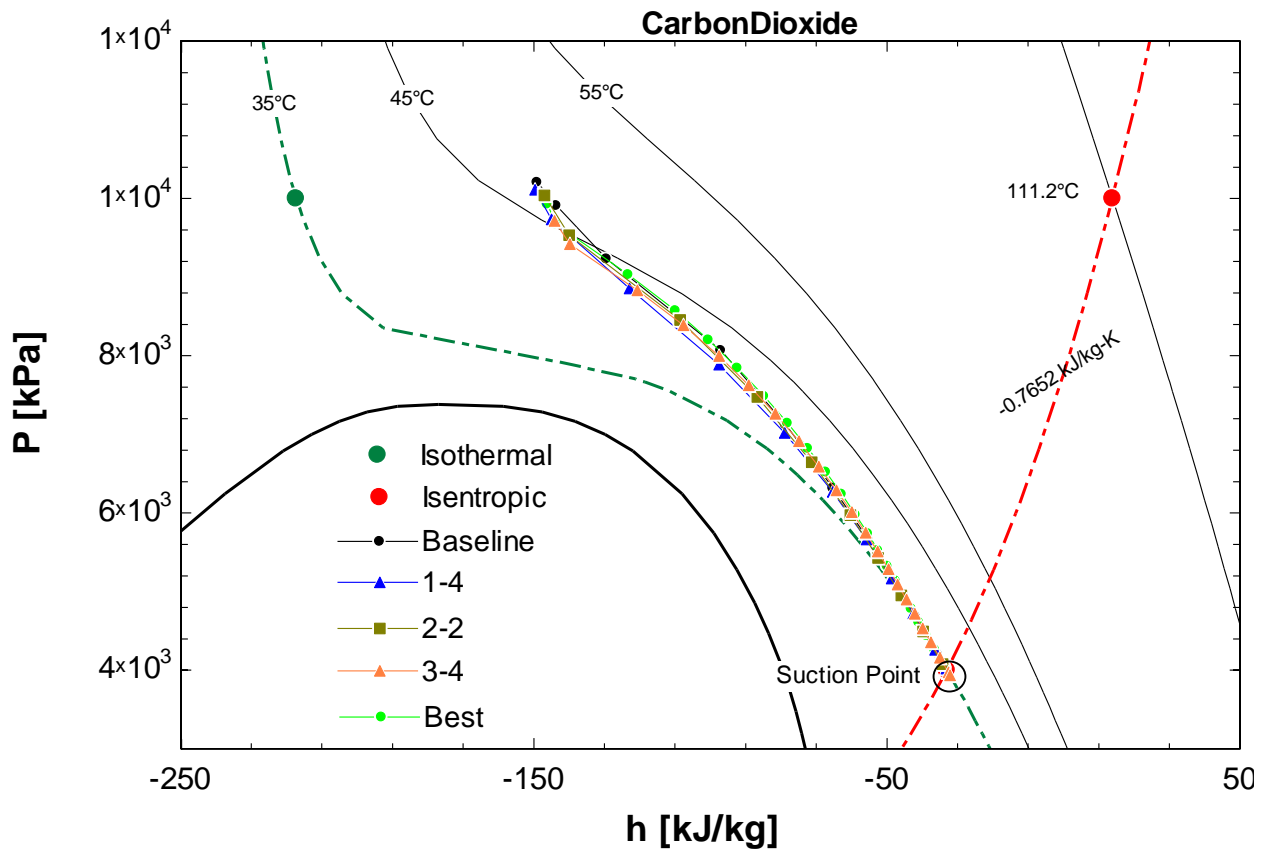
Figure 59: P-h Diagram of Best Efficiencies Versus Isentropic and Isothermal Case
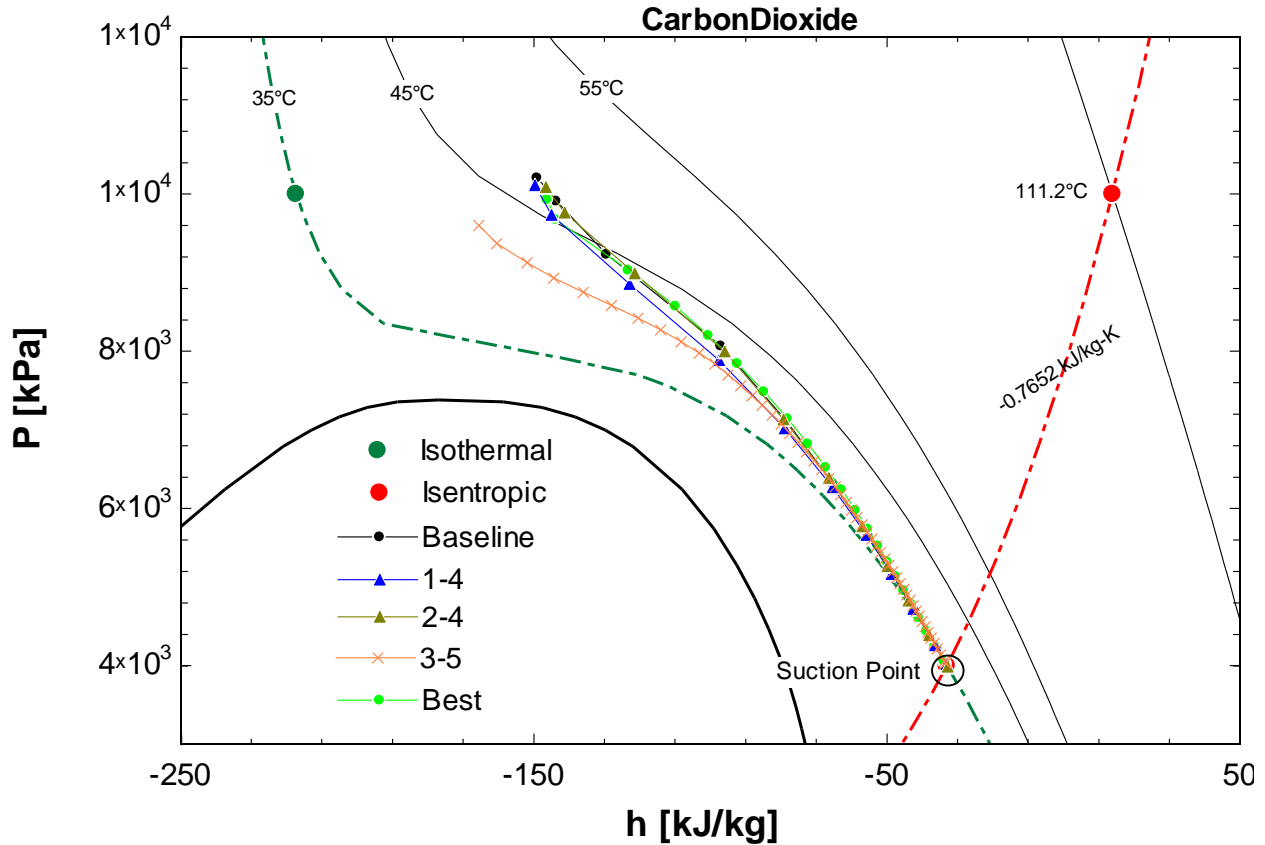
Figure 60: P-h Diagram of Best Temperatures Versus Isentropic and Isothermal Case

7.2 Steady State

Results from the steady state tests are summarized in Table 23. It should be noted that the temperature increase and isothermal efficiency are averaged over 5 cycles. Temperature increase is also taken from the highest temperature seen which may happen past the compression phase when the piston is pushing out the gas. Temperature increase for SS-B, SS-1 and SS-2 see a significant increase from their single compression counterparts. Although oil temperature and pump speed are not the same from the single compression series, the higher oil temperature was seen to not affect the temperature increase in the single compression tests considerably and having slower compression speeds was proven to decrease temperature increase. In the case of SS-B, however, temperature increase is still seen. This may be due to the HXCC being saturated

with heat during a steady state process which is not seen in the single compression tests. This limited thermal capacity would raise the overall temperature of the HXCC during operation. Overall, the isothermal efficiencies are still comparable to that of the single compression tests. Average pressure ratios and power is also recorded.

Table 23: Steady State Operation Results

Test #	Average Temperature Increase [K]	Average Isothermal Efficiency [%]	Average Pressure Ratio	Average Power [kW]
SS-B	19.8	70.4	2.44	1.46
SS-1	18.7	74.7	2.58	1.59
SS-2	16.1	82.1	2.36	1.54
SS-3	9.5	69.7	2.73	2.96
SS-4	14.5	82.7	2.33	0.77
SS-EC	8.5	91.2	2.57	0.63

Efficiency is improved by 7.4% from test SS-1 to SS-2 by increasing the fan speed as shown in Table 23. This is a significant improvement over the single compression tests going from the baseline to 1-4, which has an improvement of only 1.2%. The effect of the fan has a more pronounced impact on the efficiency during continuous operation. Additionally, when the suction temperature becomes lower than ambient temperature as seen with test SS-1, the efficiency and temperature increase is still comparable with the baseline SS-B. The effect of the fan is also still prevalent with test SS-2 where higher efficiency is seen in Figure 61. This could

be due to the pre-cooling effect of the gas inside on the chamber. The gas will pre-cool the chamber during suction and then the gas will be cooled more effectively during compression.

Interestingly, when comparing SS-3 with SS-B, isothermal efficiencies are similar as seen in Figure 61, which compares the isothermal compression efficiencies at different pump speeds with fan cooling. For this case, the effect of the fan seems to balance out the effect of higher pump speed. Additionally, the temperature profile in SS-3 is the lowest, as seen in Figure 62. In contrast, the temperature profile for SS-4 is higher in this plot even though the pump speed is considerably lower. This may be due to the nature of compressing the working fluid at a faster rate. The RTDs were installed at the suction and discharge ports. During decompression, new gas is introduced in the chamber and cools the RTD, then it is compressed, which increases the temperature. This is done so at a fast rate, which may not have given the RTD enough time to accurately gauge the temperature inside the chamber. This would explain why this is seen in the steady state test and not the single compression test. As expected, the power consumption scales with the pump speed as seen in Figure 63.
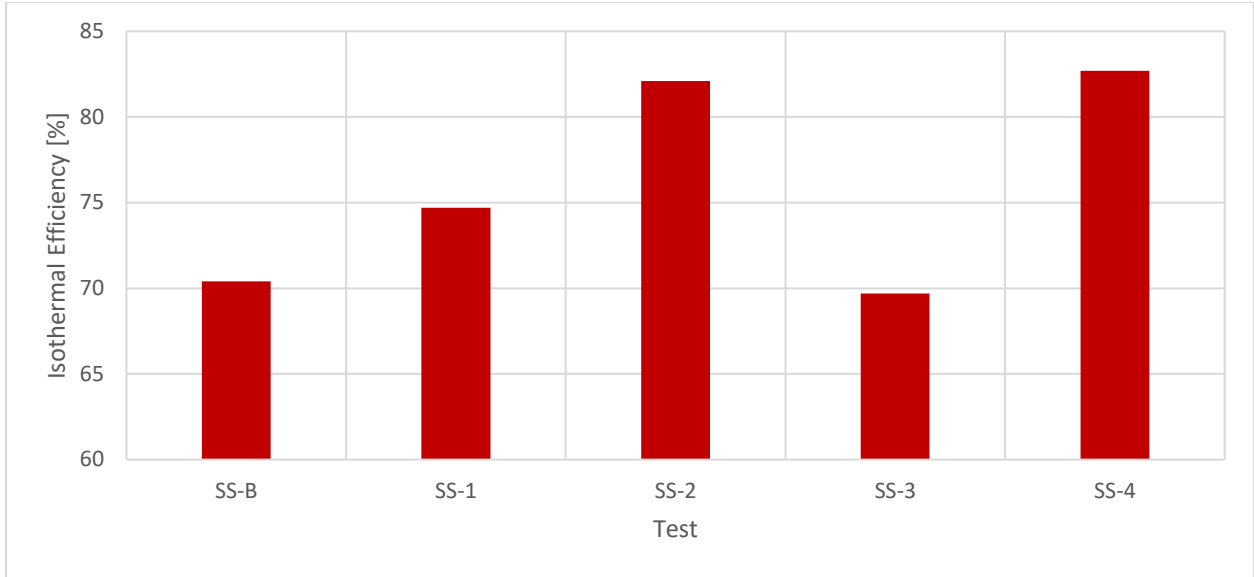
Figure 61: Isothermal Efficiency Bar Plot Comparing Combined Effect of Pump Speed and

Suction Temperature With Fan Speed
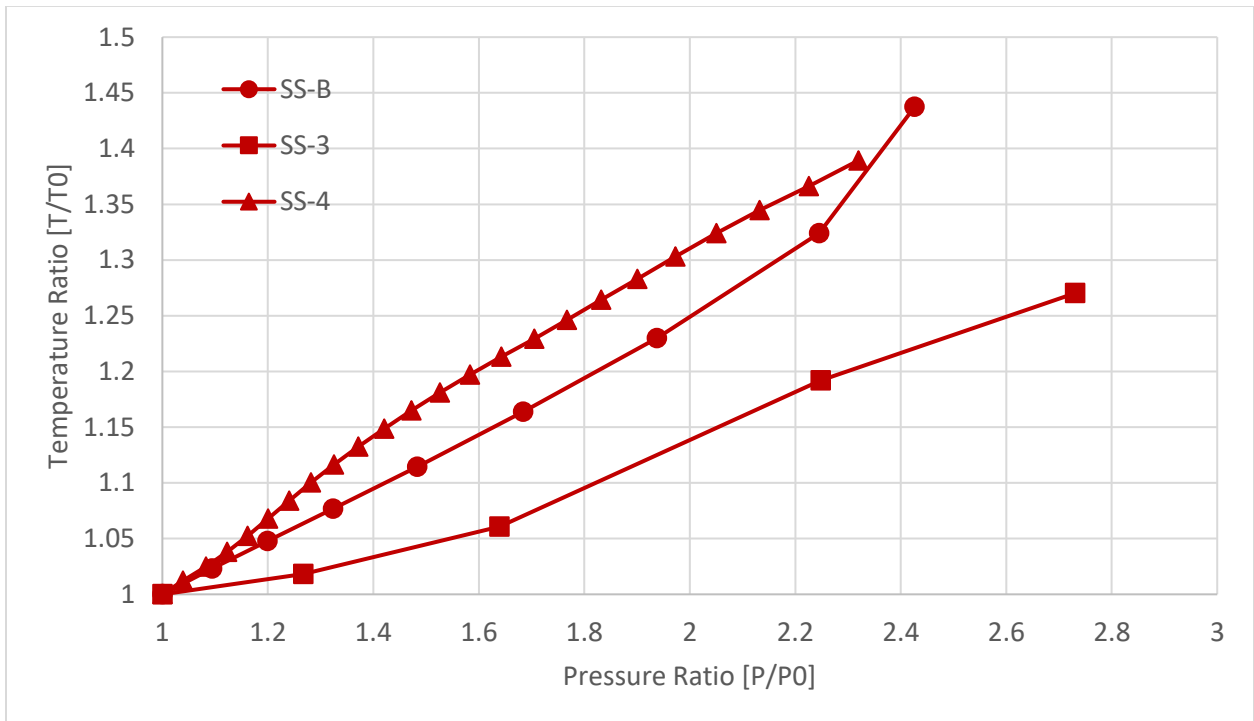
Figure 62: Temperature Ratio Versus Pressure Ratio Comparing Effect of Pump Speed
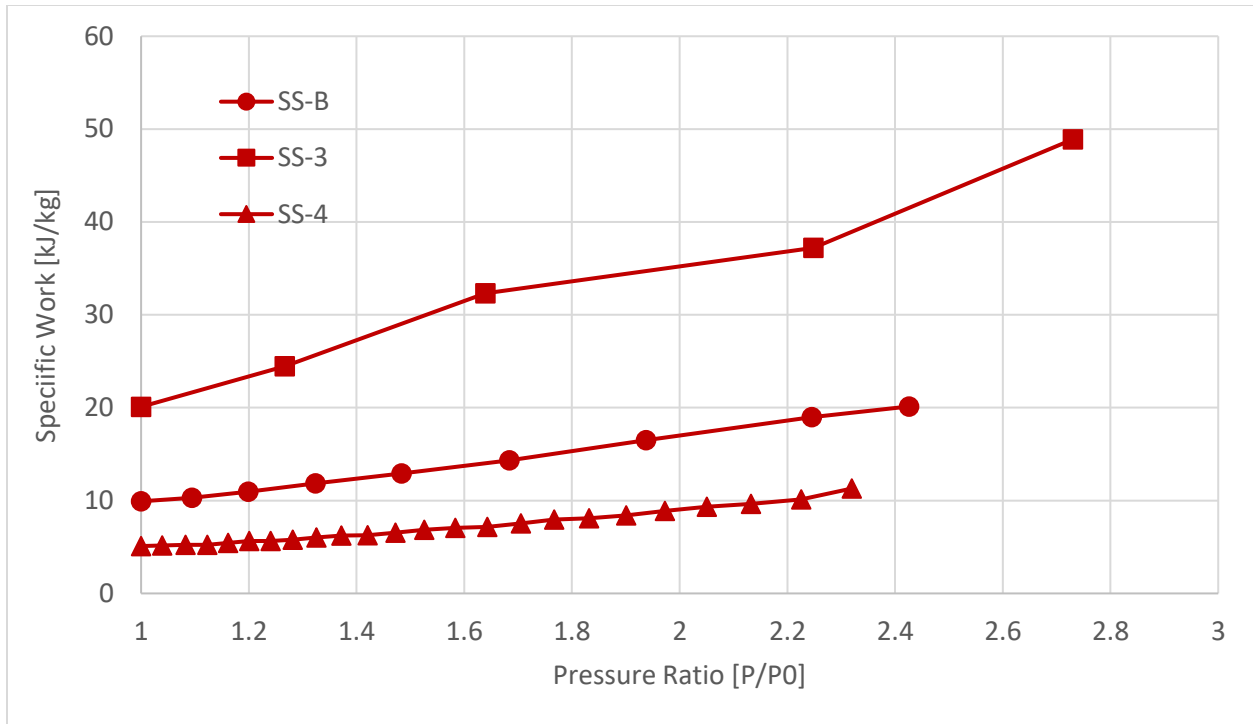
Figure 63: Specific Work Versus Pressure Ratio Comparing Effect of Pump Speed

The last test done for steady state analysis is the evaporative cooling test. With an isothermal efficiency of 91.2%, it is the highest efficiency seen in all the tests. The P-h diagram in Figure 64 shows the isothermal capability during this test against the isentropic case. The final temperature for the isentropic case would be 116.9 °C. SS-EC shows a 68.4 K decrease from the isentropic case, with only a 8.5 K temperature increase. It should also be noted that the starting temperature was increased to 40 °C which would contribute to better heat transfer compared to the tests that were done with a 35 °C starting temperature.
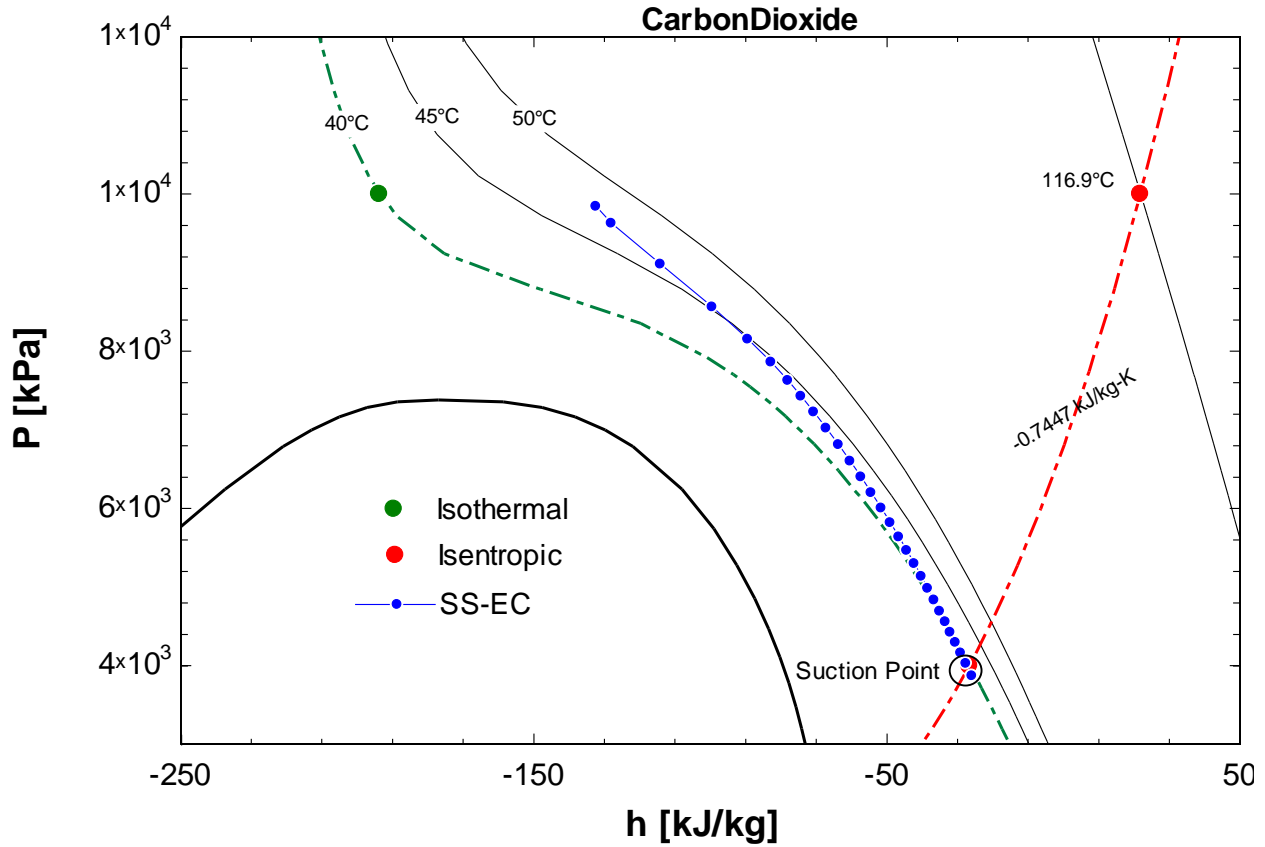
Figure 64: P-h Diagram of Steady State Evaporative Cooling Versus Isentropic and Isothermal Case

7.3 Compressor Comparison

The isothermal compressor efficiencies of different compressors for various applications (Tables 24 to 27) were compared with the test results.

Table 24: Highly ASD102SKNA6JT6A Rotary Compressor Specification

Refrigerant	Rated Capacity	Application	Suction Temp	Suction Pressure	Discharge Pressure	Isothermal Compressor Efficiency
R-410A	2,930 W	Air Conditioning	16.6 °C	989 kPa	2,236 kPa	27.2%

Highly's rotary compressor was tested at CEEE where the power draw and mass flow were directly measured to be 553 Watts and 14.9 g/s, respectively. The suction conditions as well as the discharge pressure were also directly measured as shown in Table 24. The required work for isothermal compression can be calculated in EES, knowing these values, which are in the units of kJ/kg. The isothermal efficiency can be defined as follows:

$$\eta_{iso\_Comp} = \frac{w_{iso}}{w_{actual}} = \frac{w_{iso}\dot{m}}{P_{elec}} \qquad (9)$$

Where P_{elec} is the power draw in kW, $\dot{m}$ is the mass flow rate in kg/s, w_{iso} is the required isothermal specific work in kJ/kg and w_{actual} is the actual specific work done by the compressor. Isothermal compression at these conditions requires 10.1 kJ/kg of energy. Plugging in these values, I find the isothermal efficiency to be 27.2%. The corresponding isentropic compressor efficiency is 63.2%.

Table 25: Copeland ZF06KQE Scroll Compressor Specification

Refrigerant	Rated Capacity	Application	Suction Temp	Suction Pressure	Discharge Pressure	Isothermal Compressor Efficiency
R-404A	3,870 W	Refrigeration	20.0 °C	519 kPa	2,296 kPa	28.9%

By using the capacity data and the conditions listed in Table 25, the efficiency of the Copeland's scroll compressor is calculated. Pressures are assumed to be the saturation pressures corresponding to evaporating and condensing temperatures. Reported power consumption is 2.24 kW at these conditions. The compressor has a displacement of 5.9 m³/hr. The ideal mass flow rate can be calculated by multiplying the displacement by the density at suction conditions which is 23 kg/m³. The required isothermal work is calculated to be 17.2 kJ/kg in EES. Plugging in

these values, I find the isothermal compressor efficiency to be 28.9%. The corresponding

isentropic compressor efficiency is 57.2%.

Table 26: Copeland 4MTL-05X 4 Cylinder Transcritical CO_2 Compressor Specification

Refrigerant	Rated Capacity	Application	Suction Temp	Suction Pressure	Discharge Pressure	Isothermal Compressor Efficiency
CO_2	10,008 W	Refrigeration	5.0 °C	3,050 kPa	9,000 kPa	27.0%

Calculation for the Copeland's CO_2 compressor is done like the scroll compressor. Power

draw at the conditions above is 5.6 kW. Displacement for this compressor is 4.6 m^3/hr. The

suction density is 75.7 kg/m^3. The required isothermal work is calculated to be 15.7 kJ/kg in

EES. By plugging in the values, I find the isothermal compressor efficiency to be 27.0%. The

corresponding isentropic compressor efficiency is 82%.

Table 27: Atlas Copco CO_2 22-195 50hz Reciprocating Booster Specification

Refrigerant	Flow Rate	Application	Suction Temp	Suction Pressure	Discharge Pressure	Isothermal Compressor Efficiency
CO_2	35 g/s	Gas Compression	25 °C	102 kPa	2,101 kPa	26.0%

Finally, the efficiency for the Atlas Copco's CO_2 booster is calculated in the same way.

Power draw at the conditions above is 22 kW. Mass flow rate is given at 35 g/s. The required

isothermal work is calculated to be 163.3 kJ/kg in EES. By plugging in the values, I find the

isothermal compressor efficiency to be 26.0%. The corresponding isentropic compressor

efficiency is 37.5%.

In an effort to fairly compare these compressors, the inefficiencies of the pump and motor are added back to the isothermal efficiency to get the isothermal compressor efficiency. Figure 65 plots the efficiencies of the compressors along with the evaporative cooling test, best test, and test with maximum fan cooling (SS-4). Comparing SS-EC and the Atlas Copco efficiencies, the biggest improvement can be seen with an improvement of 34.2% absolute. When comparing the next best continuous operation efficiency with the highest conventional compressor, an 18.4% improvement is seen. It should be noted that when considering all energy input including the energy needed to main pressure, efficiencies drop around the efficiency of the conventional compressors. The energy needed while pushing out the gas is also not considered in the test data efficiency analysis, which may also need to be considered for a fairer comparison.
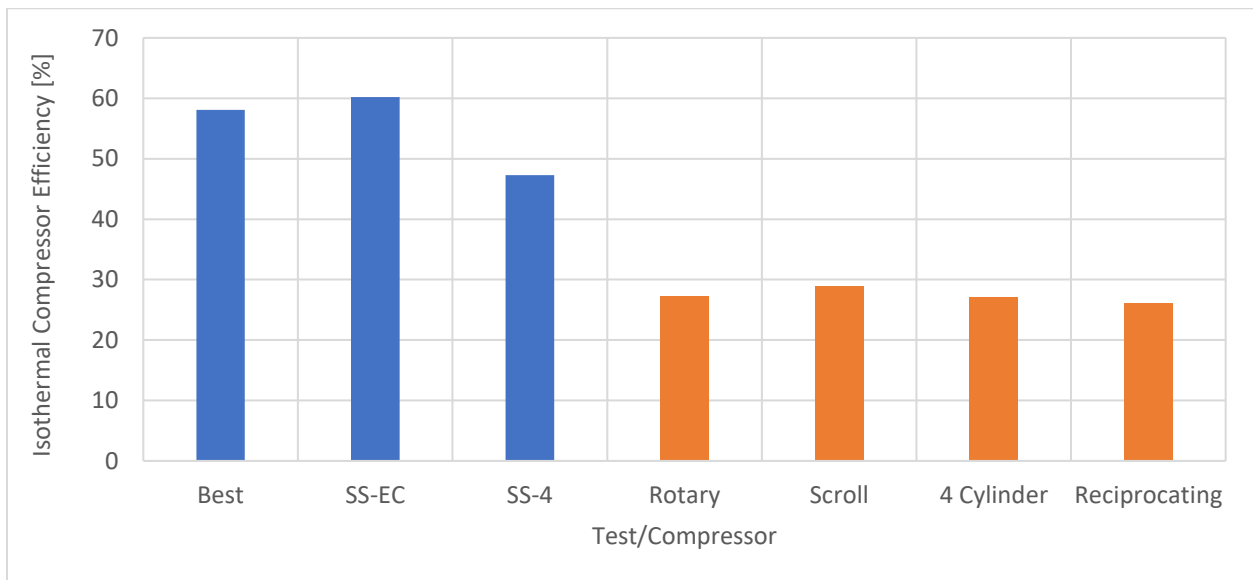

Figure 65: Isothermal Compressor Efficiency Bar Plot Comparison

7.4 Liquid Piston Comparison

Oak Ridge National Laboratory (ORNL) published the research work detailing an isothermal compressor with similar conditions, which is not addressed in the literature review

[26]. CO_2 is used as the working fluid and propylene glycol is used as a liquid piston. Their heat transfer mechanism utilizes the spray injection idea, and their target application is for heat pumps. Isothermal efficiency is not reported but comparisons can be made with SS-EC and 3-5 as detailed in Table 28. Temperature increase is 1.6 and 2.7 K lower than ORNL by SS-EC and 3-5, respectively. ORNL ran tests with a higher-pressure ratio, but the single compression and steady state tests were compressed to higher pressure near to 10,000 kPa where heat generation is most extreme. Additionally, they heated their chamber walls above ambient temperature before compression while test 3-5 did not. Test SS-EC effectively has the chamber walls heated as well because this test is run at steady state and will have the walls saturated with the heat from compression.

Table 28: Temperature and Pressure Measurement Comparison With ORNL [26]

Test	Initial Temperature [°C]	Final Temperature [°C]	Temperature Increase [K]	Initial Pressure [kPa]	Final Pressure [kPa]	Pressure Ratio
ORNL	28.6	38.8	10.2	1,870	8,580	4.59
SS-EC*	39.3	47.9	8.6	3,870	9,940	2.57
3-5	35.0	42.5	7.5	4,054	9,604	2.37

*averaged over 5 cycles

7.5 Mass Flow Rate

An additional test is run to determine the refrigerant mass flow rate. Figure 66 below shows the resulting mass flow rate when running the system at 90% pump speed and ambient air temperature of 25 °C. As shown, max flow rate is approximately 60 g/s which averages to 13.6 g/s during the entire cycle process. This matches the necessary mass flow rate of 13.3 g/s for 1.75 kW of cooling for air conditioning applications with an evaporator saturation temperature of

15 °C. As shown in Figure 66, the mass flow rate is highly intermittent, which is not desirable. Due to the high pump speed, isothermal efficiency was impacted.
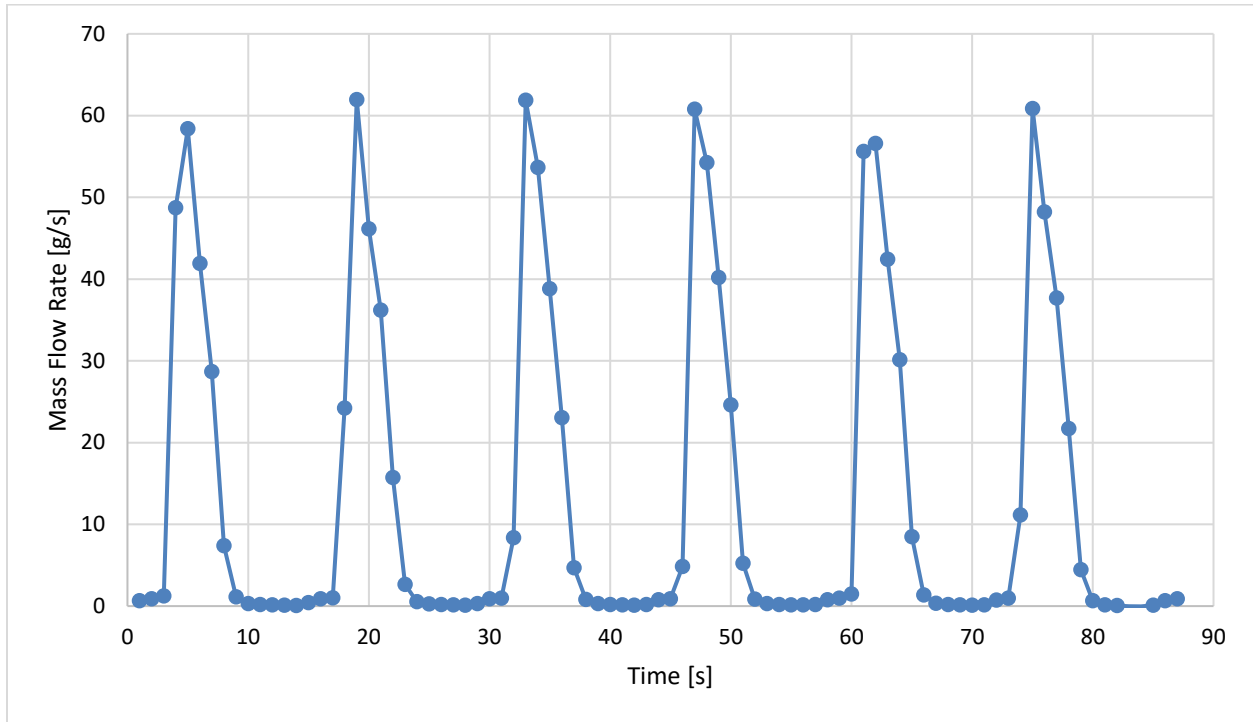
Figure 66: Mass Flow Rate of CO_2 On Suction Side

8 Conclusions

A significant amount of research has been devoted to isothermal compression of air. This thesis investigated isothermal compression toward refrigeration applications while using the CO_2 as a working fluid. Literature review suggests that spray injection can achieve high isothermal efficiencies up to 95%. However, to approach the isothermal compression process, the current study utilized the chamber geometry manipulation and a liquid piston within a bare tube HXCC design to dissipate heat during the compression process. An initial prototype was designed and built to determine its feasibility and its performance was experimentally measured and analyzed.

From the thermodynamic definition, single compression tests provide isothermal efficiencies up to 85.8%, while continuous operation tests provide isothermal efficiencies up to 82.7%. This efficiency drop is due to the heat saturation in the HXCC. With the addition of evaporative cooling on the HXCC during a steady state test, isothermal efficiency increased to 91.2%. A sensitivity analysis was also performed for the single compression tests by varying the oil temperature, fan speed and pump speed. The comparison of isothermal compressor efficiencies of current prototype compressor and four commercially available compressors shows up to 34.2% efficiency improvement absolute over commercial products. This prototype design was also able to achieve a 2.7 K lower final temperature at a lower pressure ratio but a higher final pressure over a design from the ORNL which utilized spray injection. The targeted mass flow rate for 1.75 kW cooling system was achieved but at the cost of lower isothermal efficiency. These results show sufficient performance to warrant the design of the next prototype for optimization.

9 Challenges and Future Work

9.1 Challenges

Throughout the prototyping and testing of the system, many challenges were encountered which are explained in this section. Solutions for those challenges are also suggested.

9.1.1 Heat Transfer

The highest isothermal efficiency that was achieved without the help of evaporative cooling was 82.7% for continuous operation. This is an exceptional efficiency but there is still room for improvement, especially during the latter half of the compression where the

temperature increase reaches 14.6 K. Although the chamber was designed at the maximum heat flux, many assumptions were made, so the model was inaccurate. A more robust design is needed based on a more accurate heat transfer model.

9.1.2 Refrigerant Loss

During operation, CO_2 is dissolved into the liquid piston, despite being relatively insoluble with the gas. This dissolved gas is released from the liquid piston during the decompression process when the compression chamber is open to the oil tank and is lost to the atmosphere. This can be solved with a closed loop system.

9.1.3 Oil Level Sensor

Despite the reflect sensor working in the system as is, there are some hiccups in the detection of the oil when operating at higher pump speeds and shorter suction times, making it not completely reliable. This may simply be an issue with the implemented code to run the sensor, nonetheless a more reliable, fast, and cheap sensor that can handle such working pressures may still be needed. Some likely candidates are the float, ultrasonic, and thermocouple sensors.

9.1.4 Power Density

A pump speed of 90% is needed to reach the 1.75 kW capacity currently which is not ideal. At these speeds, the isothermal efficiency is impacted severely. Conversely, lower pump speeds are necessary to reach acceptable isothermal efficiencies, therefore there is a tradeoff between efficiency and power density. This can be addressed by reducing the amount of dead volume in the compression chamber which occupies about 5% of the chamber by volume. This percentage is worse for CO_2 since it is far from an ideal gas. Using a bigger chamber combined

with a pump with a bigger displacement per rotation would also help but will need to be optimized for size. The use of the double acting piston will also help as will be explained.

9.1.5 Intermittent Mass Flow

Mass flow rate of the working fluid is highly intermittent which will pose a problem for the design of the evaporator. Since the flow time span is very short, the heat exchanger will need to be unnecessarily large. This can be aided by use of the double acting pistons and the use of a proper expansion valve.

9.1.6 Liquid Piston Loss to Refrigerant Side

During testing, the system experienced migration of some of the liquid piston into the receiver. It is believed this is due to the mixing of the liquid piston and the CO_2 near the interface. This is possible because of the nature of the geometry of the HXCC causing turbulence and the CO_2 approaching the same density of liquid piston past the critical point. This effect may be more pronounced with higher pump speeds as the interface between the piston and refrigerant gets blurred. Since this occurs, some of the liquid piston will discharge with the CO_2 and be trapped in the receiver. A similar situation is reported by Kowalski et al. (2022) [26]. This can be addressed by the addition of a separator after the back pressure regulator.

9.1.7 Water Hammer

During testing, water hammer would be experienced when shutting the solenoid valve between the pump and the HXCC. This eventually may cause microcracks in the piping, leaking the liquid piston. This can be resolved by using an expansion tank to absorb the pressure shock. The effect may also be less pronounced in the double acting piston design due to a smaller pressure difference between the inlet and outlet of the pump.

9.2 Next Prototype Improvements

With all the challenges encountered thus far, improvements to the prototype have already been thought of and a design of a work-in-progress prototype are discussed. Figure 67 shows the design of the "double acting piston" isothermal compressor.
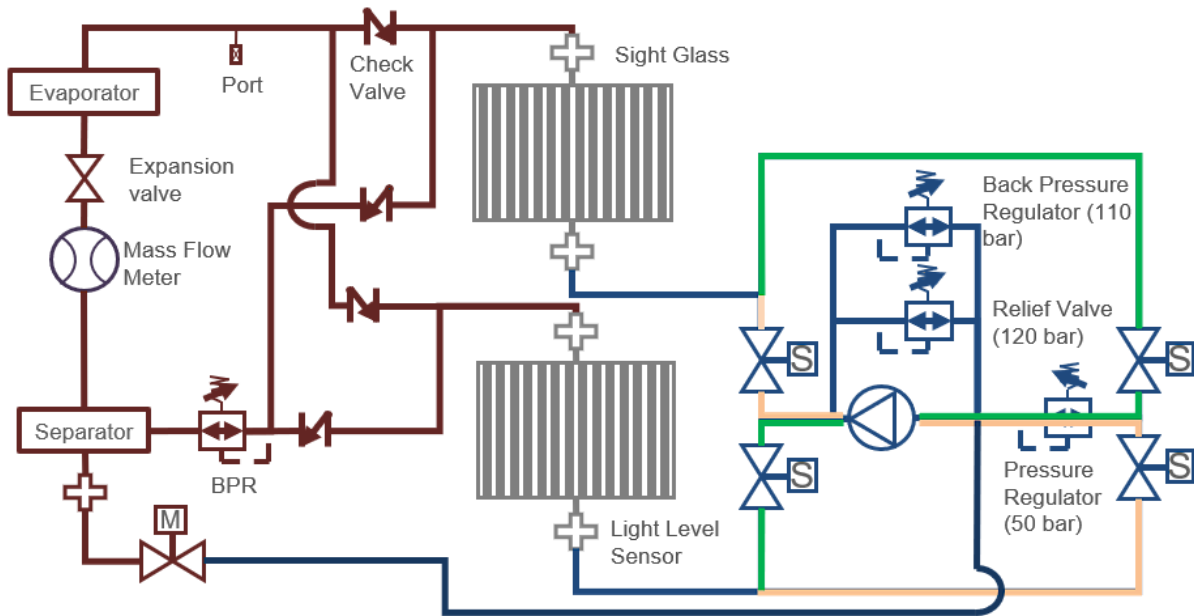
Figure 67: Double Acting Piston 2nd Prototype Design

This design will address many of the challenges that were faced with the first prototype. In addition, improvements to the integrated HXCC are being made. Currently, the most promising improvement to the heat exchanger is reducing the hydraulic diameter of the tubes to 1–2 mm inner diameter in a fractal design, as the refrigerant side heat transfer is still a limiting factor in the path to isothermal compression. More tubes can be added to offset the decrease in the size of the tube diameter to prevent higher pressure drop. Other ideas are being considered such as the use of an oil injection system much like the water injection technology discussed in the literature review and the design from ORNL. This would increase the heat transfer area

significantly. Another idea would be to use a shell-and-tube heat exchanger as the integrated compression chamber. This would change it to a water-to-refrigerant heat exchanger instead of an air-to-refrigerant heat exchanger which would have more heat transfer capability. The HXCC will also be designed for medium temperature refrigeration applications so the evaporator saturation pressure will need to be 3,000 to 3,500 kPa.

The double acting piston works by having two compression chambers. Use of a liquid piston is still present. Four solenoids are used to direct of the flow of the liquid piston much like an H-bridge used in electronics to drive a motor in forward and reverse. Use of a back pressure regulator and relief valve are still present to regulate the pressure of the liquid piston. The pressure regulator at the suction side of the pump is added to regulate the incoming liquid to the suction of the pump. Though not seen in the diagram, the use of a gas separator may be needed after the pressure regulator to ensure pure liquid flow into the pump. Flow of the liquid piston can be visualized with the green and yellow lines depicted in the diagram. For instance, if compression has completed in the bottom chamber, the top left and bottom right solenoids would open and the others would close to redirect flow from the bottom chamber to the top chamber, following the yellow path. After compression of the top chamber is completed, the flow path would follow the green line as depicted.

With the design of the double acting piston, multiple issues would be addressed as well as improvements being made. First, this design would be fully enclosed which would eliminate the issue with the loss of refrigerant being transported through the liquid piston to the environment. Second, the power density of the system would increase because time spent for decompressing the chamber would be spent for compressing the other chamber unlike with the first prototype. Third, the occurrence of highly intermittent flow would be reduced when a more balanced time

110

of compression would take place. Fourth, work recovery can be accomplished here to save more energy used for compression and energy will not be wasted re-pressurizing the liquid from atmospheric pressure to the inlet pressure. The two solenoid valves can be opened after the pump to equalize the two chambers to recover the work. Fifth, the issue of the original photoresistor/LED combination (different from the reflect sensor) can be resolved using the same sensor by placing these sensors only at the bottom of each chamber which would avoid the challenge of having to overcome the fog. Sixth, liquid piston loss would be addressed by the addition of an oil separator after the compressor to recover the lost oil.

With this new design, there come some challenges that still need to be overcome to fully realize the isothermal compressor design. The new design will require high inlet pressure into the pump which is a challenge because there does not seem to be any commercially available pumps with the specifications needed that can handle such high inlet pressures that could be found at least at the time of writing this thesis. In addition, the design may experience a possible form of cavitation to the pump which is not desirable. This is a possibility because the refrigerant will be dissolved into the liquid piston while compressing the refrigerant and then will be reduced to a lower pressure when entering the inlet of the pump which will cause the refrigerant to bubble out of the liquid piston. This challenge can be addressed with the use of a separator right before the pump inlet.

10 References

[1] ANSI/AHRI STANDARD 570 (I-P)-2012, Performance Rating of Positive Displacement Carbon Dioxide Refrigerant Compressors and Compressor Units, page 7

[2] ASME PTC 19.1-2013, Test Uncertainty, page 17-19

[3] Benson, Glendon M. Isothermalizer System. New Process Industries, Inc., Minneapolis, Minn., assignee. Patent US4446698A. 8 May 1984. Print.

[4] Bell, I.H., Groll, E.A., Braun, J.E., 2011. Performance of vapor compression systems with compressor oil flooding and regeneration. Int. J. Refrig. 34, 225–233. https://doi.org/10.1016/j.ijrefrig.2010.09.004

[5] Bell, I.H., Lemort, V., Groll, E.A., Braun, J.E., King, G.B., Horton, W.T., 2012. Liquid-flooded compression and expansion in scroll machines - Part I: Model development. Int. J. Refrig. 35, 1878–1889. https://doi.org/10.1016/j.ijrefrig.2012.07.010

[6] Bell, I.H., Lemort, V., Groll, E.A., Braun, J.E., King, G.B., Horton, W.T., 2012. Liquid flooded compression and expansion in scroll machines - Part II: Experimental testing and model validation. Int. J. Refrig. 35, 1890–1900. https://doi.org/10.1016/j.ijrefrig.2012.07.008

[7] Bell, I.H., Groll, E.A., Braun, J.E., Horton, W.T., 2013. Experimental testing of an oil-flooded hermetic scroll compressor. Int. J. Refrig. 36, 1866–1873. https://doi.org/10.1016/j.ijrefrig.2013.01.006

[8] Canales RI, Lubben MJ, Gonzalez-Miquel M, Brennecke JF. 2015 Solubility of CO2 in [1-n-butylthiolanium] [Tf2N] + toluene mixtures: liquid–liquid phase split separation and modelling.Phil. Trans. R. Soc. A 373: 20150011. http://dx.doi.org/10.1098/rsta.2015.0011

[9] "Carnot Compression." *Carnot Compression*, https://carnotcompression.com/.

[10] "Chapter 4. - Second Law of Thermodynamics." CHAPTER 4. - SECOND LAW OF
THERMODYNAMICS - Codecalculation.com 1 Documentation,
http://docs.codecalculation.com/thermodynamics/chap04.html.

[11] Cherry, Mark A.; Alderman, Robert A.; Shillinger, D. Hans. Energy recovery-recycling
turbine integrated with a capillary tube gas compressor. Carnot Compression, LLC, Scotts
Valley, CA. Justia Patent 10359055. 10 February 2017. Print.

[12] Cherry, Mark A.; Alderman, Robert A.; Shillinger, D. Hans. Method and system of
compressing gas with flow restrictions. Carnot Compression, LLC, Scotts Valley, CA. Justia
Patent 9919243. 12 October 2015. Print.

[13] Cho, H., Chung, J.T., Kim, Y., 2003. Influence of liquid refrigerant injection on the
performance of an inverter-driven scroll compressor. Int. J. Refrig. 26, 87–94.
https://doi.org/10.1016/S0140-7007(02)00017-8

[14] Coney, M.W., Stephenson, P., Malmgren, A., Linnemann, C., Morgan, R.E., 2002.
Development Of A Reciprocating Compressor Using Water Injection To Achieve Quasi-
Isothermal Compression. Int. Compress. Eng. Conf. Paper 1508.

[15] Desideri, Umberto, and Francesco Asdrubali. "High Efficiency Plants and Building
Integrated Renewable Energy Systems." *Handbook of Energy Efficiency in Buildings: A Life
Cycle Approach*, Butterworth-Heinemann Is an Imprint of Elsevier, Oxford, United
Kingdom, 2019, pp. 441–595.

[16] EPA (2022). HFC-23 Emission Standards for Production of Class II ODS. EPA.
https://www.epa.gov/ods-phaseout/hfc-23-emission-standards-production-class-ii-ods

[17] Gerstmann, Joseph, and Yizhak Friedman. Liquid Piston Heat-actuated Heat Pump and
Methods of Operating Same. Patent US4148195. 10 Apr. 1979. Print.

[18] Guanwei, J., Weiqing, X., Maolin, C., Yan, S., 2018. Micron-sized water spray-cooled quasi-isothermal compression for compressed air energy storage. Exp. Therm. Fluid Sci. 96, 470–481. https://doi.org/10.1016/j.expthermflusci.2018.03.032

[19] Guo, D., Ma, Z., Zhang, J., Liu, M., 2017. Energy Impact of Air Pre-cooling on Screw Air Compressor. Procedia Eng. 205, 937–944. https://doi.org/10.1016/j.proeng.2017.10.147

[20] Hangx, S. J. T. "Behaviour of the CO2-H2O system and preliminary mineralisation model and experiments." CATO Workpackage WP 4.1 (2005): 1-43.

[21] Heidari, M., Lemofouet, S., Rufer, A., 2014. On The Strategies Towards Isothermal Gas Compression And Expansion. Proc. 16th Int. Compress. Eng. Conf. Purdue, Lafayette, Indiana, USA. 20. 1–14.

[22] Heidari, M., Rufer, A., 2014. Fluid Flow Analysis of a New Finned Piston Reciprocating Compressor Using Pneumatic Analogy. Int. J. Mater. Mech. Manuf. 2, 297–301. https://doi.org/10.7763/ijmmm.2014.v2.146

[23] Huang, J.M., Chiang, C.P., Chen, J.F., Chow, Y. Lo, Wang, C.C., 2007. Numerical investigation of the intercooler of a two-stage refrigerant compressor. Appl. Therm. Eng. 27, 2536–2548. https://doi.org/10.1016/j.applthermaleng.2007.01.028

[24] Hugenroth, J., Braun, J., Groll, E., King, G., 2007. Thermodynamic analysis of a liquid-flooded Ericsson cycle cooler. Int. J. Refrig. 30, 1176–1186. https://doi.org/10.1016/j.ijrefrig.2007.02.012

[25] Jin, X., Zhang, K., Liu, Z., Li, X., Jiang, S., 2018. Numerical research on coupling performance of inter-stage parameters for two-stage compression system with injection. Appl. Therm. Eng. 128, 1430–1445. https://doi.org/10.1016/j.applthermaleng.2017.09.126

[26] Kowalski, Stephen; Rendall, Joseph; Abu-Heiba, Ahmad; Cheekatamarla, Praveen; Gehl, Anthony; Momen, Ayyoub; and Kashif, Nawaz, "Initial Design and Experimental Results of a Novel Near-Isothermal Compressor for Heat Pump Applications" (2022). International Compressor Engineering Conference. Paper 2776. https://docs.lib.purdue.edu/icec/2776

[27] Langston, L.; Faghri, A. "Heat Pipe Turbine Vane Cooling". Advanced Turbine Systems Annual Program Review 1995; CONF-9510109-26.

[28] Lawrence Livermore National Laboratory. "Estimated U.S. Energy Consumption in 2021: 97.3 Quads." *Flowcharts*, https://flowcharts.llnl.gov/.

[29] Lee, D., Seong, K.J., Lee, J., 2015. Performance investigation of vapor and liquid injection on a refrigeration system operating at high compression ratio. Int. J. Refrig. 53, 115–125. https://doi.org/10.1016/j.ijrefrig.2015.01.013

[30] Leibowitz, Herman M., and Somayajulu D.S.R. Karamchetty. Isothermal Compression. Mechanical Technology Incorporated, Latham, N.Y., assignee. Patent US4478553A. 23 Oct. 1984. Print.

[31] Liu, Y., Miao, N., Deng, Y., Wu, D., 2019. Efficiency evaluation of a miniature multi-stage compressor under insufficient inter-stage cooling conditions. Int. J. Refrig. 97, 169–179. https://doi.org/10.1016/j.ijrefrig.2018.09.009

[32] Luo, B., 2016. Theoretical study of R32 in an oil-flooded compression cycle with a scroll machine. Int. J. Refrig. 70, 269–279. https://doi.org/10.1016/j.ijrefrig.2016.06.002

[33] Neu, T., Solliec, C., dos Santos Piccoli, B., 2020. Experimental study of convective heat transfer during liquid piston compressions applied to near isothermal underwater compressed-air energy storage. J. Energy Storage 32, 101827. https://doi.org/10.1016/j.est.2020.101827

[34] Neu, T., Subrenat, A., 2021. Experimental investigation of internal air flow during slow piston compression into isothermal compressed air energy storage. J. Energy Storage 38, 102532. https://doi.org/10.1016/j.est.2021.102532

[35] Nethaji, N., Mohideen, S.T., 2017. Energy conservation in domestic refrigerators by cooling compressor shell - A case study. Case Stud. Therm. Eng. 10, 382–387. https://doi.org/10.1016/j.csite.2017.08.002

[36] Odukomaiya, A., Abu-Heiba, A., Gluesenkamp, K.R., Abdelaziz, O., Jackson, R.K., Daniel, C., Graham, S., Momen, A.M., 2016. Thermal analysis of near-isothermal compressed gas energy storage system. Appl. Energy 179, 948–960. https://doi.org/10.1016/j.apenergy.2016.07.059

[37] Patil, V.C., Acharya, P., Ro, P.I., 2018. Experimental Investigation of Aqueous Foam based Heat Transfer in Liquid Piston Compressor for Improvement in Compression Efficiency..Int. Compress. Eng. Conf.

[38] Patil, V.C., Liu, J., Ro, P.I., 2020. Efficiency improvement of liquid piston compressor using metal wire mesh for near-isothermal compressed air energy storage application. J. Energy Storage 28, 101226. https://doi.org/10.1016/j.est.2020.101226

[39] Patil, V.C., Acharya, P., Ro, P.I., 2019. Experimental investigation of heat transfer in liquid piston compressor. Appl. Therm. Eng. 146, 169–179. https://doi.org/10.1016/j.applthermaleng.2018.09.121

[40] Patil, V.C., Acharya, P., Ro, P.I., 2020. Experimental investigation of water spray injection in liquid piston for near-isothermal compression. Appl. Energy 259, 114182. https://doi.org/10.1016/j.apenergy.2019.114182

[41] Payne, J.W., Weinbrecht, J.F., 2002. Reflux Gas Densification Technology An Innovative Dry Compression Process. Int. Compress. Eng. Conf.

[42] PS-2018-077, High-Efficient Isothermal Compression Techniques, 2018.

[43] Qin, C., Loth, E., 2014. Liquid piston compression efficiency with droplet heat transfer. Appl. Energy 114, 539–550. https://doi.org/10.1016/j.apenergy.2013.10.005

[44] Röyttä, P., Turunen-Saaresti, T., Honkatukia, J., 2009. Optimising the refrigeration cycle with a two-stage centrifugal compressor and a flash intercooler. Int. J. Refrig. 32, 1366–1375. https://doi.org/10.1016/j.ijrefrig.2009.01.006

[45] Ramaraj, S., Yang, B., Braun, J.E., Groll, E.A., Horton, W.T., 2014. Experimental analysis of oil flooded R410A scroll compressor. Int. J. Refrig. 46, 185–195. https://doi.org/10.1016/j.ijrefrig.2014.08.006

[46] Ramaraj, S., Braun, J.E., Groll, E.A., Horton, W.T., 2016. Performance analysis of liquid flooded compression with regeneration for cold climate heat pumps. Int. J. Refrig. 68, 50–58. https://doi.org/10.1016/j.ijrefrig.2016.04.017

[47] Ren, T., Xu, W., Jia, G.W., Cai, M., 2020. A novel isothermal compression method for energy conservation in fluid power systems. Entropy 22. https://doi.org/10.3390/e22091015

[48] Saadat, M., Li, P.Y., Simon, T.W., 2012. Optimal trajectories for a liquid piston compressor/expander in a Compressed Air Energy Storage system with consideration of heat transfer and friction. Proc. Am. Control Conf. 1800–1805. https://doi.org/10.1109/acc.2012.6315616

[49] Sakama, S., Tanaka, Y., Suzuki, R., 2012. Optimization of bubble eliminator through numerical and experimental investigation. Int. J. Autom. Technol. 6, 418–425. https://doi.org/10.20965/ijat.2012.p0418

[50] "Share of Renewables in Electricity Production." *Enerdata*, 2019,

yearbook.enerdata.net/renewables/renewable-in-electricity-production-share.html.

[51] Taghavi, M., Goossens, M., Taghavi, M., Goossens, M., Syrjala, S., Joronen, T., 2021.

Experimental Investigation of a Domestic Refrigeration Appliance Based on Exergy

Destruction Experimental Investigation of a Domestic Refrigeration Appliance Based on

Exergy Destruction.

[52] Tomoya Tsuji; Daisuke Namikawa; Toshihiko Hiaki; Masayoshi Ito, "Solubility and Liquid

Density Measurement for CO 2 + Lubricant at High Pressures," no. 157.

[53] U.S. Energy Information Administration, "Table CE3.1 Annual household site end-use

consumption in the U.S. - totals and averages, 2015," 2015.

https://www.eia.gov/consumption/residential/data/2015/c&e/pdf/ce3.1.pdf.

[54] U.S. Energy Information Administration, "Table E1. Major fuel consumption (Btu) by end

use, 2012," 2016. https://www.eia.gov/consumption/commercial/data/2012/c&e/pdf/e1.pdf.

[55] Van de Ven, J.D., Li, P.Y., 2009. Liquid piston gas compression. Appl. Energy 86, 2183–

2191. https://doi.org/10.1016/j.apenergy.2008.12.001

[56] Wang, X., Hwang, Y., Radermacher, R., 2008. Investigation of potential benefits of

compressor cooling. Appl. Therm. Eng. 28, 1791–1797.

https://doi.org/10.1016/j.applthermaleng.2007.11.010

[57] Weiqing, X., Ziyue, D., Xiaoshuang, W., Maolin, C., Guanwei, J., Yan, S., 2020. Isothermal

piston gas compression for compressed air energy storage. Int. J. Heat Mass Transf. 155.

https://doi.org/10.1016/j.ijheatmasstransfer.2020.119779

[58] Working Group I (2021). Technical Summary. IPCC.

https://www.ipcc.ch/report/ar6/wg1/downloads/report/IPCC_AR6_WGI_TS.pdf

[59] Xu, X., Hwang, Y., Radermacher, R., 2011. Refrigerant injection for heat pumping/air conditioning systems: Literature review and challenges discussions. Int. J. Refrig. 34, 402–415. https://doi.org/10.1016/j.ijrefrig.2010.09.015

[60] Yan, B., Wieberdink, J., Shirazi, F., Li, P.Y., Simon, T.W., Van de Ven, J.D., 2015. Experimental study of heat transfer enhancement in a liquid piston compressor/expander using porous media inserts. Appl. Energy 154, 40–50. https://doi.org/10.1016/j.apenergy.2015.04.106

[61] Yusha, V.L., Den'gin, V.G., Busarov, S.S., Nedovenchanyi, A. V., Gromov, A.Y., 2015. The estimation of thermal conditions of highly-cooled long-stroke stages in reciprocating compressors. Procedia Eng. 113, 264–269. https://doi.org/10.1016/j.proeng.2015.07.333

[62] Zhang, C., Li, P.Y., Van De Ven, J.D., Simon, T.W., 2016. Design analysis of a liquid-piston compression chamber with application to compressed air energy storage. Appl. Therm. Eng. 101, 704–709. https://doi.org/10.1016/j.applthermaleng.2016.01.082